Studies on the host-virus interactions of coronaviruses

Zhong, Yanxin

2012

Zhong, Y. (2012). Studies on the host-virus interactions of coronaviruses. Doctoral thesis, Nanyang Technological University, Singapore.

https://hdl.handle.net/10356/49502

https://doi.org/10.32657/10356/49502

NANYANG TECHNOLOGICAL UNIVERSITY

STUDIES ON THE HOST-VIRUS INTERACTIONS

OF

CORONAVIRUSES

ZHONG YANXIN

SCHOOL OF BIOLOGICAL SCIENCES

2012

STUDIES ON THE HOST-VIRUS INTERACTIONS OF CORONAVIRUSES

ZHONG YANXIN

School Of Biological Sciences

A thesis submitted to the Nanyang Technological University

in partial fulfillment of the requirement for the degree of

Doctor of Philosophy

2012

Acknowledgements

I would like to express my heartfelt gratitude to my supervisors, Professor James Tam and Associate Professor Liu Ding Xiang, for their mentorship, guidance and advice over the years, and for granting me the opportunity to work in the Institute of Molecular and Cell Biology (IMCB) as part of their collaborative research between IMCB and Nanyang Technological University (NTU). I would also like to thank the NTU School of Biological Sciences for giving me the chance to experience research life at the University of Alberta in Canada as a visiting graduate student. These external collaborations have greatly enriched my graduate studies.

Special thanks to all the wonderful colleagues and students from both LDX IMCB and LDX NTU laboratories, especially Huihui, Ronghua, Felicia, Siti, Xiaoxing and Chen Guang from IMCB, as well as Sharhana, Elizabeth, Nafisah and Martin from NTU, for their friendship and encouragement. I am also grateful to Dr. Fang Shouguo, Dr. Yoshiyuki Yamada and Dr. Nasirudeen AMA for their kind assistance and words of wisdom.

I would like to thank NTU for the research scholarship, IMCB for allowing me to work there as an external graduate student, and the Foreign Affairs and International Trade Canda (DFAIT) for the research grant during my time in Canada.

This work would not have been possible without the unfailing support of my parents – thank you for always being there for me.

Table of Contents

ABBREVIATIONS

ALV	*Avian Leukosis and sarcoma Virus*
HCV	*Hepatitis C virus*
HCMV	*Human Cytomegalovirus*
HHV-8	*Human herpesvirus-8*
HIV	*Human immunodeficiency virus*
HSV	*Herpes simplex virus*
IBV	*Infectious bronchitis virus*
KSHV	*Kaposi sarcoma–associated herpesvirus*
MHV	*Mouse hepatitis virus*
SARS-CoV	*Severe acute respiratory syndrome coronavirus*
SV	*Sendai virus*
SV5	*Simian virus 5*
TGEV	*Transmissible Gastroenteritis Coronavirus*
$3CL^{pro}$	3C-like protease
3pRNA	5'-triphosphate RNA
AIF	apoptosis-inducing factor
AP1	activator protein 1
Apaf1	Apoptotic protease activating factor1
BAK	BCL-2-antagonist/killer 1
Bcl-2	B cell lymphoma-2
BH	Bcl-2 homology
CARD	caspase-recruitment domain
caspase	cysteine aspartyl-specific proteases
CHOP	C/EBP homologous protein
CMC	Carboxymethylcellulose
CREBP	cAMP-response element-binding protein
DBD	DNA-binding domain
DED	death effector domain
DMEM	Dulbecco's Modified Eagle Medium
dsRNA	double stranded RNA
DTT	Dithiothreitol
E	envelope protein
E. coli	*Escherichia coli*
EGFP	enhanced green fluorescence protein
ER	endoplasmic reticulum
ERGIC	endoplasmic reticulum Golgi intermediate compartment
ExoN	exonuclease
FACS	Fluorescence activated cell sorting
FADD	Fas associated death domain
FBS	Foetal bovine serum
FLIP	FLICE-inhibitory protein
GADD153	growth arrest and DNA damage-inducible gene 153
GAPDH	glyceraldehyde-3-phosphate dehydrogenase
HE	hemagglutinin esterase
hnRNPA1	heterogeneous nuclear ribonucleoprotein A1
IAD	IRF association domain
IAP	inhibitor of apoptosis

IFIT	interferon-induced protein with tetratricopeptide repeats
IFN	interferon
IGS	intergenic sequences
IKKe	IkB kinase e
IKK-I	inducible IκB kinase
IκBα	inhibitor of κB
IRAK	interleukin-1 receptor–associated kinase
IRES	internal ribosome entry site
IRF	interferon regulatory factor
ISG	interferon-stimulated gene
ISGF	interferon-stimulated gene transcription factor
ISRE	IFN-stimulated response elements
JAK-STAT	Janus kinase-Signal Transducer and Activator of Transcription
JNK	c-Jun NH2-terminal kinase
kb	kilo-base
kDa	kilo-Dalton
LGP2	laboratory of genetics and physiology 2
M	membrane protein
MAP/ERK	mitogen-activated protein/extracellular signal-regulated kinase
MAVS	mitochondrial antiviral signalling adaptor
Mcl-1	myeloid cell leukemia-1
MDA5	melanoma differentiation-associated gene-5
MOI	multiplicity of infection
MOMP	mitochondrial outer membrane permeabilization
MyD88	myeloid differentiation primary response protein 88
N	nucleocapsid protein
NendoU	endoribonuclease
NES	nuclear export signal
NFκB	nuclear factor kappa-light-chain-enhancer of activated B
NOD	Nucleotide-binding oligomerization domain
NLR	NOD-like receptor
ORF	open reading frame
PAMP	pathogen associated molecular pattern
PARP	poly (ADP-ribose) polymerase
PCR	polymerase chain reaction
PFU	plaque forming units
PI3K/Akt	phosphoinositide 3-kinase
PKR	protein kinase receptor
PL^{pro}	papain-like protease
poly(I:C)	poly-inosinic poly-cytidylic acid
PPR	pattern recognition receptor
RIG-I	retinoic acid inducible gene-I
RLH	RIG-I like helicase
RPMI1640	Roswell Park Memorial Institute medium 1640
RT	reverse transcription
S	spike protein
SDS-PAGE	Sodium dodecyl sulfate-polyacrylamide gel electrophoresis
sgRNA	subgenomic RNA
siRNA	short interfering RNA
ssRNA	single strand RNA

TBK1	tank-binding kinase 1
TIR	TLR toll-interleukin 1 receptor
TLR	Toll-like receptor
TNFR1	TNF receptor 1
TRADD	TNFR-associated death domain
TRAF	TNF-receptor-associated factor
TRIF	TIR domain-containing adaptor-inducing IFN β
TRS	transcription-regulatory sequence
TYK2	tyrosine kinase 2
UTR	untranslated region
VDAC2	Voltage-dependent anion-selective channel protein 2
vIBO	viral inhibitor of Bak oligomerization
vIRF	viral interferon regulatory factors
vMIA	viral mitochondria-localized inhibitor of apoptosis
vSIG	viral stress-inducible genes
XIAP	X-linked inhibitor of apoptosis

List of Figures

List of Tables

PUBLICATIONS

Y. Zhong, Y. Liao, S. Fang, J. P. Tam, D. X. Liu. (2012). Up-regulation of Mcl-1 and Bak by coronavirus infection of human, avian and animal cells modulate apoptosis and viral replication. PLoS ONE doi:10.1371/journal.pone.0030191

SUMMARY

Virus-induced apoptosis and host antiviral innate immunity, as well as the various mechanisms that regulate these responses, are key issues in understanding virus-host interactions and viral pathogenesis. Like many other human and animal viruses, coronavirus infection of mammalian cells induces both apoptosis and host antivral innate immune responses.

Global gene expression profiles are first determined in IBV-infected Vero cells at 24 hours post-infection by Affymetrix array, using avian coronavirus infectious bronchitis virus (IBV) as a model system. It reveals an up-regulation at the transcriptional level of both pro-apoptotic B cell lymphoma-2 (BCL-2)-antagonist/killer 1 (Bak) and pro-survival myeloid cell leukemia-1 (Mcl-1). These results were further confirmed both *in vivo* and *in vitro*, in IBV-infected embryonated chicken eggs, chicken fibroblast cells and mammalian cells at transcriptional and translational levels, respectively. Interestingly, the onset of IBV-induced apoptosis occurred earlier in short interfering RNA targeting Mcl-1 (siMcl-1) silenced mammalian cells, and was delayed in cells silenced with siBak. IBV progeny production and release were increased in infected Mcl-1 knockdown cells compared to similarly infected control cells, while the contrary was observed in infected Bak knockdown cells. Furthermore, IBV infection was shown to up-regulate the growth arrest and DNA damage-inducible gene 153 (GADD153), which in turn induced the expression of Mcl-1. Inhibition of the mitogen-activated protein/extracellular signal-regulated kinase (MEK/ERK) and phosphoinositide 3-kinase (PI3K/Akt) signalling pathways by chemical inhibitors and knockdown of GADD153 by siRNA demonstrated the involvement of ER-stress response in regulation of IBV-induced Mcl-1 expression.

Next, up-regulation of RNA helicases from the RIG-I-like receptor (RLR) family, Melanoma differentiation-associated gene 5 (MDA5) and Retinoic-inducible gene I (RIG-I) was observed at both transcriptional and translational levels in mammalian cells infected with IBV. MDA5 was also observed to be up-regulated *in vivo*, in infected chicken embryos, and *in vitro*, in infected chicken fibroblast cells. A third member of the RLR family, the Laboratory of genetics and physiology 2 (LGP2), appears to be able to regulate MDA5 and/or RIG-I antiviral signalling during IBV infection, which ultimately leads to the downstream activation of Mitochondrial antiviral signalling (MAVS) adaptor protein for the induction of interferons in response to viral invasion. While the transient expression of MAVS was able to abolish IBV infection almost entirely, the same was not observed in cells over-expressing MDA5 or RIG-I. Little or no interferon activity was also observed in the co-expression of MDA5/RIG-I with total viral RNA, nor with the fourth segment of the IBV genome encompassing IBV non-structural proteins (nsp) 13-16, confirming the ability of IBV to evade recognition by MDA5 and/or RIG-I. Co-expression of IBV nsp 15, an endonuclease, with MAVS also led to the inhibition of interferon regulatory factor 3 (IRF3) phosphoactivation, which may possibly play a part in the IBV evasion of MDA5 and/or RIG-I recognition.

Members of the RLR signalling pathway, including RIG-I, MDA5 and MAVS, were also observed to play a part in the modulation of virus-induced apoptosis during IBV infection. Full length MAVS underwent caspase-dependent cleavage in conjunction with the onset of apoptosis during the late stages of infection. The rate of apoptosis appeared to increase in infected MDA5 and/or MAVS knockdown cells, and was delayed in infected RIG-I knockdown cells. The Bcl-2 family of proteins, too, regulates the onset of apoptosis and MAVS cleavage during infection, thus further

establishing the link between MAVS, a mitochondrial protein, and intrinsic apoptotic pathway activation in the mitochondria during the induction of host innate immunity.

Altogether, these results illustrate the multiple, sophisticated regulatory strategies evolved by coronaviruses to tightly modulate both virus-induced apoptosis and host antiviral responses during their replication cycle.

CHAPTER 1. LITERATURE REVIEW

1.1 VIRUSES AND APOPTOSIS

1.1.1 Virus-induced cell deaths: apoptosis and necrosis

Virus-induced eukaryotic cell death typically follows one of the two paths: apoptosis or necrosis. The execution of either one or the other in virus-infected cells, thus, reflects the pathogenicity of viruses (Hay and Kannourakis, 2002).

Apoptosis is a highly conserved and strictly controlled physiological process by which unwanted cells are selectively eliminated. This mechanism also plays a critical role in normal development (Ren et al., 2005), stress response and adaptation (Puthalakath et al., 2007). Apoptotic cells undergo many distinct morphological and biochemical changes. Nuclear and/or cytoplasmic condensation, as well as membrane protrusion, is initiated. Nuclear fragmentation then follows suit, resulting in the subsequent encapsulation of these fragments into apoptotic bodies that are rapidly and unobtrusively phagocytosed before there is any leakage of their cytosolic contents, without an inflammatory response (Reed, 2000).

Necrosis, in contrast, is not self initiated but instead arises from an insult or injury to the cell, such as cytotoxicity or mechanical damage (Elmore, 2007). Characteristics of necrosis include significantly less DNA degradation as compared to apoptosis and a major loss of membrane integrity. The damaged cells swell and rupture, resulting in leakage of destroyed cell contents and eliciting an inflammatory response from the surrounding cells (Assuncao Guimaraes and Linden, 2004).

Increasing evidence has shown, however, that the distinction between apoptosis and necrosis might have been oversimplified, and the lines between the two have since been blurred (Zong and Thompson, 2006). Necrosis, once thought to be unmanageable and random, has been shown to be a type of programmed cell death that resembles that

of an arrested form of apoptosis. Cells can also be scheduled to undergo both necrosis and apoptosis given the same stimuli, and can similarly be safeguarded from necrotic elimination by anti-apoptotic proteins such as B cell lymphoma-2 (Bcl-2) (Proskuryakov, Gabai, and Konoplyannikov, 2002).

1.1.2 Apoptotic pathways

A number of stimuli can precipitate apoptotic events, including cell homeostatic imbalance such as cell stress, and the binding of ligands to cell surface "death" receptors; these in turn trigger the onset of major apoptotic pathways: the extrinsic or intrinsic pathway (Ferri and Kroemer, 2001) (Fig. 1-1).

The extrinsic pathway is synonymous with receptor-mediated cell death and can be induced by several cytokine "death" receptors from the tumour necrosis factor (TNF) family, such as the TNF receptor 1 (TNFR1) and Fas (Apo1/CD95) (Reed, 2000). Upon recruitment of their respective ligands, TNF and Fas ligand, via their respective adaptor molecules, TNFR-associated death domain (TRADD) and Fas associated death domain (FADD), to the death receptors' cytosolic death domains, the subsequent complexes formed then bind death effector domain (DED)-containing pro-Cysteine Aspartyl-Specific Proteases (pro-caspases), in particular pro-caspase-8, the activation and consequent oligomerization of which further serves is a signal for downstream activations, thus pledging the doomed cell towards its own death (Ashkenazi and Dixit, 1998).

The intrinsic pathway, on the other hand, is activated by the release of cytochrome *c* from the mitochondria into the cytoplasm, which is in turn precipitated by pro-apoptotic stimuli or even the activation of cell surface death receptors (Mikhailov et al., 2003). The regulation of the mitochondria and its downstream apoptotic signalling pathways will be discussed further in depth in later paragraphs. In

the cytosol, cytochrome *c* binds the apoptotic protease activating factor (Apaf1), which together form an apoptosome that leads to the release of the active caspase 9 from its inactivated pro-caspase 9 form through the binding and cleavage of the latter.

Both caspase 8, from the extrinsic pathway, and caspase 9, from the intrinsic pathway, have been observed to activate the main effector caspase 3, which in turn activates a caspase cascade, cleaving and activating downstream effector proteases caspases-6 and -7 to eventually evoke the morphological hallmarks of apoptosis such as DNA fragmentation (Assuncao Guimaraes and Linden, 2004; Elmore, 2007). Meanwhile, the X-linked inhibitor of apoptosis protein [XIAP, or inhibitor of apoptosis protein 3 (IAP3), also known as baculoviral IAP repeat-containing protein 4 (BIRC)], serves as an endogenous inhibitor of caspases-3, -7, and -9 in human cells (Chawla-Sarkar et al., 2003).

A third pathway, induced by prolonged endoplasmic reticulum (ER) stress (Fig. 1-2), has also been shown to activate multiple downstream apoptotic targets, including caspase 12, growth arrest and DNA damage-inducible gene 153 (GADD153), also known as the transcription factor C/EBP homologous protein (CHOP) as well as activation of the pro-apoptotic c-Jun NH2-terminal kinase (JNK) (Li, Lee, and Lee, 2006). It must be noted that while the rodent caspase 12 is found to be critically important in ER-stressed induced apoptosis, it is absent in many humans as a result of polymorphism (Kim, Xu, and Reed, 2008). However, human pro-inflammatory caspase 4, a nearly identical paralogue of the rodent form of caspase 12, has been shown to possess comparable roles in ER-stressed apoptosis (Hitomi et al., 2004). The activation of JNK is mediated by ER transmembrane protein kinases, themselves activated in times of stress, while CHOP is triggered by ER stress at the transcriptional level (Li, Lee, and Lee, 2006). The downstream apoptotic activities of both JNK and

CHOP have been shown, at least in part, to be connected with the Bcl-2 family of proteins, as BCL-2)-antagonist/killer 1 (Bak) and BCL-2-associated X (Bax) can be recruited to the ER and initiate apoptosis in response to stress (Li, Lee, and Lee, 2006). As these pro-apoptotic proteins are better known to govern apoptotic events at the mitochondria, it has been postulated that the mitochondria may well serve as an assimilator of the ER cell stress-related death pathway (Oyadomari and Mori, 2004).

While caspases are fundamental to the programmed pathway of cell death, apoptosis can also occur in a caspase-independent manner. Bak and Bax have been shown to induce apoptosis in yeast, which are naturally caspase-deficient, without any DNA fragmentation (Jurgensmeier et al., 1997). It is likely that in the event of caspase inhibition or deficit, the apoptosis-inducing factor (AIF) is released following mitochondrial dysfunction and mitochondrial outer membrane permeabilization (MOMP) to activate the onset of apoptosis (Susin et al., 1999).

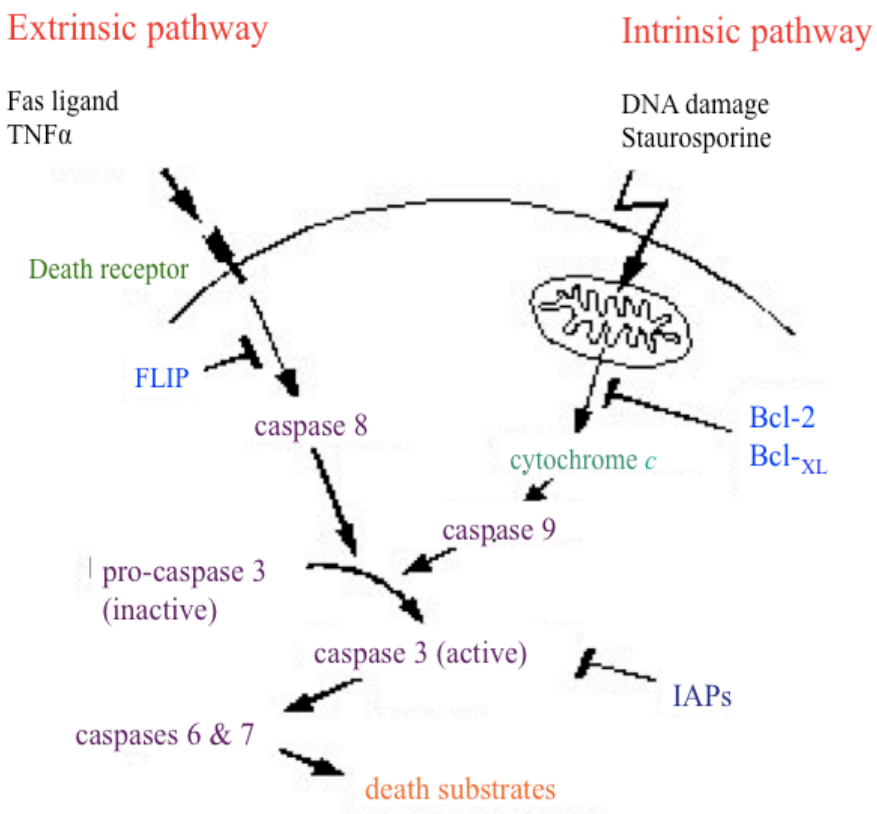

Figure 1-1

Schematic overview of the major extrinsic and intrinsic apoptotic pathways, as adapted from (Nishihara et al., 2003). **Extrinsic pathway**: Fas ligand first transmits signals to Fas receptor on a target cell by inducing its trimerization. Activation of Fas subsequently recruits FADD via interactions between their respective death domains. Pro-caspase-8 then binds FADD via interactions between the death effector domains of FADD and pro-caspase-8, leading to the cleavage and subsequent activation of caspase-8. Activation of caspase-8 triggers a caspase cascade that activates other caspases and ultimately leads to apoptosis. Caspase-8 activation can also activate Bid, leading to activation of the intrinsic apoptotic pathway. Fas-induced apoptosis can be effectively blocked at several stages by either FLICE-inhibitory protein (FLIP).

Intrinsic pathway: Proapoptotic Bcl-2 family members, such as Bax and Bak can promote the release of apoptogenic factors such as cytochrome *c* from the mitochondrial inter-membranal space into the cytosol, which subsequently leads to the activation of caspases that ultimately lead to apoptosis through nuclear damage such as DNA fragmentation. In addition, Smac/Diablo is released, which blocks the IAP inhibition of caspase activity.

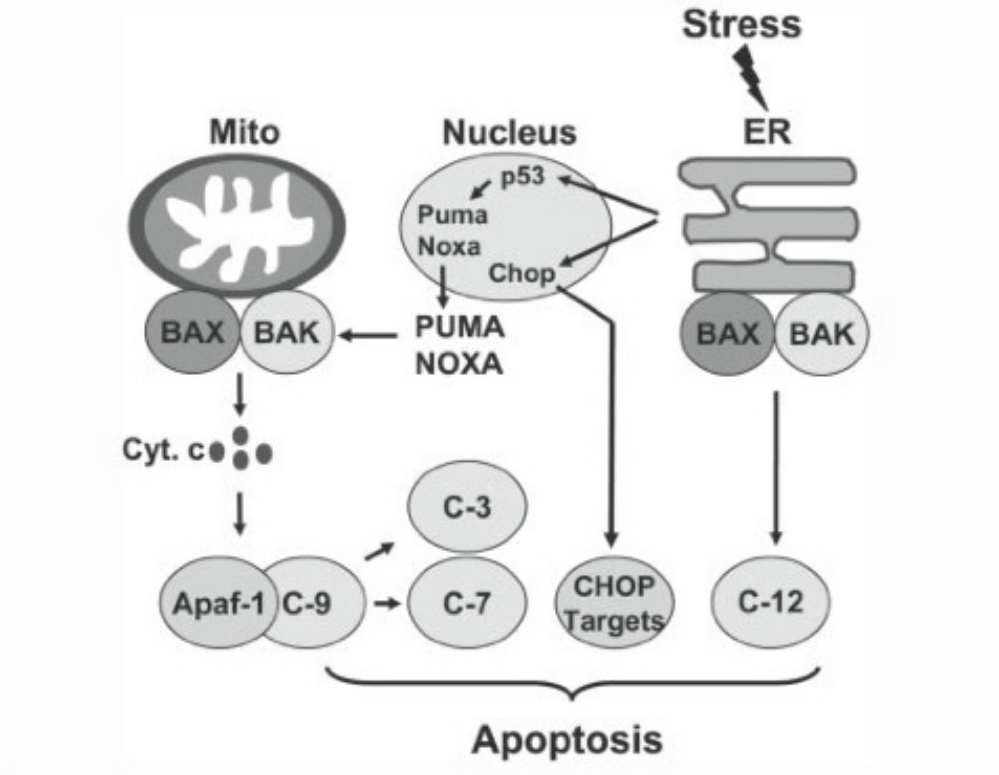

Figure 1-2

ER stress-induced apoptotic pathways, as adapted from (Li, Lee, and Lee, 2006). ER stress activates Bax/Bak localized at the ER, which targets and cleaves downstream murine caspase 12 (human caspase 4 paralogue) for its activation. ER stress transcriptionally induces BH3 family members, PUMA and NOXA, via p53-dependent mechanisms, as well as CHOP via p53-independent pathways, leading to the downstream activation of CHOP targets, which then induce ER stress-dependent apoptosis. PUMA and NOXA activate Bax/Bak localized at the mitochondria, which subsequently induces apoptosis via mitochondrial signalling pathways.

1.1.3 The mitochondrial pathway of apoptosis and its regulation

Of note is the mediation of apoptosis through the permeabilization of the outer mitochondrial membrane, as this is the main cellular organelle on which different cell death signals and pathways merge (Green, 2006). Apoptotic mitochondrial events are regulated primarily through the activation of pro-survival and pro-apoptotic proteins (Adams and Cory, 2001). The Bcl-2 family of proteins constitutes a critical control point in the regulation of apoptosis. Depending on the number Bcl-2 homology (BH) domains they share, which can range anywhere from one to four domains, they form three major protein subgroups: the BH3-only proteins [e.g., BH3-interacting domain death agonist (Bid), BCL2-associated agonist of cell death (Bad)], Bax-like proteins (e.g., Bax, Bak) and the Bcl-2-like factors [e.g., Myeloid cell leukemia-1 (Mcl-1), Bcl-extra large (Bcl-X_L)] (Galonek and Hardwick, 2006). BH3-only and Bax-like proteins are essential initiators of apoptosis while the Bcl-2-like proteins are pro-survival factors that safeguard the cells against apoptosis. The complex interaction among the family members that lead to the onset of apoptosis has been a subject for debate over the years.

A popular theory that most subscribe to is the direct activation model where pro-apoptotic proteins such as Bax and Bak heterodimerize with Bcl-2-like anti-apoptotic factors like Mcl-1 and Bcl-X_L in unstressed, healthy cells, thus rendering the former inactive (Leu et al., 2004; Willis et al., 2005). In response to distinct cell death signals, BH3-only proteins are activated, which act to bind the anti-apoptotic inhibitors and release the pro-apoptotic activators from their clutches (Galonek and Hardwick, 2006). As such, the expression of pro-apoptotic proteins of the Bcl-2 family such as Bax and Bak increases, which undergo homo-oligomerization and form pores in the outer mitochondrial membrane in a process known as

mitochondrial outer membrane permeabilization, resulting in a series of mitochondrial dysfunctions that includes an alteration in the mitochondrial membrane potential ($\Delta\Psi_m$) and the production of reactive oxygen species, culminating in the opening of the permeability transition pore that induces the efflux of cytochrome-*c* from the mitochondrial inter-membranal space into the cytosol (Korsmeyer et al., 2000). Cytochrome-*c* then complexes with Apaf-1 and pro-caspase 9 to activate caspase 9, which leads to the subsequent activation of caspase-3 and -7 (Ferri and Kroemer, 2001) (Fig. 1-3).

A

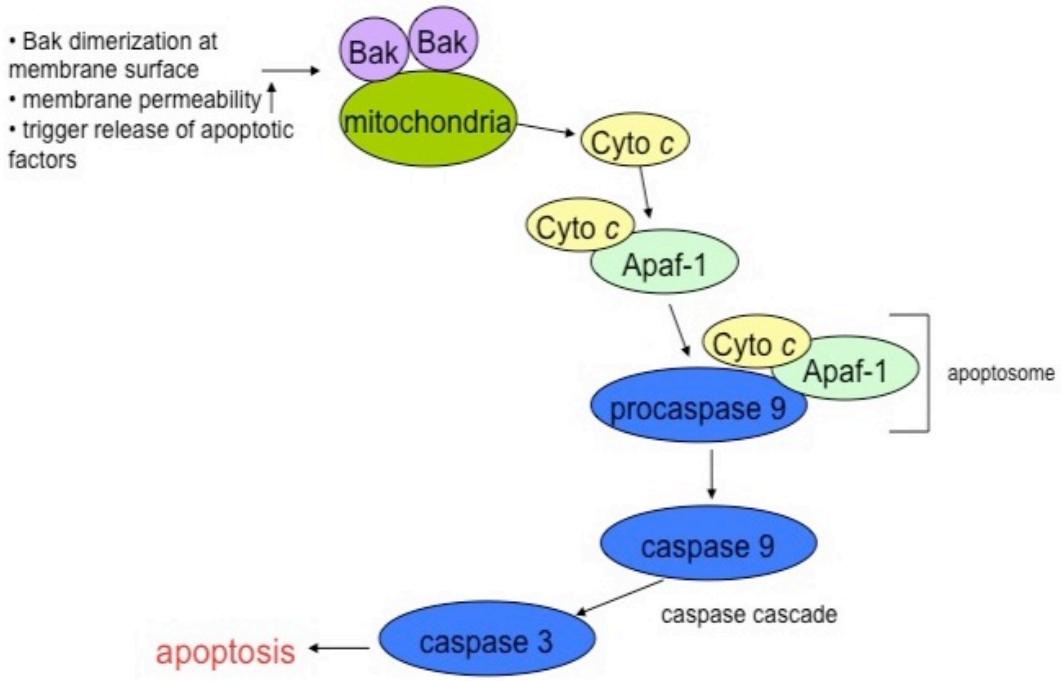
• Bak dimerization at membrane surface
• membrane permeability
• trigger release of apoptotic factors
Bak
Bak
mitochondria
Cyto c
Cyto c
Apaf-1
Cyto c
Apaf-1
apoptosome
procaspase 9
caspase 9
caspase cascade
caspase 3
apoptosis

B

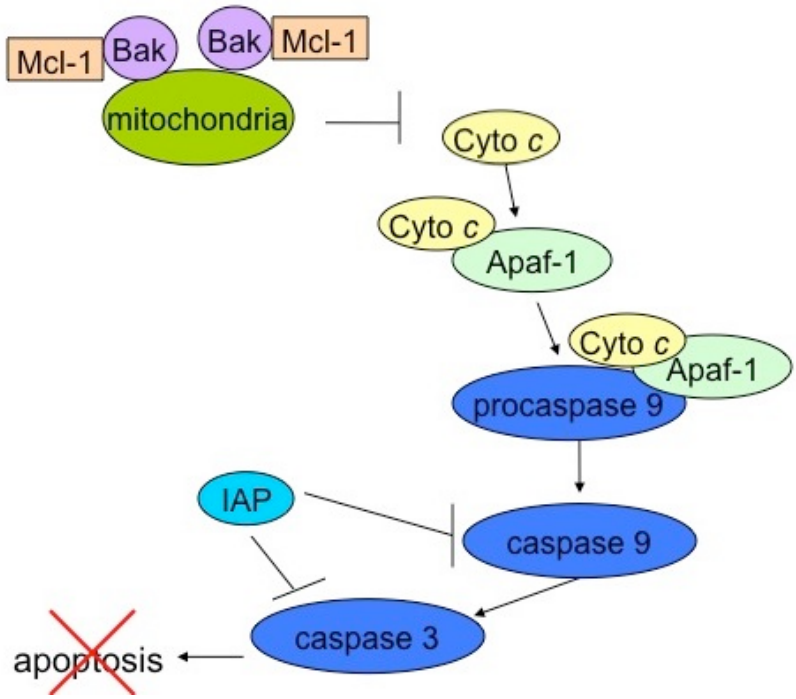
Mcl-1
Bak
Bak
Mcl-1
mitochondria
Cyto c
Cyto c
Apaf-1
Cyto c
Apaf-1
procaspase 9
IAP
caspase 9
caspase 3
apoptosis

Figure 1-3

A simplified model of the activation and inhibition of the mitochondrial pathway.

(A) Activation of the mitochondrial pathway. Pro-apoptotic Bak dimerizes at the cell membrane surface and act to increase mitochondrial membrane permeability, triggering the release of apoptotic factors from the mitochondrial inter-membranal space into the cytosol. One such factor is cytochrome *c*, which activates and forms a complex with apoptotic effector Apaf-1 and pro-caspase 9 to form the apoptosome. Caspases are downstream effectors of the apoptosome, and are processed into proteolytically active forms. This begins a caspase cascade, resulting in apoptosis through nuclear damage (DNA fragmentation), thus disrupting normal cell functions.

(B) Inhibition of the mitochondrial pathway. Inhibition of the mitochondrial pathway occurs when anti-apoptotic protein Mcl-1 heterodimerizes with Bak, preventing mitochondrial membrane permeabilization and thus inhibiting the subsequent release of apoptotic factors.

Another model, the hierarchy model of activation, has been proposed where the BH3-only proteins are categorized into two sub-groups depending on their functions (Kim et al., 2006). BH3-only proteins that function as inactivators (e.g., Bad) bind and inactivate anti-apoptotic factors upon the stimulation of cell death signals. The inactivated anti-apoptotic branch of proteins is thus unable to confine the second sub-group of BH3-only activator proteins [truncated BID (tBID), Bcl-2-interacting mediator of cell death (BIM) and p53 up-regulated modulator of apoptosis (PUMA)], which are now free to either associate directly with and activate both Bak and Bax, or indirectly with negative regulators of Bak and Bax like the mitochondrial outer membrane channel voltage-dependent anion-selective channel protein 2 (VDAC2).

A third contradictory theory disputes the role of BH3-only "activator" proteins, as it has been shown that cells were still able to undergo apoptosis even in the absence of tBID, BIM and PUMA (Willis et al., 2007). Instead, all BH3-only proteins are postulated to target only the anti-apoptotic fraction such that the latter group is forced to relinquish their restrictive hold on Bak and Bax, thereby allowing the onset of apoptosis.

Recently, however, it has come to light that the activation of Bak and Bax require the direct intervention of BH3-only activating proteins for MOMP to occur (Du et al., 2011). It has been suggested that Bak and Bax function in a semi-activated form after being released from the confines of pro-survival proteins, and requires further direct activation from BH3 only proteins before they become fully functional.

1.1.4 The role of apoptosis in virus infection

As viruses depend on the host cells they infect in order to reproduce, apoptosis is often employed as an important antiviral defence mechanism of the host cell that, as a protective measure, leads to the abortion of virus infection such that viral productivity

and persistent infectivity is consequently limited (Barber, 2001). In many cases, p53 and the Bcl-2 family of proteins have been shown to be the main mediators that induce the beleaguered cell to undergo self-induced death at almost every stage of the infection cycle (Levine, 1997).

Viruses can induce apoptosis as early as during virus entry. For example, retroviruses like avian leukosis and sarcoma virus (ALV) utilize their envelope protein (Env) to attach to the cell surface death receptor CAR1, a member of the TNF receptor family, thereby triggering downstream apoptotic signalling cascades (Brojatsch et al., 1996). In the case of polioviruses, the poliovirus receptor (PVR/CD155), important in facilitating virus entry, has also been shown to trigger downstream JNK-mediated activation of the mitochondrial apoptotic pathway, although the mechanism is currently unknown (Danthi, 2011).

Once through to the cell, enveloped viruses such as coronaviruses undergo uncoating in host endosomes while non-enveloped viruses like reoviruses are deconstructed in the same organelles. Host endosomal membranes are forced to undergo conformational changes for the fusion of virus and host cell membranes during virus uncoating; membrane integrity is also antagonized during the process of virus disassembly. As such, these drastic alterations to membranes, as well as the unveiling of viral components in the case of non-enveloped viruses, may then elicit downstream pro-death signals, prompting the infected cells to commit suicide (Danthi, 2011).

Post-uncoating/-disassembly, in the cytosol or within the nuclear membrane, viruses such as adenoviruses require further processing of their viral components, for example from the viral nucleocapsid to its inner capsid, and cytosol events bringing about this transport process may also inadvertently trip the initiation of apoptosis

(Danthi, 2011).

However, certain viruses have rather cleverly sought to turn the tables on their hosts and evolved strategies to both counteract and induce apoptosis in order to maximize the production of virus progeny and promote its spread to neighbouring cells. An increasing number of known viruses from different families, such as those from the adenoviridae, parvoviridae, papillomaviridae families, as well as some coronaviruses, have been found to induce apoptosis during their infection cycles, which may possibly contribute to the cytotoxicity associated with virus infections, especially during the late stages of infection (O'Brien, 1998). During apoptosis, membrane-bound cell fragments are produced which bulges off of the cell as apoptotic bodies to be swallowed up by surrounding cells via phagocytosis. This provides an excellent method for a virus to disperse its progeny without eliciting host immune response (Teodoro and Branton, 1997). Of related interest to this project, the avian coronavirus IBV has been shown to induce apoptosis in infected African green monkey Vero cells (Liu, Xu, and Liu, 2001).

1.1.5 Viral genes that regulate apoptosis

Several viral genes from different viruses have been found to manipulate to the induction of apoptosis to their benefit. In adenoviruses, for example, the pro-survival adenovirus Bcl-2 homologue, E1B 19K, inhibits apoptosis in adenovirus-infected cells by binding Bak to prevent its homo-oligomerization (Cuconati et al., 2002). The Hepatitis C virus (HCV) core protein interacts with another HCV non-structural NS5A protein and mediates the caspase-dependent cleavage of the latter as well as downstream apoptosis events (Goh et al., 2001). Tat, Nef and Vpu are three HIV viral proteins that are reported to be able to inhibit apoptosis in HIV-infected cells, while Env, Vpr, Vpu, and Tat function to induce apoptosis mainly in the uninfected cell

population during HIV infection (Ross, 2001). This dual function serves to increase the percentage of infected cells in the total cell population in the course of an infection so as to prolong virus replication and dissemination of virus progeny. The β-herpesvirus human cytomegalovirus (HCMV), too, has devised ways to thwart apoptosis during virus infection by encoding viral homologs of inhibitor proteins, such as the viral mitochondria-localized inhibitor of apoptosis (vMIA) – which binds and suppresses apoptotic activities of Bax – and a viral inhibitor of Bak oligomerization (vIBO) which, true to its name, impedes the homo-oligomerization of Bak (Cam et al., 2010; Poncet et al., 2006). In the case of coronaviruses, the unique SARS-CoV (Severe Acute Respiratory Syndrome coronavirus) encoded protein, 7b, and a 58-kDa mature cleavage product from the 1a/b polyprotein encoded by mRNA1 of the IBV are also discovered to have caspase-dependent, pro-apoptotic functions (Liu, Xu, and Liu, 2001; Tan et al., 2004).

1.1.6 Apoptosis and innate immunity

The maintenance of apoptosis is also important in the establishment and governance of immune responses in a cell. A loss in the control of apoptosis leads to an imbalance in cell homeostasis, which ultimately affects immune sensitivity (Opferman and Korsmeyer, 2003). The presence of apoptotic cells, particularly in existence with infectious agents, may also lead to the mobilization and initiation of innate immune defences (Lucas et al., 2003). This crosstalk between apoptosis and innate immunity is therefore of considerable importance during pathogenic infection and can be manipulated by both host and pathogen, either as a form of immune defence or immune evasion, respectively (Alcami and Koszinowski, 2000).

1.2 VIRUSES AND HOST INNATE IMMUNITY

1.2.1 Pathogen detection and host antiviral defence

When the host immune system is exposed to viral pathogens, it reacts straightaway by triggering a diverse array of defence mechanisms in order to establish a more efficacious shield. The first line of defence is the mounting of an innate immune response, characterized by the increased production of type I interferons (IFN-α and IFN–β) and other inflammatory cytokines. These, in turn, choreograph the expression of downstream IFN-stimulated genes (ISGs) and activate several signalling pathways, all of which collaboratively lead to the induction of a protective antiviral state and, subsequently, the inhibition of both viral replication and proliferation (Stetson and Medzhitov, 2006).

1.2.2 Interferons and the antiviral response

The cytokine family of interferons is dedicated to the conveyance of the presence of intracellular infection, as well as the expedition of numerous connections among the cells that provide protection against, or eradication of, foreign pathogens. Other than interfering with viral progeny production in host cells – hence the name 'interferon' – IFNs are also able to induce Natural Killer (NK) cells and macrophages to 'kill' or engulf infected cells, increase antigen presentation to thymus (T) cell lymphocytes for rapid recognition of infected cells and bring about virus resistance to new uninfected cells (Fensterl and Sen, 2009). IFNs are conventionally classified into three types: Type I (IFN-α, IFN-β and IFN-ω), Type II (IFN-γ) and the more recently identified Type III (IFN-λ1, IFN-λ2 and IFN-λ3) (de Veer et al., 2001; Zhou et al., 2007). Over time, mammalian hosts have gradually developed a multitude of cellular sensors for the detection viral infection, and it is the involvement and operation of these cellular protein receptors that eventually leads, through an intricate network of pathways, to the

expression of type 1 IFNs. Major receptor systems that conduct immune surveillance and trigger the production and subsequent release of type I IFNs are known as pattern recognition receptors (PPRs), which detect viral infection through the identification of pathogen-associated molecular patterns (PAMPs); PPR families include the toll-like receptor (TLR), RIG-like helicase (RLH) and Nucleotide-binding oligomerization domain (NOD)-like receptor (NLRs) families (Takeuchi and Akira, 2010).

1.2.3 Pattern recognition receptor families

The TLR family is mainly made up of transmembrane proteins, which conduct surveillance from the cell surface, endosome or ER, constantly scanning the extracellular environment for PAMPs that can be derived from a wide range of microorganisms, including viruses and bacteria. TLRs convert extracellular PAMP 'danger' signals into specific intracellular responses through the direct interaction of the TLR toll-interleukin 1 receptor (TIR) domain with one of its cytoplasmic TIR-containing signalling adaptor molecules, such as myeloid differentiation primary response protein 88 (MyD88) and TIR domain-containing adaptor-inducing IFNβ (TRIF) (Kumar, Kawai, and Akira, 2009). The eleven TLR molecules identified so far recognize specific PAMPs, and four of which appear to be essential in identifying viral molecular patterns: TLR3, as a general viral sensor, detects mainly through double stranded RNA (dsRNA), a replication intermediate of both DNA and RNA viruses; TLR7 and TLR8 have been identified to recognize RNA viruses like Human immunodeficiency virus (HIV); TLR9 detects DNA viruses such as herpesviruses (Kumar, Kawai, and Akira, 2009).

NLRs are stimulated by microbial agonists and collaborate with TLRs in evoking intracellular immune responses through mitogen activated protein kinase (MAPK) and caspase signalling cascades upon sensing bacterial components (Shaw et al., 2008).

The RLH family of purely cytoplasmic PRRs is made up of the following: retinoic acid inducible gene-I (RIG-I or DDX58), melanoma differentiation-associated gene-5 (MDA5 or IFIH1), and laboratory of genetics and physiology 2 (LGP2). RIG-I and MDA5 are PRRs with two N-terminal caspase-recruitment domains (CARDs) followed by a DExD/H box RNA helicase domain; LGP2 lacks the signalling caspase recruitment domains but shares a helicase domain of similar homology and is thought to serve as a regulator of the former (Yoneyama et al., 2005). RIG-I and MDA-5 both sense cytoplasmic dsRNA, which the host recognizes as 'non-self', via the N-terminal CARDs (Takeuchi and Akira, 2008). However, the different RNA viruses each recognizes differentiate the two PRRs. In addition to long dsRNAs (> 2kb) such as the synthetic dsRNA analogue poly-inosinic poly-cytidylic acid (poly(I:C)), MDA5 also recognizes picornaviruses. RIG-I, on the other hand, recognizes mostly short relatively short dsRNA (19-mer to 1 kb), or ssRNA (single stranded RNA) preferably with the presence of a 5'-triphosphate end, and responds to paramyxoviruses, flaviviruses, orthomyxoviruses and rhabdoviruses (Bowie and Fitzgerald, 2007; Takeuchi and Akira, 2010).

It is worthwhile to note that while the elicitation of TLRs and RLRs by PAMPs trigger their distinct signalling cascades through divergent downstream effectors at varying efficacies, they ultimately cross paths at the juncture of transcriptional activation of NFκB (nuclear factor kappa-light-chain-enhancer of activated B cells) and interferon regulatory factor 3 (IRF3), both of which lead to the downstream expression of IFN-α and -β genes that eventually culminates in the concerted induction and development of adaptive antiviral immune response.

1.2.4 The Toll-like receptor (TLR) signalling pathway – a brief overview

Upon viral sensing, the TIR domain of TLR3 associates with TRIF, turning on

both IkB kinase e (IKKe) and tank-binding kinase 1 (TBK1) and resulting in the phosphorylation of IRF3, which in turn undergoes dimerization and translocates to the nucleus to trigger IFN gene expression. TRIF also stimulates NFκB via the kinase complex IκB kinase (IKKa/b/g), which releases the former from its inhibitory IκBα (Inhibitor of κB), as well as induces activator protein 1 (AP1) by the MAPK cascade. The TIR domains of TLR-7, -8 and -9 associate with another adaptor protein, MyD88, which recruits the interleukin-1 receptor–associated kinases, IRAK1 and IRAK4, and the tumour necrosis factor receptor–associated factor 6 (TRAF6) to also bring about the activation of NFκB and AP1 through the IκB kinase complex and MAPK cascades, respectively. These transcription factors – IRF3, NFκB, and AP1 – work together to bring about the transcriptional regulation of IFN-α and -β genes for a coordinated inflammatory immune response (Kumar, Kawai, and Akira, 2009). MyD88 and TRAF6 also form a complex with IRF7 and trigger activation of the latter through the TRAF6 ubiquitin ligase activity; the trio of MyD88, TRAF6 and IRF7 then induce the expression of IFN-α (Kawai et al., 2004) (Fig 1-4).

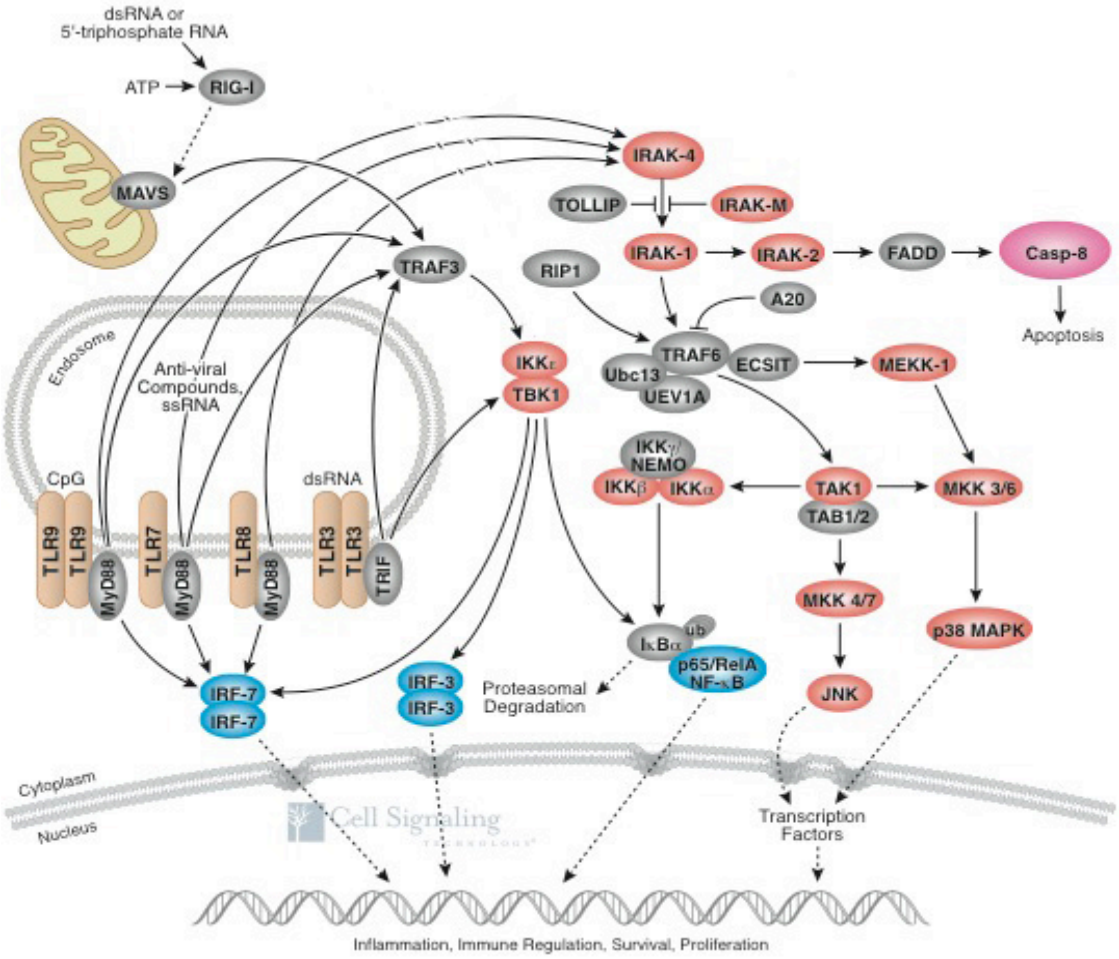

Figure 1-4

A simplified model of the Toll-like receptor(s) pathway, as adapted from Cell Signalling Technology references. Toll-like receptors TLR-3, -7, -8 and -9 are localized to the endosomal compartment. The TLR signalling pathway is activated when the TIR domain associates with its TIR domain-containing adaptor, MyD88. Upon specific ligand stimulation, MyD88 recruits IRAK4 to TLRs through the interaction of their respective death domains, following which phosphoactivated IRAK1 associates with TRAF6, leading MAP kinases and NF-κB activation. RIP1 is also able to undergo TRIF-dependent induction of TRAF6 signalling. MyD88-independent pathways serve to induce IRF3 phosphoactivation and IFN-β expression.

1.2.5 The RIG-I Like Helicase (RLH) signalling pathway – a brief overview

RIG-I and MDA5 signal through their caspase recruitment domains, which associate with a CARD-containing mitochondrial antiviral signalling adaptor (MAVS); the latter in turn binds TNF-receptor-associated factor (TRAF) 3, an E3 ubiquitin ligase which serves to recruit two IKK-related kinases, TBK1 and inducible IκB kinase (IKK-i), the induction of which then serve to phosphorylate and activate interferon regulatory factors IRF-3 and -7, and NFκB, respectively, prompting their translocation to the nucleus to trigger the expression of type I IFN genes by binding to IFN-stimulated response elements (ISREs), and inflammatory cytokines, respectively (Moore and Ting, 2008) (Fig. 1-5).

In addition to dsRNA, RIG-I is also able to sense dsDNA (Ablasser et al., 2009). Adenine-Thymine (AT)-rich dsDNA is converted to dsRNA by RNA polymerase III through the formation of a 5'-triphosphate RNA (3pRNA) intermediate that acts as a ligand for RIG-I signalling through the latter's C-terminal regulatory domain, activating downstream expression of NFκB and type I IFN genes. RIG-I is thus important in sensing Epstein-Barr virus (EBV) through this pathway (Ablasser et al., 2009).

While they share a high percentage of sequence homology, MDA5 and RIG-I each recognizes a differing subset of viruses. Table 1-1 summarizes the different viruses and their specific host PRR identified to date (Wilkins and Gale, 2010). Of note are the reoviruses, Dengue virus and West Nile virus, all of which can be recognized by both MDA5 and RIG-I (Loo et al., 2008).

Table 1-1 The specificity of RIG-I-like receptors in virus recognition. Receptors listed are classified according to the different classes of virus, as adapted from an immunological review of cytoplasmic PRRs (Wilkins and Gale, 2010).

Virus	Genome RNA	Host cytosolic PRR
Vesicular stomatitis virus	Non-segmented negative-sense, single strand	RIG-I
Respiratory syncytial virus	Non-segmented negative-sense, single strand	RIG-I
Influenza A virus	Eight RNA segments, negative-sense, single strand	RIG-I
Ebola virus	Non-segmented negative-sense, single strand	RIG-I
Reovirus	Ten double-stranded segments	RIG-I and MDA5
Hepatitis C virus	Non-segmented positive-sense, single strand	RIG-I
Dengue virus	Non-segmented positive-sense, single strand	RIG-I and MDA5
West Nile virus	Non-segmented positive-sense, single strand	RIG-I and MDA5
Polio virus	Non-segmented positive-sense, single strand	MDA5

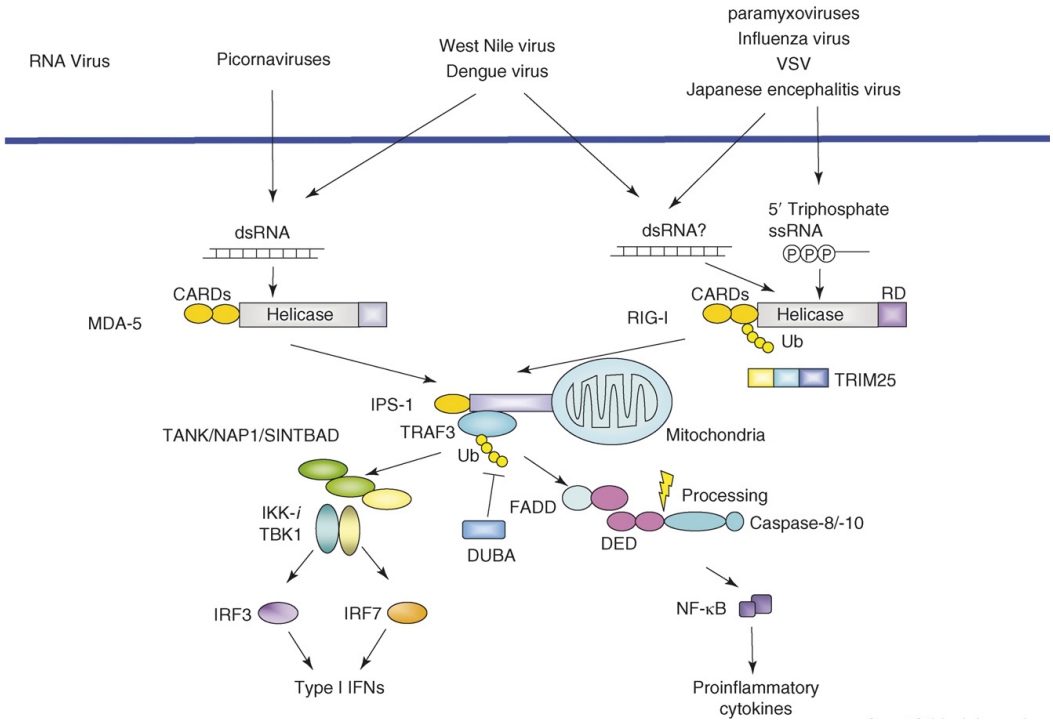

Figure 1-5

RIG-I/MDA5 and virus recognition, as modified from (Takeuchi and Akira, 2008). RIG-I and MDA5 recognize 5'-triphosphate RNA and dsRNA from RNA viruses, respectively, and interact with their downstream signalling adaptor MAVS. MAVS in turn binds TRAF3, which recruits TANK and TBK1/IKK-I for the phosphorylation of IRF-3 and IRF-7, the activation of which prompt their nuclear translocation to induce the expression of type I IFN genes. NFkB can also be activated by MAVS via a separate FADD and caspase-8/caspase-10-dependent pathway.

Reports on the functions of LGP2 have been varied and contradictory. Although a protein with high sequence homology to RIG-I and MDA5, the structure of LGP2 lacks a N-terminal CARD and has thus been proposed to be a negative regulator of RIG-I and MDA5 signalling (Rothenfusser et al., 2005). In line with this hypothesis, LGP2 has been shown to interact with MAVS, with the downstream RIG-I/MDA5 activating kinase IKK-i as a binding competitor, independently of viral infection and/or dsRNA stimulation (Komuro and Horvath, 2006). The hetero-oligomerization of LGP2 C-terminal region and the RIG-I repressor domain of the C-terminal region has also been observed (Saito et al., 2007), likely to prevent the homo-oligomerization of RIG-I for the activation of RIG-I downstream signalling components (Cui et al., 2008). The first sign of discrepancy regarding the functions of LGP2 was demonstrated in one study that simultaneously highlighted insignificant role LGP2 plays in the inhibition of type I IFN gene expression, and the sensitivity of LGP2-/- mice to encephalomyocarditis virus infection, which triggers MDA5-dependent signalling under wildtype circumstances (Venkataraman et al., 2007). On the other hand, in mice that are deficient in LGP2, type I IFN responses were gravely compromised when the knockout mice were challenged with viruses that are normally sensed by either MDA5 or RIG-I (Satoh et al., 2010). The authors of the aforementioned findings also proposed a mechanism in which LGP2 promotes RIG-I- and MDA5-mediated viral RNA sensing through its ATPase domain.

1.2.6 Type I interferon response

The expression and induction of interferons from the cells occurs in response to viral insults and tumour growth. Type I interferons, the major group of cytokines in innate anti-virus defence, bind a specific cell surface heteromeric receptor, the

interferon-α/β receptor (IFNAR), which composed of two subunits, IFNAR1 and IFNAR2 (Theofilopoulos et al., 2005). Type I IFNs can be classified into two groups, the immediate-early genes (such as IFNβ) that are triggered by the initial response to virus infection, and the delayed-set (such as IFNα subtypes) that rely on a secondary *de novo* protein synthesis pathway (Marie, Durbin, and Levy, 1998). The expression of IFNs is regulated by IFN regulatory factors. To date, 9 IRFs have been identified, all with a homologous DNA binding domain in the N-terminus (Mamane et al., 1999). In particular, IRF3 plays a major role in innate immune response through its antiviral response. IRF3 has been functionally characterized to consist of a nuclear export signal (NES), a DNA-binding domain (DBD), a C-terminal IRF association domain (IAD), as well as a number of phosphorylation sites as well as two auto-inhibitory domains that prevents a constitutive activation of the NES, DBD and IAD (Lin et al., 1999). Normally found in an inactive cytoplasmic form, IRF3 is phosphorylated as a consequence of virus infection. This activation signal exposes the DBD and IAD and results in the dimerization of IRF3, allowing the activated IRF3 to form a complex with the transcriptional co-activator cAMP-response element-binding protein (CREBP) to translocate to the nucleus and bind to DNA to trigger the transcription and expression of immediate-early IFNs, which signals the JAK-STAT (Janus kinase-Signal Transducer and Activator of Transcription) pathway through the binding of the IFNAR (Lin et al., 1999). In this pathway, type I IFNs trigger the phosphorylation activity of two JAKs, JAK1 and tyrosine kinase 2 (TYK2). These in turn stimulate the phosphorylation of STAT2 tyrosine, which subsequently recruits STAT1, establishing the formation of a STAT heterodimer. The STAT dimer then team up with the interferon regulatory DNA binding factor IRF9, which together constitute an activated heterotrimeric factor, the interferon-stimulated gene

transcription factor ISGF3, that, through the recognition and binding of specific ISREs, induces downstream expression of innate immunity genes for host defence against virus invasion (Aaronson and Horvath, 2002) (Fig. 1-6). ISGF3 also plays an important role in the up-regulation of IRF7 transcription, where the phosphorylation and consequent activation of the latter further leads to the induction of delayed-type IFNs (Lin et al., 1999).

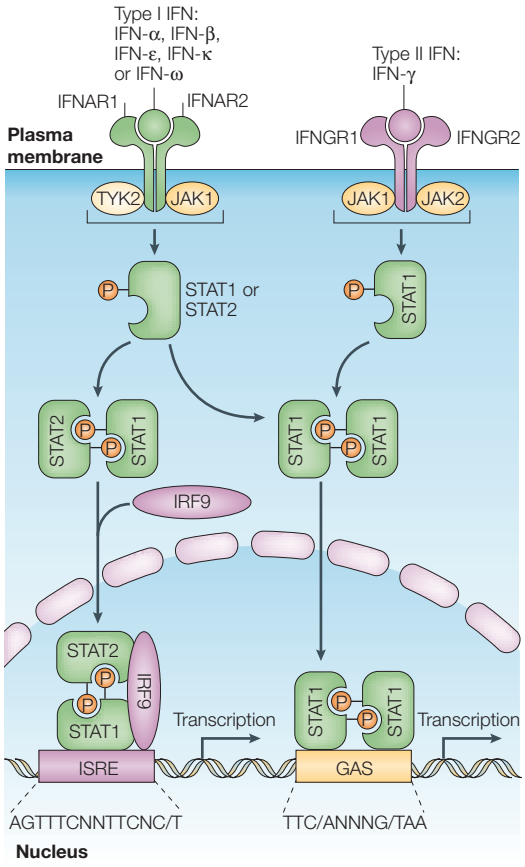

Figure 1-6

Interferon receptors and activation of classical JAK–STAT pathways by types I and II interferons, as adapted from (Platanias, 2005). Only type I interferon response is described here and in the text. All type I interferons bind the type I IFN receptor at the cell surface of human cells. The type I IFN receptor consists of two subunits, IFNAR1 and IFNAR2, which are associated with TYK2 and JAK1, respectively. JAK1 activation results in the phosphorylation of STAT1 and STAT2, and the latter two subsequently form ISGF3 complexes with IFN regulator factor IRF9. These complexes will translocate to the nucleus and bind ISREs in DNA to initiate gene transcription. Type I IFNs are also capable of inducing the formation of STAT1-STAT1 homodimers that translocate to the nucleus and bind GAS (IFNγ-activated site) elements that are present in the promoter region of some ISGs to initiate their transcription. The consensus GAS element and ISRE sequences are indicated. N, any nucleotide.

1.2.7 Interferon-Stimulated Genes (ISGs)

The IFN response activates JAK kinases to undergo auto-phosphorylation, as well as phosphorylation of the STAT family of transcription factors, inducing their homo- and hetero-dimerization as well as the formation of complexes with other transcription factors to trigger the expression of IFN-stimulated genes (ISGs) (de Veer et al., 2001). Over three hundred ISGs have been identified so far, all with varying functions and belonging to specific groups such as host defence (e.g. protein kinase receptor PKR) and signalling (MyD88 and TRADD, for example) (de Veer et al., 2001). Of interest are viral stress-inducible genes (vSIGs), especially those from the ISG56 gene family (ISG56/IFIT1, ISG54/IFIT2, ISG60/IFIT3, and ISG58/IFIT5; where IFIT is an acronym for interferon-induced protein with tetratricopeptide repeats), the expression of which are strongly induced by viruses, type I IFNs and dsRNA (Fensterl and Sen, 2011). These ISGs are involved in a variety of both cellular and viral related activities, including virus replication suppression and dsRNA signalling. Importantly, ISG56, an interferon stimulated gene whose transcription is regulated by transcription factors such as IRF3, has also recently been shown to be a negative-feedback regulator of type I IFN-mediated cellular antiviral response through the disruption of the association between MAVS and its adaptor protein MITA (mitochondrial mediator of IRF3 activation) as well as the association between TBK1 and MITA (Li et al., 2009). This helps to curb excessive production of type I IFNs, which may inadvertently cause more harm than good to the host cell.

1.2.8 Immune evasive strategies of viral proteins

Many viruses encode homologs of cellular immune regulators. For example, viral interferon regulatory factors (vIRFs) are that resemble cytokines and/or are able to participate in cytokine signalling pathways (Mamane et al., 1999). In the case of

Human herpesvirus-8 (HHV-8), otherwise known as Kaposi sarcoma–associated herpesvirus (KSHV), several viral proteins inhibit host innate antiviral immune response. These include vIRF1, vIRF2 and viral interleukin 6 or vIL-6, to name a few (Lagos et al., 2007). In particular, vIRF1 competes with host IRF1 and IRF3 for binding with their respective cellular transcriptional co-activators, thereby repressing downstream activation of IFN-induced signal transduction. Viruses can also block IFN-induced downstream responses by targeting the JAK-STAT pathway. Both adenoviruses and simian virus (SV5), for example, encode viral proteins that act to decrease STAT1 levels and/or target STAT1 for degradation in order to prolong the rate of virus replication (Alcami and Koszinowski, 2000). Poxviruses, on the other hand, have evolved to encode cytokine receptor homologs, which are compete with host receptors for the binding of IFNs and other cytokine ligands, thus preventing the onset of downstream signalling pathways (Ploegh, 1998). Coronaviruses, too, encode viral proteins that may possibly be involved in the evasion of host immune responses. SARS-CoV open reading frame ORF6 is known to prevent the nuclear import of STAT1, while the structural nucleocapsid N protein was able to hinder the activation of the NFκB promoter, thus possibility allowing the virus to escape from the clutches of the host innate immune system (Frieman, Heise, and Baric, 2008). The fact that viruses have developed various counterattacks to thwart the defence mechanisms of their hosts only serves to highlight the complexity of the relationship and interaction between viruses and their host. This is made all the more convoluted as viruses, especially large DNA viruses, tend to evolve together with their host and often rather shrewdly appropriate certain host immunomodulators and modify them to the virus' advantage.

1.2.9 The dual roles of mitochondria in antiviral signalling and virus-induced apoptosis

One of the most indispensible adaptor proteins in the RLH signalling pathway is MAVS. Otherwise known as virus-induced signalling adaptor (VISA), interferon β (IFNβ) promoter stimulator-1 (IPS-1) or CARD-adaptor inducing IFN-β (Cardif), it was discovered independently by four different research groups in 2005 (Kawai et al., 2005; Meylan et al., 2005; Seth et al., 2005; Xu et al., 2005), and contains a N-terminal CARD-like domain, which interacts with the CARD domains of RIG-I and MDA5, and a C-terminal transmembrane (TM) region that lodges the protein in the mitochondrial membrane, thus pioneering the connection between mitochondria and innate immunity. The mitochondrion, indisputably one of the most essential organelle in eukaryotic cells, possesses its own DNA (mitochondrial mtDNA) and a double membrane that is imperative to many functions, including the regulation of apoptosis and energy (adenosine triphosphate ATP) production through mitochondrial fusion and fission events (Hyde, Twig, and Shirihai, 2010). A deficiency in, or the cleavage of, MAVS from the mitochondrial membrane results in an arrested antiviral immune response, highlighting the pivotal role MAVS plays in mitochondria-mediated innate antiviral immunity (Kumar et al., 2006). The mitochondria has also been discovered be physiologically impertinent in MAVS-mediated antiviral signalling; the deletion of mitochondrial fusion mediators Mfn 1 and Mfn2 (mitochondrial outer membrane guanosine triphosphatase (GTPase) mitofusins), as well as a disruptive change in the mitochondrial membrane potential, both resulted in an inoperative innate immune signalling pathway (Koshiba et al., 2011). Moreover, while MAVS signalling has been routinely associated with the downstream activation of IFN type I gene expression, it has also been shown to concomitantly induce NFκB nuclear translocation via the

interaction of the two adaptor proteins TRADD and FADD, which cleaves and activates caspases-8 and -10 for the induction of NFκB and subsequent cytokine expression (Moore and Ting, 2008). As genes induced by NFκB are also involved in apoptosis and modulation of immune responses, this brings to light the pivotal roles the mitochondrion plays in both host innate immune response and virus-activated apoptosis. However, whether or not these two host responses to virus infection are linked in any way still remains to be seen.

1.2.10 Regulation of RLH proteins through apoptosis during virus infection

Recent studies have shown that, during virus infection, the major components of the RLH-signalling pathway, including MAVS, RIG-I and MDA5, are earmarked for inactivation by both viral and host counterparts in an attempt to assist in and prolong viral replication (Castanier et al., 2010; Komuro, Bamming, and Horvath, 2008; Matsumiya et al., 2011). MAVS, in particular, has been shown to undergo caspase-dependent cleavage by the HCV NS3/4A serine protease (Li et al., 2005), and targeted for cleavage by host proteases during poliovirus infection (Rebsamen et al., 2008). Other studies have also correlated the antiviral properties of MAVS with the onset of apoptosis during virus infection, thus highlighting the ability of viruses to effectively thwart the activation of MAVS-mediated host antiviral signalling pathways, at least during the early stages of infection (Lei et al., 2009). MDA5, too, has been shown to be a target for cleavage together with PARP cleavage – a stalwart hallmark of apoptosis – during poliovirus infection, thus prompting a link between MDA5 degradation and virus-induced apoptosis (Barral et al., 2007). However, while RIG-I is proteolytically degraded during the late stages of HCMV infection to allow persistent infection and abrogate innate immune responses, both RIG-I and MDA5 are prevented from cleavage by caspases via the viral apoptosis inhibitor protein vMIA to possibly

aid in viral survival during the early stages of infection (Scott, 2009). The ability of RIG-I and MDA5 to trigger IFN-independent apoptosis could also be a host antiviral response tactic to circumvent prolonged virus replication, especially in tumour cells or immunocompromised hosts (Besch et al., 2009). These widely divergent regulatory pathways thus reflect the differing strategies individual viruses may exploit in a bid for their survival and propagation.

1.3 CORONAVIRUS

1.3.1 Coronaviruses – an introduction

The *Coronaviridae* are a family of large, non-segmented, positive sense and single stranded RNA viruses, and consist of the following subfamilies: *Coronavirinae* and *Torovirinae* (Cavanagh et al., 1993). They are grouped in the order *Nidovirales*, which in Latin ('nidus') means 'nest', which also contains the families *Arteriviridae* and *Roniviridae* (Gonzalez et al., 2003), as all viruses in this order produce a extensive 3'-nested set of subgenomic mRNAs for transcription during infection (Cavanagh, 1997). The name "coronavirus" is derived from the Latin word 'corona', which means crown. Coronaviruses, as befit their name, are visible under electron microscopy as enveloped, spherical structures of around 110nm in diameter, with protrusions formed by viral 'spike' proteins that determine the infectivity of potential host cells (Casais et al., 2003) (Fig. 1-7). Some viruses, specifically those from the betacoronavirus group of the family of coronaviruses and toroviruses, also form shorter projections on the surface of the virus by way of the hemagglutinin-esterase (HE) protein (de Groot, 2006).

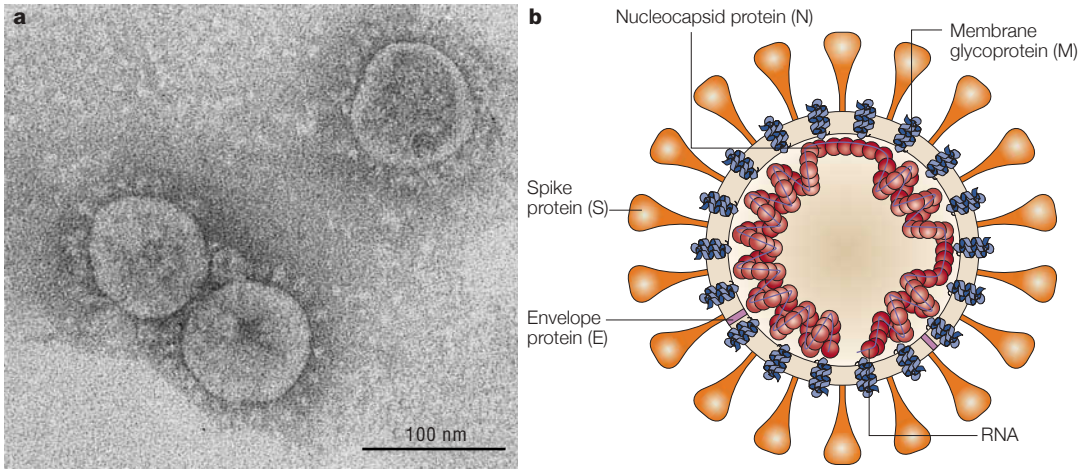

Figure 1-7

Coronavirus morphology, as adapted from (Stadler et al., 2003).

(A) Electron micrograph of coronavirus cultivated in Vero cells.

(B) Schematic representation of the coronavirus. A lipid bilayer comprising the spike (S) protein, the membrane (M) glycoprotein and the envelope (E) protein encloses the helical nucleocapsid, which comprises the nucleocapsid (N) protein associated with the viral RNA.

As important pathogens of both human and animals (Cavanagh, 2005), coronaviruses are commonly associated with mild respiratory and enteric diseases, although they are also known to cause more critical lower respiratory tract illness, such as the severe acute respiratory syndrome coronavirus (SARS-CoV) epidemic that occurred in 2003 (Peiris, Guan, and Yuen, 2004). The pathogenicity of coronaviruses is typically species-dependent, as is the severity of infection; they infect mainly their natural hosts and/or species that are closely related. Certain coronavirus infections can cross the species barrier, the prime example being the zoonotic SARs-CoV, that is thought to have originated from bats before it adapted to its intermediate host, civet cats, and finally to humans (Wang and Eaton, 2007). Coronavirus infections are also tissue-specific – the Transmissible Gastroenteritis Coronavirus (TGEV), for example, affects mainly the gastrointestinal tract (Laude et al., 1990) while human coronaviruses mostly cause respiratory infections (Wevers and van der Hoek, 2009).

1.3.2 The coronavirus genome

Coronaviruses have large genomes – between 27 and 32kb – that are capped at the 5'-terminus and polyadenylated at the 3'end. The classic gene order in all coronaviruses is a very large gene (gene 1) of around 21kb at the 5' end which constitutes slightly more than two-thirds of the whole genome and encodes the replicase, and four structural proteins clustered at the 3' distal end that follows sequentially: the Spike (S) protein, the envelope (E) protein, membrane (M) protein and the nucleocapsid (N) protein (Lai, 1990) (Fig. 1-8). The order of the HE gene, if any, typically falls between the replicase and the S gene (de Groot, 2006). Interspersed among the structural proteins are assorted accessory and non-structural proteins. These will be discussed in more detail in later paragraphs. Only the replicase polyprotein stems from the genome; all other downstream ORFs are derived from subgenomic

mRNAs (Brian and Baric, 2005). The genome also acts as a template for replication and transcription, and is involved in virion assembly as well, assisting in the assimilation of progeny genomes into progeny virions.

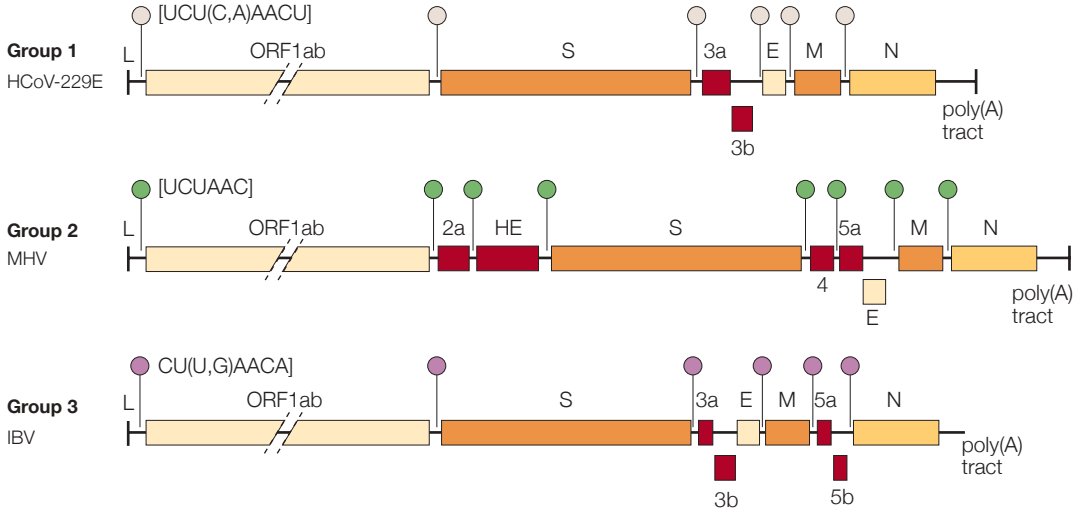

Figure 1-8

Coronavirus genome organization, as adapted from (Stadler et al., 2003). Genome organization of coronavirus representatives of group 1, or alphacoronaviruses, (human coronavirus 229E, HCoV-229E), group 2, or betacoronaviruses, (mouse hepatitis virus, MHV) and group 3, or gammacoronaviruses (avian infectious bronchitis virus, IBV). The positions of the leader sequence (L) and poly(A) tract are also indicated. Circles of different colour at specific positions on the individual genomes represent group-specific transcription-regulatory sequences (TRS).

1.3.3 The gene 1 polyprotein

The virion RNA serves as a messenger RNA (mRNA) and, being a positive sense strand RNA, is infectious on its own. It first acts as an mRNA that translates the gene 1, a single large gene that contains two protein-coding sequences with overlapping open reading frames (ORFs), 1a and 1b, into two large polyproteins pp1a (around 500kDa) and pp1ab of around 800kDa, the expressions of which are executed via a mechanism known as ribosomal frame shifting. Characteristics of the ribosomal slippage signal include a psuedoknot structure and a 7-nucleotide long 'slippery' sequence of UUUAAAC at the region where the two ORFs overlap (Ziebuhr, 2006). Although pp1a and pp1ab are predicted to be large translation products of around 500-800kDa, proteins of these sizes have not been detected in coronavirus-infected cells. This is probably due to the fact the polyproteins undergo co-translational polyprotein processing, via functional internal protease domains, and are cut into 15-16 polypeptides that synthesize viral RNA for the replication and transcription of the genome (Liu et al., 1998). These processed polypeptides will be discussed further in later paragraphs.

Depending on the group of coronaviruses, there are, in sequential order, typically two papain-like cysteine protease (PL^{pro}) domains in between an X domain that in conserved in IBV and MHV, a picornavirus-3C-like protease domain ($3CL^{pro}$) flanked by a membrane associated domain (MD) on either side, and a cysteine-rich growth factor-related protein (GFL) domain in ORF1a. In the ORF1b, the functional domains have been identified as follows: the RNA-dependent RNA polymerase (pol), a zinc finger nucleic acid metal-binding motif (MB) and a nucleoside triphosphate (NTP)-binding helicase (hel). The functional domains located within ORF1b are connected with mRNA synthesis, while the PL^{pro} domains in ORF1a are autocatalytic

proteases that cleave the ORF1a polyprotein from the N-terminus, and the $3CL^{pro}$ has autocatalytic proteolytic activity for the cleavage of certain downstream sites in both ORF1a and 1b to facilitate negative strand RNA synthesis (Lai, 1990; Liu et al., 1998).

1.3.4 Coronavirus structural proteins

The following is a brief overview of the four main structural proteins of coronavirus.

1.3.4.1 Spike (S) protein

The S protein is an extensively N-linked glycosylated type I glycoprotein of about 150kDa (kilo Dalton) in size that is a protein component of the viral envelope of coronaviruses that is responsible for cell entry through virus-cell fusion (Brian and Baric, 2005). It has an N-terminal ectodomain, a transmembrane domain and a short carboxy (C)-terminal endodomain in the virus interior. The S protein forms homodimers and homotrimers, which account for the bulbous projections on the spherical virus structure seen under electron microscopy. The binding of S protein to a host cell receptor initiates a fusion event between the virion envelope and a host cell membrane, either plasma or endosomal, resulting in the entry of the virion and subsequent internalization of the nucleocapsid into the cytoplasm. In some cases, it is also able to extend across the plasma membrane of infected cells to initiate the fusion of adjacent cells for the formation of a syncytium (Yamada et al., 2009). Moreover, the S protein is the primary viral antigen, and host antibodies against S are neutralizing.

1.3.4.2 Envelope (E) protein

The E protein is a minuscule polypeptide of only around 8-10kDa. While small in size, it is rather important in stature as it is an integral membrane protein that interacts with M protein to facilitate viral budding by designating the site of budding through its carboxy-terminal end – budding sites can either be the endoplasmic

reticulum Golgi intermediate compartment (ERGIC), or the Golgi (Lai, 1990).

1.3.4.3 Membrane (M) protein

The 25kDa M protein is the main component of the virion envelope and the most abundant constituent of coronaviruses. Contrary to S protein, most of M is embedded within the interior of the virus; the amino-terminal ectodomain is very short while the carboxy-terminal endodomain is large and interacts with the viral nucleocapsid to aid in its attachment to the membranes of internal structures such as the Golgi apparatus (Masters, 2006). M protein also possesses three transmembrane domains, of which the last one is most important for the insertion and anchoring of M protein in intracellular membranes. M protein also plays the decisive factor in the establishment of virion morphogenesis, recruiting S protein as well as singling out N protein for assimilation into the virion during assembly (Arndt, Larson, and Hogue, 2010).

1.3.4.4 Nucleocapsid (N) protein

The N protein is the protein component of the helical nucleocapsid in the virus interior and is between 43 and 50 kDa in size. N protein functions to bind viral RNA through its N-terminal leader sequence and central region, a two-domain region (domains 1 and 2) that is highly basic (arginine- and lysine-rich) to facilitate RNA-binding (Schelle et al., 2006). The C-terminus of N, with more acidic than basic residues, has an overall negative charge that allows binding to the M protein during virion assembly. N is also a phosphoprotein. However, the function of N protein phosphorylation remains undetermined. Phosphorylation may have regulatory significance through the promotion of N protein interaction with intracellular membranes, and also allow N to boost the translation of certain virus mRNAs during infection (Schelle et al., 2005).

1.3.4.5 Hemagglutinin esterase (HE) accessory protein

The aforementioned HE gene that is present only in betacoronaviruses is not found in any other coronavirus group. The gene encodes HE glycoprotein, an accessory protein, which, together with S protein, can be found on the surface of certain betacoronaviruses and contributes to the crown-like morphology of the virus. The HE protein of betacoronaviruses is related to the hemagglutinin, esterase, and fusion (HEF) glycoprotein of influenza C virus; the two share approximately 29% amino acid homology. It has been proposed that the HE gene was acquired by horizontal transfer from an ancestral influenza C virus, as a result of recombination between the two viruses (Zhang, Kousoulas, and Storz, 1992).

1.3.5 Coronavirus replicase non-structural proteins

As mentioned earlier, translation of the replicase gene through ribosomal frame shifting results in the production of two polyproteins pp1a and pp1ab. These are in turn processed by their own internal proteases, which then auto-proteolytically cleave the polyproteins to give rise to 15-16 non-structural proteins (nsps). The pp1a gives rise to 11 nsps, numbered 1-11, while pp1ab produces 15, from 1-10 and 12-16 (Ziebuhr, 2006). The nsps, with the exception of nsp11, that are derived from pp1a is therefore identical to those from pp1ab and appear to facilitate cell infection by assembly the necessary components required for RNA synthesis. The nsp products derived from pp1ab, on the other hand, are required in expediting the de facto control of RNA replication and transcription (Harcourt et al., 2004). Nsp11 is unique in that it is generated when ribosomal frame shifting fails to occur. The location and the number of nsps present depend on the coronavirus group.

For example, avian IBV and turkey coronavirus, both gammacoronaviruses from the family of coronaviruses, has only 15nsps and lacks nsp1 (Cao, Wu, and Lin, 2008).

They are numbered 2-15 for conformity to the other coronaviruses.

Progress has been made in recent years in the crystallization of either the full structures or main domains of several non-structural proteins, which may be correlated with their relative functions. The elucidation of crystal structures, together with the recent development in reverse genetics systems, has been imperative in the demystification of the responsibilities of different nsps: nsp1, the first translational product derived from most coronaviruses, has been shown to have a role in cell cycle arrest, presumably to prepare a more conducive cellular environment for infection and subsequent viral RNA replication (Brockway and Denison, 2005; Eckerle et al., 2006); nsp3 has an ADP-ribose-1"-monophosphatase domain that has been hypothesized to be superfluously involved in viral RNA replication (Putics et al., 2005), in addition to the proteolytic abilities of $PL1^{pro}$ and/or $PL2^{pro}$ it encode; the dimeric main $3CL^{pro}$ (or M^{pro}) is composed entirely of nsp5 and is able to undergo considerable pH-dependent conformational changes in regulation of its proteolytic activity (Harcourt et al., 2004); nsp3, nsp4 and nsp6 all encompass transmembrane domains that assist in securing the replicase complex to intracellular membranes (Oostra et al., 2008); nsp7-nsp8 is a hexadecameric complex that is comprised of 8 monomers of each nsp and has been proposed to confer processivity to the RNA polymerase (Zhai et al., 2005); nsp9 contains an RNA-binding protein domain in that is likely involved in RNA synthesis (Egloff et al., 2004; Sutton et al., 2004). Nsp12-nsp16 are products of pp1ab that are actively involved in viral RNA replication and transcription; nsp12 contains the indispensible coronavirus RNA-dependent RNA polymerase (RdRp) and also consists of a coronavirus-specific amino-terminal domain that has the ability to interact with intracellular membranes as well as other nsps; nsp13 contains the superfamily 1 RNA helicase with RNA-dependent NTPase and dNTPase activities, which allows the

unwinding of both DNA and RNA with a 5'-3' polarity for processing in the RdRp while supplying the necessary energy required for its movement along the RNA templates (Ivanov et al., 2004b; Ivanov and Ziebuhr, 2004); nsp14, nsp15, and nsp16 have been either postulated or established to confer 3'-5' exonuclease (ExoN), endoribonuclease (NendoU), and 2'-O-ribose methyltransferase activities, respectively (Bhardwaj, Guarino, and Kao, 2004; Decroly et al., 2008; Eckerle et al., 2006; Ivanov et al., 2004a).

Not much is known about the functions of the other non-structural proteins, as they are presumed to be mostly non-essential and do not play a part in pathogenesis. A brief description of the coronavirus non-structural proteins and their known functions is summarized in Table 1-2.

1.3.6 Coronavirus replication cycle

Coronavirus genome replication occurs exclusively in the cytoplasm and commences with the binding of virus to specific receptors on the cellular membrane of target cells. Once the virus attaches to its receptor, S protein then effectuates the fusion of the viral envelope with the cellular membrane – either plasma or endosomal – through conformational changes, thereby allowing the virus to insinuate itself through the cell surface and into the interior of the cell (Masters, 2006).

Table 1-2 A summary of coronavirus non-structural proteins and their known functions.

Protein	Functions
Nsp1	Host mRNA degradation; translation inhibition; cell cycle arrest; IFN signalling inhibition
Nsp2	Unknown
Nsp3	Papain-like proteases ($PL1^{pro}$, $PL2^{pro}$) in polyprotein processing; poly(ADP-ribose) binding; IFN antagonist; nucleic acid binding; deubiquitinating activity; double membrane vesicle formation (putative)
Nsp4	Double membrane vesicle formation (putative)
Nsp5	Main protease (M^{pro}, $3CL^{pro}$) in polyprotein processing
Nsp6	Double membrane vesicle formation (putative)
Nsp7	Single-stranded RNA binding
Nsp8	Primase
Nsp9	Replicase complex component
Nsp10	Replicase complex component
Nsp11	Unknown
Nsp12	RNA-dependent RNA polymerase
Nsp13	Helicase; nucleoside triphosphatase activity; RNA 5'-triphosphate activity
Nsp14	3'→5' exoribonuclease; RNA cap formation (guanine-N7)-methyltransferase
Nsp15	Endonuclease
Nsp16	RNA cap formation (2'-*O*-methyltransferase)

Virus penetration is followed by its uncoating, after which the nucleocapsid and, subsequently, genomic viral RNA is deposited into the cytoplasm and serves as a template for the primary translation and consequent processing of the gene 1 polyprotein (Lai and Cavanagh, 1997). Similar to eukaryotic host RNAs, the viral RNA also has a 5'-methylated cap and a 3'-polyadenylated end, and this resemblance to its host RNA allows its attachment to host ribosomes for translation, resulting in the construction of the large replicase polyprotein, on which many non-structural proteins are attached (Brian and Baric, 2005). One of them, an autocatalytic proteinase, is able to process the polyprotein and detach the individual proteins, which collectively function to facilitate RNA synthesis and transcription (Ziebuhr, Snijder, and Gorbalenya, 2000). As such, the virus is able to economize by encoding the maximum number of genes in a minimal amount of nucleotides. The RNA-dependent RNA polymerase derived from the replicase recognizes the 3'-distal end of the genome, and produces a full-length negative-strand copy of the genome. Using this negative strand copy to serve as a template, viral RNA replication and mRNA transcription then follow suit, synthesizing both progeny genomic RNA and subgenomic mRNAs by the polymerase; the latter are transcribed in multiple steps and which are then subsequently translated into structural and accessory proteins (Shi and Lai, 2005). A simplified model depicting the general life cycle of a coronavirus is shown in Figure 1-9.

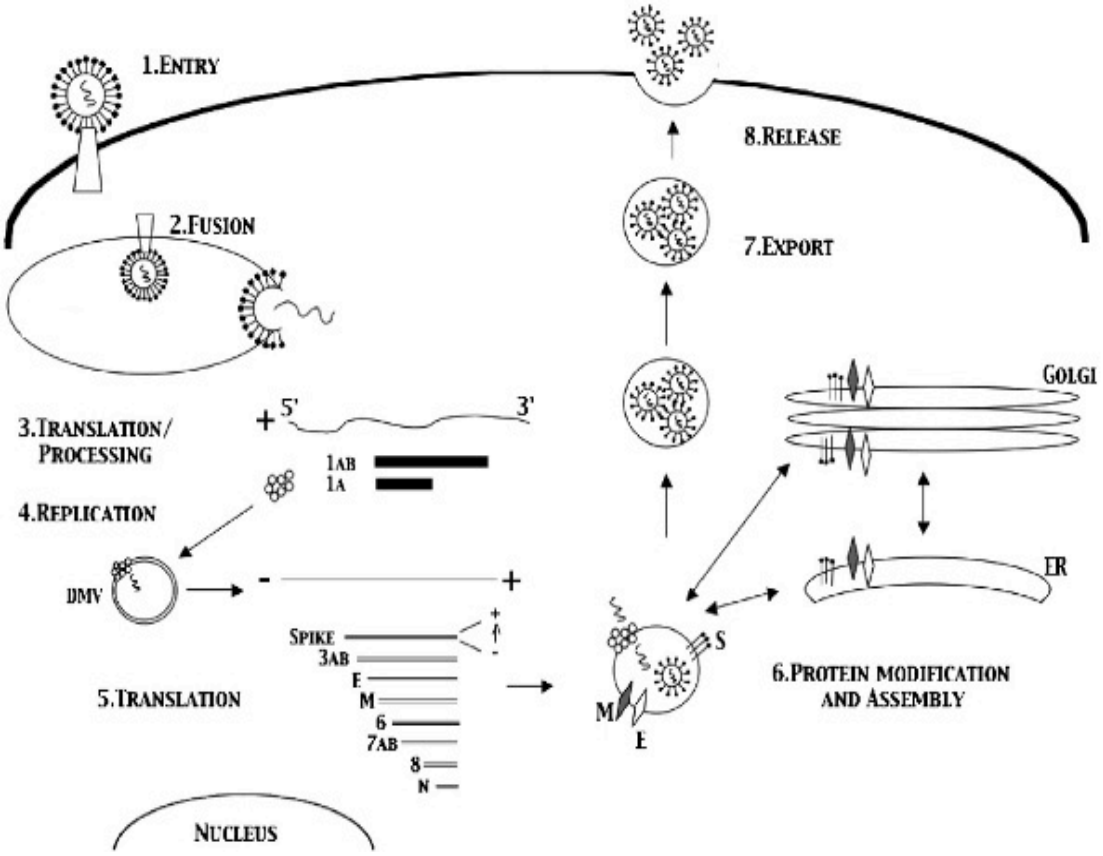

Figure 1-9

Life cycle of coronaviruses, as adapted from (Frieman, Heise, and Baric, 2008). Coronavirus entry into the cell through membrane fusion is mediated by binding of the spike protein, followed by the subsequent activation of a fusion peptide in its S2 domain that mediates entry through cellular endocytic compartments. Following fusion with the endosomal compartment, the viral RNA genome is released into the cytoplasm, where replication takes place. ORF1a/1b is first translated by host translation machinery, through a ribosomal frame-shifting mechanism, to produce a single polyprotein. This polyprotein is then cleaved by virally encoded proteases into the individual proteins necessary for replication. Subgenomic RNA synthesis occurs from a discontinuous transcription strategy adopted by the virus, which joins leader

RNA sequences encoded at the 5'-end of the genome to the body sequences of each subgenomic RNA to produce a nested set of subgenomic mRNAs. These different subgenomic negative strands thus act as templates for the synthesis of their respective subgenomic mRNA counterparts, which are then translated into viral proteins for the localization to their relevant compartments. N protein and genomic RNA first assemble in the cytoplasm to form the helical nucleocapsid. This core structure acquires its envelope by budding through intracellular membranes between the ER and the Golgi apparatus. The M, E and S proteins are transported through the ER to the budding compartment for the assembly of progeny virions in vesicles. The vesicles are then exported to the host cell surface where fusion of virion-containing vesicles with the plasma membrane occurs before their release into the exterior environment.

1.3.7 The discontinuous model of mRNA synthesis

Subgenomic mRNAs form a 3' nested set, and all of them share a common leader sequence of between 70 and 100 nucleotides at the 5'-end, which is fused to various downstream internal sites of genomic RNA to form the main segment, or 'body', of the subgenomic RNA, each of which is identical to the 3'-distal end of the genome (van Vliet et al., 2002). The common leader sequence is also found at the 5'-end of the genomic RNA. While the process of coronavirus RNA synthesis is complex and not yet completely decipherable, the general consensus supports the discontinuous model of mRNA synthesis during coronavirus mRNA transcription – a template switch mechanism that joins the internal sequence to the 5' leader sequence – that occurs during the negative strand synthesis of the subgenomic mRNAs, which uses the genomic RNA as a template (Sawicki, Sawicki, and Siddell, 2007). Each of the resultant subgenomic RNAs (sgRNAs) serves as a message for translation of one of the downstream genes for the production of all other proteins, such as the various viral structural proteins. Transcription of negative strand sgRNAs is initiated at their 3'-distal end, which is homologous to that of the genomic RNA template (Sawicki and Sawicki, 1995). The minimal 3'-terminus required for replication signalling includes a variable part of the N gene – which differs from virus to virus – as well as the complete 3'UTR (untranslated region), which spans 301 nucleotides and includes a conserved motif, 5'-GGAAGAGC-3' (Goebel et al., 2004). The site of fusion between leader and body is a consensus motif, conserved within each coronavirus group, which is more or less homologous to the 3'-end of the leader sequence; these are known as transcription-regulating sequences (TRSs) or intergenic sequences (IGSs). The sequences of the core consensus TRS are as follows: 5'-AACUAAAC-3' for alphacoronaviruses; 5'-AAUCUAAAC-3' for betacoronaviruses with the exception of

SARS-CoV, which has the sequence ‘5-AAACGAAC-3’; and 5’-CUUAACAA-3’ for gammacoronaviruses (Zuniga et al., 2004). Elongation of the negative-strand sgRNA, via the viral polymerase, is initiated at the 3’end of the genomic RNA template, and proceeds along the body of the negative sense strand until an internal TRS is reached, which triggers a template-switching event, re-initiating synthesis at its corresponding TRS copy at the 3’end of the genomic RNA template leader sequence (Zuniga et al., 2004). The resultant negative strand sgRNA then complexes with the positive genomic RNA, and this functions as a template for the subsequent synthesis of its positive strand subgenomic counterpart.

Both viral and cellular proteins are required for viral RNA replication and transcription (Enjuanes et al., 2006). Known cellular host factors involved in coronavirus RNA synthesis include the heterogeneous nuclear ribonucleoprotein A1 (hnRNPA1) (Shi and Lai, 2005), while the viral structural N protein is required for viral RNA synthesis (Hurst et al., 2010), and has been discovered to possess RNA chaperone activity that may possibly play a role during template switch (Enjuanes et al., 2006; Mir and Panganiban, 2006). The structural proteins M, E and S are incorporated into the ER en route to the ERGIC. Meanwhile, encapsidation follows suit after the synthesis of viral RNA, where N protein binds to the newly produced progeny viral RNA to form a long, flexible helical nucleocapsid (Escors, Capiscol, and Enjuanes, 2004). N binds to the cytoplasmic portion of M protein that is fused with the ER membrane as well, under the direction of packaging signals that direct the eventual incorporation of the nucleocapsid into virion progeny (Hurst, Koetzner, and Masters, 2009). Once bound to M, the newly packaged nucleocapsid virus core enters the ER lumen and become encircled within its membrane, which are already interspersed with membrane bound structural proteins, for the assembly of virion progeny that buds into

the ERGIC (Snijder et al., 2006).

1.3.8 Virion assembly and the spread of virion progeny

Contrary to other RNA viruses, coronavirus does not include the RNA polymerase when assembling progeny virion particles; instead, the polymerase is produced only after the infection of a target host cell, via the usage of its positive sense genomic RNA as a messenger RNA template (Brockway et al., 2003). The newly assembled virion progeny are transported by smooth-walled golgi vesicles to the surface of the plasma membrane and released by exocytosis into the extracellular space (Cohen, Lin, and Machamer, 2011). This thus has an exponential effect: one virus enters an uninfected cell, while more than a thousand progeny can leave the cell after infection.

The S protein of some coronaviruses, such as IBV, can mediate the fusion of an infected cell with its adjacent uninfected neighbours to stimulate the formation of sizable syncytia with containing several nuclei (Yamada et al., 2009). This facilitates the extension of infection to neighbouring cells without mobilizing extracellular virus, thus allowing the evasion of host antiviral immune responses.

1.3.9 Recombination and mutation

One unique factor with regards to coronavirus RNA synthesis is the incidence of RNA-RNA recombination, which has a high rate of occurrence that is atypical of non-segmented RNA viruses. This may be due in part to the discontinuous model of RNA replication through a template-switching mechanism where RNA polymerase will copy one template (to make the 5' leader sequence) then 'jump' to another strand by detaching itself from the original template, while still attached to the emerging nascent RNA strand that is being made, and reattaching itself to the same relative position on the new template to resume synthesis, thus generating RNA recombinants

with deletion mutations. This results in the expeditious evolution of the virus, as well as the emergence of new viral strains (Han et al., 2011).

The substantial size of the coronavirus genome, coupled with the absence of proof-reading proficiency in their RNA polymerases, also leads to an extensive mutation frequency in coronaviruses. As the coronavirus RNA genome is replicated using a coronavirus-encoded polymerase, and RNA polymerases have a high error rate of 1 in 10,000 nucleotides, a number of mutations can occur in each virion progeny as the large genome allows more room for error (Holmes and Rambaut, 2004).

1.3.10 The manipulation of coronaviruses through reverse genetics

As the genomic positive sense RNA is, on its own, infectious, an infectious clone can be made with a full-length cDNA copy of the genome cloned into a suitable transcription vector. However, this posed some difficulties in coronaviruses owing to the large sizes of their genomes and the presence of relatively unstable regions in the replicase. Another method of reverse genetic system for coronaviruses is through the manipulation of the high frequency of RNA recombination during coronavirus RNA synthesis. A synthetic RNA with a mutation of interest is introduced into cells infected with a parent virus that contains certain attributes that can be selected against, for example, a thermolabile mutant that arose due to an internal deletion in the N gene (Masters and Rottier, 2005). Mutant recombinants are then recovered by way of a heat-killing selection in which they are survivors. However, this method can only be used to characterize structural protein genes of MHV coronavirus, and those of other coronaviruses as well, as only the last one-third of the genome from the 3' distal terminal can be constructed. A slightly different method was devised to construct the replicase together with the structural proteins. To do this, full-length infectious clone systems were constructed by *in vitro* ligation of at least five smaller – and therefore

more stable – subclones of cDNA fragments of the full length genome (Pasternak, Spaan, and Snijder, 2006; Yount, Curtis, and Baric, 2000). Infectious RNA can then be obtained from the ligated product through *in vitro* transcription. Through this method, the porcine TGEV, the 229E, MHV, and infectious bronchitis virus have all been made, and many have employed this system to create mutant viruses through site-directed mutagenesis to elucidate and characterize viral RNA replicase (Casais et al., 2001; Thiel and Siddell, 2005). These methods also have implications on vaccine development and the construction of gene delivery vectors.

1.3.11 Coronavirus taxonomy

While all coronaviruses belong to the genus *Coronavirus*, which is itself within the family of *Coronaviridae*, different species of coronaviruses can be classified into three different groups based on antigenic relationships and gene/protein sequence comparisons (Figure 1-10; Table 1-3). Of note is the classification of SARS-CoV, which was first deemed to be the pioneer member in a new fourth group due to the phylogenetic comparison of its full length genome sequence but was later surmised to be more closely related to betacoronaviruses based on recently constructed phylogeny of its gene 1b instead (Snijder et al., 2003). Two other novel human coronaviruses, HCoV-NL63 and HCoV-HKU1, were also characterized in the wake of the SARS epidemic, and were classified under alpha- and beta-coronaviruses, respectively.

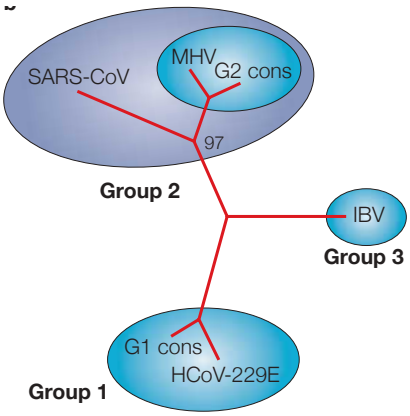

Figure 1-10

Phylogenetic analysis of coronaviruses, as adapted from (Stadler et al., 2003). Phylogenetic tree is obtained using the sequences of the S1 domain of the spike protein. The multiple sequence alignment was constructed using consensus sequences generated from group 1, or alphacoronaviruses, and group 2, or betacoronaviruses, the sequence of IBV (group 3) and of SARS-CoV. The neighbour-joining algorithm was used to build the tree. Numbers represent the result of a bootstrap analysis performed with 100 replicates.

Table 1-3 Coronavirus species and groups, as adapted from (Masters, 2006).

Group	Designation	Species	Host
alpha	TGEV	Transmissible gastroenteritis virus	Pig
	PRCoV	Porcine respiratory coronavirus	Pig
	FIPV	Feline infectious peritonitis virus	Cat
	Bat-CoV-61	Bat coronavirus strain 61	Bat
	HCoV-229E	Human coronavirus strain 229E	Human
	HCov-NL63	Human coronavirus strain NL63	Human
beta	MHV	Mouse hepatitis virus	Mouse
	BCoV	Bovine coronavirus	Cow
	RCoV	Rat coronavirus	Rat
	ECoV	Equine coronavirus	Horse
	SARS-CoV	Severe acute respiratory syndrome coronavirus	Human
	HCoV-HKU1	Human coronavirus strain HKU1	Human
	Bat-SARS-CoV	Bat SARS coronavirus	Bat
gamma	IBV	Infectious bronchitis virus	Chicken
	TCoV	Turkey coronavirus	Turkey
	PhCoV	Pheasant coronavirus	Pheasant
	DCoV	Duck coronavirus	Mallard
	GCoV	Goose coronavirus	Goose

1.3.12 Infectious Bronchitis Virus – an introduction

Avian infectious bronchitis virus was the first coronavirus to be identified; it was isolated from domestic chicken fowl and subsequently propagated back in the 1930s. IBV is the etiological agent of infectious bronchitis, an acute disease that renders the respiratory and urogenital tracts of chicken irreparable, which might eventually lead to inflammation of the kidneys (nephritis), respectively (King and Cavanagh, 1991; Picault et al., 1986). While it extensively destroys the mucosae of the respiratory tract, the impact of IBV infection is greatly magnified as a consequence of its enhancement of diseases associated with fatal co-infections by bacteria and mycoplasmas (Landman and Feberwee, 2004; Matthijs et al., 2003).

Despite its name, IBV can also replicate at many epithelial surfaces, including much of the alimentary canal, as well as kidney, gonads and bursa (Cavanagh, 2003). The capacity of the virus to replicate in so many tissues possibly contributes to the sequence diversity of its proteins, especially that of the spike protein (Ignjatovic and Sapats, 2000). Distinct strains of IBV differ in their virulence, and the genetic background of the host can influence the outcome of infection (Bacon et al., 2004).

Although IBV is an avian virus, it is reported to adapt well to primate cells and has also been shown to overcome the host species barrier and become zoonotic, infecting both human and animal cells (Fang et al., 2005; Shen, Wen, and Liu, 2003).

IBV undergoes a cytolytic life cycle after it adapts to a cell culture system (such as Vero cells) and results in typical cytopathic effects (CPE). A hallmark of IBV infection of cultured cells is the formation of multi-nucleated syncytia, which spread rapidly from a virus-infected cell to its surrounding cells (Fig. 1-11). The syncytium is progressively destroyed, and the cells round up and detach from the substratum,

concomitant with the secretion of virions, ultimately leading to cell lysis and death (Liu, Xu, and Liu, 2001).

IBV infection and the consequent host cell response involve complicated interaction between host cellular and viral networks. Previous studies on the infection of different hosts by IBV have shown various modifications in the immune and stress responses, cell cycle, cytoskeleton, autophagy and apoptotic pathways of the former (Cavanagh, 2007; Cottam et al., 2011; Emmott et al., 2010).

More specifically, IBV induces the p38 mitogen-activated protein kinase (MAPK) signalling pathway, which in turn up-regulates production of pro-inflammatory cytokines, interleukin (IL)-6 and IL-8, in infected host cells and mount an immune response against virus infection in these cells. Negative modulation of p38 MAPK is through an up-regulation of the dual-specificity phosphatases 1 (DUSP1) feedback loop during IBV infection, which reduces cytokine production by dephosphorylation of phosphor-threonine and phosphor-tyrosine residues on activated p38 MAPKs (Liao et al., 2011).

IBV infection of cultured cells also resulted in cell cycle arrest, at both S and G2/M phases, to boost viral replication. This p53-independent growth inhibitory outcome was catalyzed by regulation of the expression of multiple cell cycle regulatory genes such as corresponding cyclin/cyclin-dependent kinases (Cdk) complexes (Li, Tam, and Liu, 2007), as well as through systemic modulation of ataxia-telangiectasia mutated (ATM)/Rad3-related (ATR)-dependent cellular DNA damage response (Xu et al., 2011). Moreover, death processes such as apoptosis are induced by IBV at late stages of the cytolytic infection cycle, which thus lead to the eventual death of infected cells. Specifically, IBV-induced apoptosis has been shown to be both caspase-dependent (Liu, Xu, and Liu, 2001) and p53-independent (Li, Tam,

and Liu, 2007) in cultured mammalian cells, with a 58-kDa protein encoded in the open reading frame (ORF) 1b region of the virus believed to function as a possible source of virus-derived apoptotic signal (Liu, Xu, and Liu, 2001).

Host proteins are also play a role in the replication and transcription of IBV RNA. This was confirmed with a yeast two-hybrid screen that was performed using IBV nonstructural protein 14 (nsp14) as a bait protein, which ultimately led to the discovery of DDX1, a cellular RNA helicase in the DExD/H helicase family, as a potential interacting partner that translocates from the nucleus to the cytoplasm and enhances IBV replication in cultured mammalian cells through subcellular colocalization with nsp14 during infection (Xu et al., 2010).

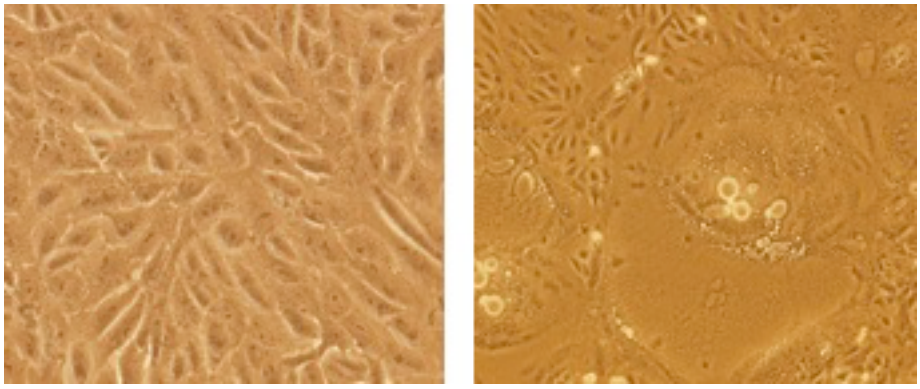

Figure 1-11

Morphological differences between a normal Vero cell (left) and an IBV-infected Vero cell (right). 100% confluent Vero cells (right) were infected with IBV at an MOI of 1 and harvested at 16 hours post-infection for comparison with uninfected wildtype Vero cells (left).

1.4 OBJECTIVES AND SIGNIFICANCE

Host-virus interactions embody the fundamental basis of viral pathogenesis. This dissertation therefore focuses on two aspects of host-antiviral response: virus-induced apoptosis, and the initiation of host innate immune response. Using IBV as a model system, the underlying effects of pro- and anti-apoptotic protein expression on coronavirus infectivity and virus-induced apoptosis was studied through the systematic characterization of pro-apoptotic Bak and anti-apoptotic Mcl-1 expression in IBV-infected cells. Likewise, again with IBV as a model system, virus recognition via the RIG-I-like helicase pathway and the subsequent initiation of host antiviral responses was investigated through the systematic characterization of pathogen recognition receptors MDA5 and RIG-I, as well as its downstream adaptor, MAVS, in IBV-infected cells.

By studying these two examples, the interplay between viral and host factors in shaping the outcome of coronavirus infection can be more effectively elucidated. Specifically, the objectives are:

1. The characterization of Bak and Mcl-1 expression, at both transcriptional and translational levels, and in different IBV-infected mammalian and chicken cell lines;
2. The targeted down-regulation of Bak and Mcl-1 proteins by RNA interference and its effect on virus-induced apoptosis and virus replication efficiency;
3. The characterization of Mda5 and RIG-I expression, at both transcriptional and translational levels, and in different IBV-infected mammalian and chicken cell lines;
4. The targeted knockdown of Mda5 and RIG-I proteins by RNA interference and its effect on coronavirus-induced host-antiviral innate immune response;

5. The effects of down-regulated Mda5 and RIG-I expression on coronavirus-induced apoptosis in relation to host immune response;
6. The role of MAVS in mediating downstream signalling activity in the RLH signalling pathway in response to coronavirus infection and the elucidation of possible viral mechanisms that may inhibit this activity.

The mechanisms studied here could identify potential antiviral targets and provide new insights for the development of antiviral drug design or antiviral therapy in the near future. For example, studies on the regulation of virus-induced apoptosis may provide more in depth details of the mechanisms that control the balance between onset of apoptosis and virus pathogenesis. Likewise, studies on the initiation of host immune response in the event of a viral invasion and the possible mechanisms viruses devise to circumvent host defence may play a part in the elucidation of new drug and/or vaccine targets.

In Chapter 1, a general overview of the regulation of apoptosis in virus infection, the onset of innate immune response to virus infection, as well as the family of coronaviruses was covered, while Chapter 2 describes the materials and methods used in this study. Chapter 3 describes the study of IBV infection on the onset of apoptosis and its regulation. In Chapter 4, the study of the RLH pathway in coronavirus recognition and virus-induced apoptosis is covered. In conclusion, Chapter 5 summarizes the findings of this project in conjunction with general discussion and the proposal of future work directions.

CHAPTER 2. MATERIALS AND METHODS

2.1 MATERIALS

2.1.1 General Reagents and Chemicals

Below is an alphabetical list of general reagents and chemicals utilized in this study, and the corresponding sources from which they were obtained.

Agarose	Bio-Rad
Ampicillin	Sigma-Aldrich
β-mercaptoethanol	Merck
Bromophenol blue	Sigma-Aldrich
Carboxymethylcellulose (CMC)	Merck
CDP-Star chemiluminescent substrate	Roche
Dulbecco's Modified Eagle Medium (D-MEM)	Gibco
Dithiothreitol (DTT)	Sigma-Aldrich
Ethidium bromide	Bio-Rad
Foetal bovine serum (FBS)	Hyclone
Formaldehyde	Sigma-Aldrich
G418 Geneticin® reagent	Invitrogen
Kanamycin	Sigma-Aldrich
Luria Broth (LB) medium	Biopolis Shared Facilities
Molecular Weight markers	
100bp DNA ladder	New England Biolabs
1kb DNA ladder	New England Biolabs
BenchMark™ Pre-Stained Protein Ladder	Invitrogen
Penicillin-Streptomycin stock solution	Invitrogen
Polyriboinosinic polyribocytidylic acid [poly(I:C)]	Sigma-Aldrich

Propidium iodide	Sigma-Aldrich
Protease inhibitor cocktail	Roche
Roswell Park Memorial Institute medium (RPMI 1640)	Gibco
Sodium Dodecyl Sulfate (SDS)	Bio-Rad
Staurosporine	Sigma-Aldrich
Toluidine blue	Bio-Rad
TRI Reagent ®	Molecular Research Centre
Tris	1st Base
Triton® X-100	Promega
Trypsin-EDTA solution	Invitrogen
Tween® 20	Promega
Z-VAD-FMK Caspase Inhibitor VI	Merck

The phosphate-buffered saline (PBS) used in all experiments is composed of 137mM NaCl, 2.7mM KCl, 4.3mM KH_2PO_4 and 1.4mM $K_2HPO_4 \cdot 7H_2O$, pH 7.3.

2.1.2 Enzymes

All restriction enzymes, as well as T4 DNA ligase and calf intestinal alkaline phosphatase (CIP), were obtained from New England Biolabs. *Pfu* DNA polymerase and *Taq* DNA polymerase were purchased from Fermentas.

2.1.3 Antibodies

Below is an alphabetical list of primary antibodies used, and the sources from which they were obtained.

Actin polyclonal antibody	Santa Cruz Biotechnology
Bak monoclonal antibody	Calbiochem
Bax monoclonal antibody	Santa Cruz Biotechnology
Bcl-2 monoclonal antibody	Cell Signalling Technology

CHOP/GADD153 monoclonal antibody	Cell Signalling Technology
Digoxigenin-Alkaline Phosphatase (AP) antibody	Roche
Flag M2 monoclonal antibody	Sigma-Aldrich
HA polyclonal antibody	Sigma-Aldrich
IRF3 polyclonal antibody	Santa Cruz Biotechnology
ISG56 polyclonal antibody	Santa Cruz Biotechnology
LC3B polyclonal antibody	Cell Signalling Technology
MAVS polyclonal antibody	Abcam
Mcl-1 monoclonal antibody	Santa Cruz Biotechnology
MDA5 polyclonal antibody	Axxora Platform
Myc polyclonal antibody	Sigma-Aldrich
RIG-I polyclonal antibody	Axxora Platform
PARP monoclonal antibody	Cell Signalling Technology
Tubulin monoclonal antibody	Sigma-Aldrich

Polyclonal IBV-S and IBV-N antibodies were raised in rabbits as described previously (Liu and Inglis, 1991), using IBV-S and IBV-N proteins as antigens, respectively. They were obtained from Mr. Benson Ng and Dr. Xiao Han, previously of the Institute of Molecular and Cell Biology in Singapore.

Polyclonal goat anti-Mouse, polyclonal goat anti-Rabbit and polyclonal rabbit anti-Goat secondary antibodies were obtained from Dako.

2.1.4 Commercial kits

Below is an alphabetical list of commercial kits used, and the sources from which they were obtained.

AxyPrep™ Plasmid Miniprep Kit	Axygen Biosci
ApoAlert® DNA Fragmentation Assay Kit	Clontech

CDP-Star® Chemiluminescent Substrate for Alkaline Phosphatase	Roche
DharmaFECT transfection reagent	Thermo Sci
Dual-Glo® Luciferase Assay kit	Promega
ECL plus chemiluminescence substrate kit	GE-Amersham
Effectene transfection reagent	Qiagen
Expand^{TM} First Strand cDNA Synthesis Kit for RT-PCR	Roche
Lipofectamine 2000 transfection reagent	Invitrogen
Luciferase Assay System kit	Promega
mMESSAGE mMACHINE® T7 Kit	Ambion
PCR DIG Probe Synthesis Kit	Roche
Power SYBR Green PCR Master Mix	Roche
QIAquick Gel Extraction Kit	Qiagen
QIAquick PCR Purification Kit	Qiagen
Western Lightning Plus Enhanced Chemiluminescence	PerkinElmer

2.2 CELLS AND VIRUSES

2.2.1 Cell lines

Vero cells (African green monkey kidney cells), H1299 cells (human non-small cell lung carcinoma cells), Huh7 (human hepatocarcinoma cells) and A549 (human lung adenocarcinoma epithelial cells) were used in this study.

H1299 cells stably expressing the *Renilla* luciferase gene were a kind gift from Ms. Felicia Tay (senior research officer, NRP-A*STAR, Singapore).

Mitochondrial AntiViral Signalling (MAVS) protein stable knockdown A549 cells were a kind gift from Dr. Wang Li (formerly of NTU, Singapore).

2.2.2 Cell culture

Vero, Huh7 and A549 cells were maintained in high glucose (4500mg/L) Dulbecco's modified Eagle's medium (DMEM) supplied with 10% fetal bovine serum (FBS) and 1% Penicillin-Streptomycin (PS) antibiotics.

H1299 cells were maintained in RPMI 1640 containing 10mM HEPES with 10% FBS and 1% PS.

H1299 cells stably expressing the *Renilla* luciferase gene were maintained in RPMI 1640 with 10% FBS, 1% PS and 100ug/ml G418 solution.

MAVS stable knockdown A549 cells were maintained in DMEM with 10% FBS, 1% PS and 200ug/ml G418 solution.

All cells were grown in a 37ºC incubator at 90% humidity level supplied with 5% CO2.

Confluent monolayers were subcultured using PBS as a wash buffer, after which, a buffered, Ca^{2+}- and Mg^{2+}-free salt solution containing 0.5% (w/v) trypsin and 0.2% (w/v) EDTA was used to dissociate adherent cells from tissue culture flasks. Dissociated cells were further washed down by DMEM and collected by centrifugation at 500 x g for 5 min. After re-suspension in fresh DMEM with 10% FBS and 1% PS, cells were seeded in new culture flasks.

2.2.3 Cell stock preparation

To prepare cell stocks, cells were trypsinized as above and collected by centrifugation at 500 x g for 5 min. After re-suspension in cell stock medium (DMEM with 10% FBS, 1% PS, and 20% glycerol), cells were transfer to 2 ml cryo-tubes by aliquots and stored in liquid nitrogen.

2.2.4 Viruses

Vero cell-adapted Beaudette strain of IBV stock (Liu and Inglis, 1992; Shen,

Law, and Liu, 2004; Shen, Wen, and Liu, 2003) was prepared by infection of Vero cells with 0.1 plaque forming unit (pfu) of IBV per cell, followed by incubation at 37°C in a humidified 5% CO_2 atmosphere. Virus stocks were made through three repeated freeze-thaw cycles and kept at -80°C in 0.5-1ml aliquots until use. Mock virus stocks were similarly made using three repeated freeze-thaw cycles of Vero cells.

A recombinant IBV containing luciferase reporter gene (IBV-Luc) was constructed by replacing 3a3b ORF with the firefly luciferase gene, and another recombinant IBV (rIBV) generated from an infectious clone was used as the wildtype control (Shen et al., 2009).

All recombinant and wildtype IBVs were propagated in Vero cells in FBS-free DMEM.

2.2.5 Virus infection

Confluent monolayers were first subcultured and seeded in appropriate culture vessels overnight. Cells were then washed once with PBS and changed to FBS free medium prior to virus infection, and inoculated with either recombinant or wildtype IBV at appropriate multiplicities of infection (MOI) depending on the experiment performed.

2.2.6 Infection of chicken embryos

Ten-day-old embryonated, pathogen-free chicken eggs (Lim Chu Kang Veterinary Station, Singapore) were inoculated with rIBV as described previously (Shen et al., 2009). Briefly, the inoculation of rIBV was done at an MOI of 0.1 and incubated for 72 h in a 37°C incubator with 5% CO_2. The allantoic fluid and different organs were harvested after the embryos were chilled at 4°C overnight. Total RNA was extracted from the homogenized tissues and used for RT-PCR with oligo(dT)[18].

2.2.7 UV inactivation of IBV

IBV was exposed to 120 000 mJ/cm2 of 254-nm shortwave UV radiation for 10 minutes within a CL-1000 cross-linker. To confirm that IBV had been inactivated, Western blotting was used to determine the presence or absence of viral proteins in cells infected with UV-inactivated virus.

2.2.8 Virus titration

60% confluent monolayers of H1299 cells grown on 6-well plates were transfected with siRNAs targeting Mcl-1 (siMcl-1), Bak (siBak), MDA5 (siMDA5), RIG-I (siRIG-I) and EGFP (siEGFP) using DharmaFECT transfection reagent according the manufacturer's instructions. At 72 hours post-transfection, cells were infected with IBV at an MOI of 0.1, and frozen down at various time points within a 0-24 hour interval post-infection for virus titration through plaque assay after three rounds of freeze-thaw cycles.

Confluent monolayers of Vero cells on six-well plates were infected with 100µl of 10-fold serially diluted virus stock. After 1 hour of incubation at 37 ºC, cells were washed twice with PBS and cultured in 3 ml of DMEM containing 0.5% carboxymethyl cellulose for 3 days. The cells were fixed and stained with 0.1% toluidine blue. The number of plaques was counted and the virus titre was calculated as pfu/ml.

2.3 MOLECULAR CLONING

2.3.1 Preparation of *E. coli* competent cells

Escherichia coli strain DH5α was streaked onto a fresh LB plate (1% bacto-tryptone, 0.5% bacto-yeast extract, 1% NaCl and 1.5% agar, pH 7.0) and incubated at 37°C overnight. A single colony was picked and grown in 10 ml LB broth

at 37°C overnight with shaking at 220 rpm. An inoculum of the culture was diluted 1:100 into 500 ml LB medium and incubated at 37°C with vigorous shaking until the absorbance at 660 nm (A_{660}) reached 0.6-0.8. The culture was chilled on ice for 30 min and bacterial cells were collected with centrifugation at 4,000 g for 10 min at 4°C. The pellet was re-suspended in 40 ml pre-cooled 0.1M $CaCl_2$ solution and incubated on ice for 1 hr. After centrifugation at 4,000 g for 15 min at 4°C, the pellet was re-suspended in 4 ml solution of 0.1M $CaCl_2$ with 20% sterile glycerol. The competent cells were stored in aliquots at -80°C.

2.3.2 Polymerase chain reaction (PCR)

Briefly, the PCR reaction mixture contains 10-20ng of DNA template, 0.1-0.5uM of both the forward and the reverse primers (Proligo-Sigma), 1 unit (U) DNA polymerase, 1X PCR buffer supplemented with 1.75mM $MgCl_2$, together with 200μM each of deoxy-adenine (dATP), deoxy-cytosine (dCTP), deoxy-guanine (dGTP) and deoxy-thymidine (dTTP) nucleotides (Promega). The reaction was typically carried out by 1 cycle of denaturation at 94°C for 2 min, followed by 30-35 cycles of denaturation at 94°C for 30 sec, primer annealing for 30-60 sec (annealing temperature to be determined by primer length and sequence) and DNA extension at 72°C. The final cycle of DNA extension was carried out at 72°C for 7 min. The reagent mixture and thermal cycle set-up were routinely adjusted to optimize product yield and specificity.

Taq polymerase was used for PCR colony screening and other routine PCR reactions. Pfu DNA polymerase, which possesses a 3'-5' exonuclease proofreading activity resulting in lower error rate, was used for high fidelity DNA synthesis.

Primers targeting mammalian genes used in this project include:

Mcl-1 Fw: 5'-ATCTCTCGGTACCTTCGGGAGC-3'

Mcl-1 Re: 5'-CCTGATGCCACCTTCTAGGTCC-3'

Bak Fw: 5'-AGGAGCAGGTAGCCCAGGAC-3'

Bak Re: 5'-CCAGTTGATCCGCTCTCAAAC-3'

Mda5 Fw: 5'-ATCTGCCTCCCTACAGGGAGTG-3'

Mda5 Re: 5'-ACACCAGGTGAAGCTGTTAGTCC-3'

RIG-I Fw: 5'-AGATCCCAGTGTATGAACAGC-3'

RIG-I Re: 5'-GCTCCAGTTCCTCCAGATTGT-3'

LGP2 Fw: 5'-AGAAGTTCCAAGATGGAAC-3'

LGP2 Re: 5'-AGCCACCATGCAGTTGAT-3'

IFNb Fw: 5'-GCTCTCCTGTTGTGCTTCTC-3'

IFNb Re: 5'-AGTCTCATTCCAGCCAGTGC-3'

ISG56 Fw: 5'-TCTCAGAGGAGCCTGGCTAAG-3'

ISG56 Re: 5'-CCACACTGTATTTGGTGTCTAGG-3'

GAPDH Fw: 5'-GACAACTTTGGTATCGTGGAA-3'

GAPDH Re: 5'-CCAGGAAATGAGCTTGACA-3'

2.3.3 DNA agarose gel electrophoresis

DNA fragments were separated by electrophoresis in the 1.0-1.5% (w/v) agarose gels prepared with TAE buffer (40mM Tris-acetate and 2mM EDTA), supplemented with 1μg/ml ethidium bromide. 6X DNA loading buffer [0.25% (w/v) of bromophenol blue and 0.25% (w/v) xylene cyanol FF and 20% (w/v) glycerol in H_2O] was added to each DNA sample before loading. DNA bands were visualized under UV illumination.

2.3.4 Gel purification of DNA

DNA gel purification was performed using the QIAquick^{TM} Gel Extraction Kit. PCR reaction products were first separated by 1-1.5% DNA agarose gel electrophoresis. Visualized under 302 nm UV-transilluminator, under which DNA/EB

complexes will fluoresce, the DNA bands of interest were excised using a scalpel and the gel slices dissolved in an appropriate volume of dissolving buffer QG according to the manufacturer's instructions. Complete melting of the gel slices was achieved by incubation at 55°C for 10 min with occasional vortex. The dissolved mixture was applied separately onto individual QIAquick™ columns for DNA purification. After two rounds of washing, the DNA fragments of interest were eluted with nuclease free water to a desired volume and quantitated using a NanoDrop™ 1000 Spectrophotometer to determine DNA concentration and purity levels.

2.3.5 PCR purification

PCR products were purified using a QIAquick PCR Purification kit. Briefly, 250µl of PB buffer were added to a 50µl PCR reaction. The mixture was applied onto a QIAquick column. After two rounds of washing, the DNA fragments of interest were eluted with nuclease free water to a desired volume and quantified using a NanoDrop™ 1000 Spectrophotometer to determine DNA concentration and purity levels.

2.3.6 Restriction enzyme digestion of DNA

Restriction endonuclease digestion mixtures were prepared as follows: 1-3µg of DNA, appropriate restriction digestion buffers and 10U of each restriction enzyme. The mixture was topped up with distilled H_2O to a total volume of 20-50µl and incubated at 37°C for 2 h. Experimental details vary according to the manufacturer's instructions for different restriction enzymes.

To prevent a singly digested vector from self-ligation, calf intestinal alkaline phosphatase (CIP) was used to remove 5' phosphates from DNA. Typically, 1U of CIP was added directly to the restriction reaction mixture in the end of the 2 h digestion and incubated for another 30 min at 37°C.

2.3.7 DNA Ligation

The purified vector and insert DNA fragment were mixed at a molar ratio of 1:3, together with 1U T4 DNA ligase and 1X T4 ligation buffer in a total volume of 10µl. The ligation mixture was incubated at 16°C overnight, or at room temperature for 3-4 hours.

2.3.8 Transformation of competent cells

An aliquot of *E. coli* competent cells were pre-thawed on ice before transformation. DNA plasmid (10ng) or ligation products were added to competent cells and incubated on ice for 30 min. The mixture then underwent heat shock at 42°C for 1 min and immediately was chilled on ice after, for 2 min. 1 ml LB broth was then added into the mixture and incubated at 37°C with vigorous shaking for 60 min. The suspension was subsequently spread onto LB plates containing 100µg/µl ampicillin or 50µg/µl kanamycin. The LB plates were incubated at 37°C overnight and single colonies were picked for DNA preparation and further characterization.

2.3.9 DNA preparation

The QIAprep® Spin Miniprep Kit was used for small-scale DNA preparation from *E. coli* cells. A single colony was inoculated into 5ml LB medium with appropriate antibiotics at 37°C with shaking overnight. Briefly, cells were pelleted by centrifugation at 14,000 rpm for 1 min and re-suspended in P1 solution containing 100mg/ml RNase A. Cells were subsequently lysed in P2 solution and neutralized by P3 solution prior to centrifugation at 14,000 rpm for 10 min. The supernatant was applied onto a QIAprep® spin column. After two rounds of washing, the DNA was eluted with 30-50µl of nuclease free water.

2.3.10 Automated DNA sequencing

Plasmid DNA (300ng) was added to a mixture of total volume of 10µl containing 3.2pmol of appropriate primer, 1X Big Dye termination mix (1stBase) and topped up with ddH_2O. Thermal cycle sequencing was carried out by 25 cycles of denaturation at 96°C for 10 sec, annealing at 50°C for 5 sec and extension at 65°C for 4 min. The reaction mixture was purified by adding 2 volumes of 100% ethanol, 0.1 volume of 3M sodium acetate (pH 5.2), and incubated on ice for 10 min before centrifugation at 14,000 rpm for 20 min. The pellet was washed twice with 70% ethanol and air-dried. Sequence was determined on an Applied Biosystems Model 3730XL automatic DNA sequencer and analyzed by Chromas program.

2.3.11 Plasmids

pXJ40 is a plasmid that was constructed by J.H. Xiao in 1990 with an ampicillin selection marker. pXJ40-Flag and pXJ40-myc was derived from pXJ40 by inserting a Flag-tag (MDWKDDDDK) and a myc-tag (EQKLISEEDL) sequence between the T7 promoter and the multiple cloning site (MCS).

The pGEM®-T Vector System (Promega) and the pXL-TOPO cloning kit (Invitrogen) were commercially obtained.

pXJ40-flag-MDA5, pXJ40-flag-RIG-I; the following IBV structural proteins: pXJ40-flag-IBV-N, pXJ40-flag-IBV-S; the following IBV fragments: pKTO-IBV-A (1-5752), pGEM-IBV-B (5748-8694), pXL-IBV-C (8689-15532), pGEM-IBV-D (15511-20930) and pXL-IBV-E (20887-27611) were constructed by Dr Fang Shouguo (senior research scientist, NTU, Singapore).

pXJ40-HA-MAVS was constructed by Dr. Wang Li (formerly of NTU, Singapore).

pXJ40-myc-IRF3 was constructed by Ms. Le Tra My (formerly of NUS,

Singapore) and Ms. Wong Hui Hui (IMCB, Singapore).

The IFNβ luciferase reporter was a kind gift from Dr. Xiao Han (formerly of University of St. Andrews, Scotland).

The following IBV non-structural proteins (nsp): pXJ40-flag-nsp12, pXJ40-flag-nsp13, pXJ40-flag-nsp14, pXJ40-flag-nsp15 and pXJ40-flag-nsp16 were constructed by Dr. Wang Xiaoxing (formerly of IMCB, Singapore).

The Mcl-1 plasmid is a full length Mcl-1 cloned into pXJ40-myc plasmid, with the following primers:

Mcl-1 fw: 5'- AGGATCCATGTTTGGCCTCAAAAGAA -3', and

Mcl-1 re: 5' TTTCTGCAGCTATCTTATTAGATATGC -3'.

The Bak plasmid is a full length Bak cloned into pXJ40-myc plasmid, with the following primers:

Bak fw: 5'- AGGATCCATGGCTTCGGGGCAAGGCC -3', and

Bak re: 5'- TTTGGTACCTCATGATTTGAAGAATCT -3'.

2.4 IN VITRO TRANSCRIPTION

5µg plasmid DNAs of not more than 5kb were linearized with an appropriate restriction enzyme downstream of the insert and purified by phenol/chloroform (equal volume) and precipitated with ethanol before transcription. The reaction was performed using mMESSAGE mMACHINE® RNA transcription kit according to the manufacturer's instructions. The transcription reaction mixture contains 1µg linearized DNA, 1X transcription buffer, 2.5mM ribonucleotides (NTPs), 2µl Enzyme Mix in a total volume of 20µl. Transcription was done by incubating the mixture at 37°C for 1-2 h, followed by DNase I digestion at 37°C for 15 min to remove the template DNA.

2.5 RNA MANIPULATION

2.5.1 Total RNA isolation from mammalian cells

Total RNA was isolated from monolayer cells using TRI Reagent® according to the manufacturer's instructions. Briefly, cells were washed twice with PBS followed by the addition TRI Reagent®. After incubation at room temperature for 10-15 min with shaking, cells were scraped and transferred to sterile 1.5ml microcentrifuge tubes. Chloroform (0.2 volume of TRI Reagent®) was added to the lysates and subjected to vigorous shaking before centrifugation at 14,000 rpm for 20 min at 4°C. The aqueous phase was transferred to a new tube and was mixed with an equal volume of isopropanol. After centrifugation at 14,000 rpm for 8 min at room temperature, the aqueous phase was transferred to a new tube and RNA was precipitated with 100% ethanol at -80°C for at least 30 min. The mixture was centrifuged at 14,000 rpm for 8 min at 4°C and the resultant pellet washed with 70% ethanol. RNA was re-suspended with an appropriate volume of RNase-free water. The concentration of the total RNA extracted was quantified using a NanoDrop^{TM} 1000 Spectrophotometer.

2.5.2 Northern blotting

RNA was separated on 1.0% agarose gel and blotted to a positively-charged nylon Hybond-N+^{TM} nylon membrane (Amersham) overnight at room temperature via capillary transfer and using a 20X SSC high-salt transfer buffer (3M NaCl, 300mM $Na_3Citrate.H_20$, pH 7.0). After the transfer, the membrane was UV-crosslinked at 120mJ/cm2 twice using a UV Stratalinker^{TM} 2400 (Stratagene), followed by pre-hybridization (Roche) at 50ºC for 1 h. After pre-hybridization, DIG-labelled DNA probe was denaturated at 100ºC for 5 min and immediately cooled on ice. Hybridization was then performed with the denatured DIG-labelled DNA probe at 50ºC for 16-20 h. After hybridization, the membrane was washed in 2X SSC (with

0.1% SDS) and 0.2X SSC (with 0.1% SDS). The membrane was then blocked in 1x Blocking Buffer (Roche) for 1 h. The signal was detected by probing with anti-Digoxigenin-AP, Fab fragments from a sheep anti-digoxigenin antibody conjugated with alkaline phosphatase, at 1:10,000 dilution followed by addition of the substrate CDP-Star chemiluminescent substrate according to the manufacturer's instructions.

2.5.3 PCR probe labelling for Northern blotting

PCR digoxigenin (DIG)-labelled DNA was used as probes for mRNAs of interest. These include the following genes: Mcl-1, Bak, Mda5 and RIG-I. The DNA probe for the pXJ40-myc-Mcl-1 plasmid corresponding to 251-715 nucleotides (nt) within the open reading frame (ORF) was labelled by incorporation of DIG-11-dUTP (Roche) during PCR. Likewise, the DNA probes for the pXJ40-myc-Bak plasmid corresponding to 332-615 nt, for pXJ40-flag-RIG-I plasmid corresponding to 896-1331 nt, for pXJ40-flag-MDA5 plasmid corresponding to 979-1456 nt within the respective ORFs, were similarly labelled. As an infection control, the DNA probe for IBV is taken from its 3'-UTR, from nucleotides 27104–27510. As a loading control, glyceraldehyde-3-phosphate dehydrogenase (GAPDH)-specific probes were also synthesized. The oligonucleotides for GAPDH-specific probe amplification are as follows:

sense GTCAGTGGTGGACCTGACCT, and

anti-sense TGCTGCAGCCAAATTCGTTG.

2.5.4 Reverse transcription (RT)

Reverse transcription was performed with Expand reverse transcriptase (Roche) according to the manufacturer's instructions. RNA was reverse transcribed using an Expand^{TM} first-strand cDNA synthesis kit according to the manufacturer's instructions.

Briefly, 1-5µg of total RNA was mixed with 20pmol oligo(dT)^{18} primers and nuclease-free H_2O to a total volume of 11ul and denatured at 65°C for 10 min. The mixture was immediately chilled on ice before the addition of a RT reaction mixture consisting of 4µl of 5X Expand reverse transcriptase buffer, 2µl of 100mM DTT, 20U RNase inhibitor, 2µl of 10 mM dNTPs and 50U of Expand reverse transcriptase to a total volume of 20ul. The reaction was incubated at 43°C for 1 h. An aliquot of the reaction was used for PCR.

2.5.5 Quantitative real-time PCR (qPCR)

Quantitative real-time PCR was used to validate gene expression changes in infected cells. Total RNA (1-5ug) was reversed transcribed to cDNA, and the resulting cDNA was subjected to qPCR using Power SYBR Green PCR Master Mix.

Primers for human Bak, Mcl-1, MDA5, RIG-I, ISG56, IFNβ and GAPDH genes are as follows:

Bak forward 5'-TGAGTACTTCACCAAGATTGCCA-3'

Bak reverse 5'-AGTCAGGCCATGCTGGTAGAC-3';

Mcl-1 forward 5'-GTAATAACACCAGTACGGACGG-3'

Mcl-1 reverse 5'-TCCCGAAGGTACCGAGAGAT-3';

MDA5 forward 5'-ATCTGCCTCCCTACAGGGAGTG-3'

MDA5 reverse 5'-ACACCAGGTGAAGCTGTTAGTCC-3';

RIG-I forward 5'-AGATCCCAGTGTATGAACAGC-3'

RIG-I reverse 5'-GCTCCAGTTCCTCCAGATTGT-3';

ISG56 forward 5'-TCTCAGAGGAGCCTGGCTAAG-3'

ISG56 reverse 5'-CCACACTGTATTTGGTGTCTAGG-3';

IFNβ forward 5'-AAACTCATGAGCAGTCTGCA-3'

IFNβ reverse 5'-AGGAGATCTTCAGTTTCGGAGG-3'

GAPDH forward 5’-CAACTACATGGTTTACATGTTC-3’

GAPDH reverse 5’-GCCAGTGGACTCCACGAC-3’.

Primers for monkey MDA5, RIG-I and ISG56 are as follows:

MDA5 forward 5’-TCCAACTGCTGAACCTCCT-3’

MDA5 reverse 5’-TGCCCATGTTGCTGTTATGT-3’;

RIG-I forward 5’-GATGGCAGGTGCAGAGAAA-3’

RIG-I reverse 5’-GGAGTTAAAATGATGATGTC-3’;

ISG56 forward 5'-TCTCAAAGGAGCCTGGCTAAG-3'

ISG56 reverse 5'-CCACATTGTATTTGGTGTCTAGG-3'.

Primers for chicken Mcl-1, Bak, MDA5, IFNβ and GAPDH are as follows:

Mcl-1 forward 5’-AATCCCTGGAGCTCTCCTCCGG-3’

Mcl-1 reverse 5’-AGATGAGCGTGACAACTCGGCC-3’;

Bak forward 5’-GCGCAGGCCATCACGAGAGA-3’

Bak reverse 5’-CCGGCCCCAGTTAATGCCGC-3’;

MDA5 forward 5’-GCCATGTGGTGCCAGATACAG-3’

MDA5 reverse 5’-TGTGGACCTGGGGCAGCAGT-3’;

IFNβ forward 5’-TCACTGGGTGTTGAGACG-3’

IFNβ reverse 5’-GATGAGGCTGTGAGAGGAGC-3’;

GAPDH forward 5’-GGGCTGATCTGAAGGGTGCTA-3’

GAPDH reverse 5’-GTGGACGCTGGGATGATGTTCTGV-3’.

Amplification and data collection were performed as per manufacturer’s instruction (Applied Biosystems 7500 real-time PCR system). The relative mRNA expression levels were calculated using GAPDH as an internal reference, and normalized to mRNA expression in mock-infected cells. All experiments were performed in duplicates.

2.5.6 RNA interference (RNAi)

The following siRNA sequences were designed for RNAi:

Mcl-1 siRNA (+): 5' GGACUUUUAGAUUUAGUGA dTdT 3',

Bak siRNA (+): 5' GCGAAGUCUUUGCCUUCUC dTdT 3',

RIG-I siRNA (+): 5' AAUUCAUCAGAGAUAGUCA dTdT 3',

(monkey) RIG-I siRNA (+): 5' GAGGUGCAGUAUAUUCAGG dTdT 3',

MDA5 siRNA (+): 5' UGAUAGAUGCGUAUACUCA dTdT 3',

(monkey) MDA5 siRNA (+): 5' GGAGUAUGCUCAUAAGAUU dTdT 3', and

non-targeting EGFP siRNA (+): 5' GCAACGUGACCCUGAAGUUC dTdT 3'.

These were purchased in duplex of OD5 (solution form) from Sigma-Proligo (Sigma-Aldrich). GADD153 siRNA and its non-targeting control were both purchased from Ambion. Transfection of siRNA into H1299 and Vero cells grown to 60% confluence was performed using DharmaFECT transfection reagent (Dharmacon) according to the manufacturer's instructions. Briefly, a 2uM siRNA solution in serum-free medium was mixed with the appropriate cell-line-specific DharmaFECT transfection reagent, also in serum-free medium of equal volume, mixed briefly and incubated at room temperature for 20 min. The total volume of the transfection mix is dependent on the size of the plate format used. Culture medium was then removed from the cells, and the transfection mix added to them. Transfection of siRNA into Huh7 cells grown to 90% confluence was performed using Lipofectamine 2000 transfection reagent according to the manufacturer's instructions. The amount of siRNA and Lipofectamine 2000 reagent used is also similarly dependent on the size of the culture vessel. In the case of Lipofectamine 2000 RNAi transfection, a second transfection was performed 24 h after the first transfection for greater knockdown efficiency. Transfected cells are incubated at 37°C with 5% CO_2 for 48 h (for mRNA

analysis) or 72 h (for protein analysis).

2.6 PROTEIN EXPRESSIONS AND ANALYSIS

2.6.1 Transient expression of plasmid DNA in mammalian cells

Cells of 80-90% confluence in 6-well plates were transfected using a recombinant vaccinia virus system. Cells were infected with recombinant vaccinia/T7 virus (vTF7) at a multiplicity of infection (M.O.I) of 1 for 1 h at 37°C with 5% CO_2. The supernatant was subsequently removed, cells were washed once with PBS and thereafter transfected with 0.4μg plasmid DNA each, using the Effectene transfection reagent according to the manufacturer's instructions, and incubated at 37°C with 5% CO_2 for 18-24 h. Cells were then harvested for further analysis.

Transfection using a non-recombinant vaccinia virus system was performed using Lipofectamine 2000 according to the manufacturer's instructions. Briefly, cells of 90-100% confluence were transfected with a serum-free DNA transfection mixture containing DNA and Lipofectamine 2000 transfection reagent at a concentration dependent on the size of the culture vessel and incubated at 37°C with 5% CO_2 for 6 h, following which the transfection mixture was removed and culture medium containing 10% FBS and 1% PS was added to the cells. The cells were then incubated for another 16-24 h before harvesting for further analysis.

2.6.2 Sodium dodecyl sulfate-polyacrylamide gel electrophoresis (SDS-PAGE)

Proteins were prepared by adding 2X Laemmli's sample buffer [100mM Tris-HCl pH 6.8, 4% SDS, 0.2% (w/v) bromophenol blue, 20% (v/v) glycerol and 10% (v/v) ß-mercaptoethanol] and heated at 95°C for 5 min before loading onto SDS-PAGE. The resolving gels of various concentrations (8%, 10%, 12% or 15%) and 5% stacking gels were cast between two glass plates (Bio-Rad). The gels were run in the Bio-Rad

Mini-PROTEAN II system in a reservoir of running buffer [25 mM Tris-HCl pH 8.3, 192 mM glycine and 0.1% SDS] at 20 mA per gel.

The gels were then electrophoretically transferred to nitrocellulose membranes (Bio-Rad) at 4°C using the Bio-Rad Trans-Blot^{TM} system. The transfer buffer contains 24mM Tris-base, 192mM glycine and 20% methanol.

2.6.3 Immunoblotting

After transfer, membranes were blocked in blocking buffer [PBS with 10% skim milk powder and 0.1% Tween 20] at room temperature for 1 h, and incubated for 1 h at room temperature or at 4^0C overnight in a dilution of a specific antiserum in blocking buffer. After 3 washes with PBST [PBS with 0.1% Tween 20] at 10 min per wash, membranes were incubated with appropriate IgG conjugated with horseradish peroxidase (HRP) diluted in blocking buffer for 60 min at room temperature. After three washes with PBST as above, membranes were subjected to chemiluminescence detection with appropriate ECL kits (Amersham/PerkinElmer), depending on the strength of the signals. To re-probe the same membrane with another antibody, the membrane was incubated in stripping buffer [62.5mM Tris-HCl pH 6.7, 100mM ß-mercaptoethanol, 2% SDS] at 55°C for 20 min, washed thrice with PBST as above, followed by blocking again.

2.7 DENSITOMETRY

Quantification of the intensity of the protein and RNA bands from Northern, Western and PCR analysis was performed using ImageJ (version 1.43), a Java-based image processing program that was developed at the National Institute of Health (NIH), with normalization to their respective consistent background (loading control) bands.

2.8 LUCIFERASE ASSAYS

2.8.1 Luciferase assay with IBV-luc

60% monolayer of H1299 cells were grown on 6-well plates and transfected with Mcl-1, Bak, MDA5, RIG-I and EGFP siRNAs, respectively, according the manufacturer's instructions. At 72 hours post-transfection, cells were infected with IBV-Luc containing the luciferase reporter gene at an MOI of 1, and harvested at the indicated time points (0-24 hours post-infection). Cells were washed with PBS and lysed with 1X Passive Lysis Buffer (Promega). Luciferase reporter assay was performed in duplicates using the Luciferase Assay System kit, according to the manufacturer's instructions. Briefly, 10ml of luciferase assay buffer was added to the luciferase assay substrate (solid form) and resuspended evenly before adding to the lysed cells in a 1:10 ratio with a total volume of 50ul per sample. Luminescence was measured with TD-20/20 luminometer (Turner Biosystems).

2.8.2 Dual Luciferase assay

H1299 cells stably expressing *Renilla* luciferase were seeded in 96-well plates (10,000 cells/well) and reverse transfected with 0.1ug each of either pXJ40-flag-MDA5, pXJ40-flag-RIG-I or pXJ40-flag-empty vector and 0.1ug of IFNβ firefly reporter using Lipofectamine 2000 reagent, and incubated at 37ºC with 5% CO_2.

At 6 h post-transfection, the transfection mixture was replaced with fresh culture medium supplemented with 10% FBS, 1% PS, and incubation was resumed for another 16 h, after which the cells were then transfected with various IBV fragments obtained from in vitro transcription using Lipofectamine 2000 reagent, with poly(I:C) as a positive control.

At 6 h post-transfection, the transfection mixture was replaced with fresh culture

medium supplemented with 10% FBS, 1% PS, and incubation was resumed for another 16 h, after which Dual-Glo® Luciferase Reagent was directly to the cells in growth medium and incubated with shaking for 10 min at room temperature, inducing cell lysis and providing a substrate for the firefly luciferase while producing the initial stable luminescent signal, which is read using an Infinite® 200 PRO plate reader (Tecan).

Subsequent addition of the Dual-Glo® Stop & Glo® Reagent with a 10 min incubation on the shaker at room temperature then quenched the luminescence from the firefly reaction, providing a substrate for *Renilla* luciferase in a reaction that was also read using the plate reader. Each transfection and luciferase assay was repeated in triplicates.

2.9 TUNEL ASSAY

The terminal deoxynucleotidyltransferase-mediated dUTP-biotin nick end-labelling (TUNEL) assay was performed using the ApoAlert® DNA Fragmentation Assay Kit according to the manufacturer's instructions. Briefly, cells were fixed with 4% formaldehyde/PBS and permeabilized with Triton X-100 at room temperature. After equilibration, each specimen was overlaid with 100µl TUNEL reaction mixture and incubated in a humidified atmosphere for 60 min at 37°C in the dark. Samples with the incorporated fluorescein were directly analyzed under a fluorescence microscope using an excitation wavelength of 488 nm.

2.10 FLUORESCENCE-ACTIVATED CELL SORTING (FACS) ANALYSIS

Cells were harvested, pelleted and washed with pre-chilled PBS before fixing with 70% ethanol and incubation at 4°C for at least 90 min. The cells were subsequently pelleted and washed with PBS twice prior to the addition of 10ug RNase

A to each tube. The cells were then incubated at room temperature for 5 min prior to the addition of 10ug of propidium iodide to each tube, and another round of incubation for 20-30 min in the dark. FACS analysis was performed on a BD™ LSR II Flow Cytometer System (BD Biosciences) with the kind assistance of Ms. Geraldine Lee (FACS Core Facility, NTU, Singapore).

2.11 STATISTICAL ANALYSIS

Data were reported as the mean +/- standard deviation (stdev). Luciferase assay results were repeated thrice and real-time PCR results were repeated twice. Calculations of the means and standard deviation were done with Microsoft Office (Excel) software (Microsoft).

CHAPTER 3. CHARACTERIZATION OF MCL-1 AND BAK IN IBV-INFECTED CELLS

3.1 INTRODUCTION

The manipulation of apoptosis is often regarded as a double-edged sword in the line of host cellular defence against viral invasion – a virus can easily turn the tables on its host and exploit the onset of apoptosis to its own advantage. One classic example is the modulation of apoptosis by HIV. HIV encoded viral proteins are able to cleverly activate apoptotic signals in instructing healthy, uninfected cells to die, while simultaneously protecting HIV-infected cells from committing 'suicide' through the up-regulation of anti-apoptotic proteins in these cells (Ross, 2001). This thus ensures the progression of the HIV life cycle and viral progeny production with minimal intervention from the host defence.

The regulation of apoptosis is also a rather complicated affair – many signalling pathways may be involved in the control of cell death and crosstalk may be involved in the activation and/or inactivation of apoptotic modulators (Elmore, 2007). For example, apoptotic pathways that occur in the mitochondria are sometimes dependent on ER stress-induced apoptosis *in vivo* (Li, Lee, and Lee, 2006).

In this study, the role of apoptosis in the coronavirus life cycle was studied using IBV as a model system. While it has been shown that apoptosis is induced in IBV-infected culture cells in a caspase dependent manner (Liu, Xu, and Liu, 2001), the role of Bcl-2 family proteins in instigating apoptosis during virus infection has not been well defined.

Here, the underlying effects of pro- and anti-apoptotic protein expression on coronavirus infectivity and virus-induced apoptosis was investigated through the systematic characterization of Bak and Mcl-1 expression at both transcriptional and translational levels in IBV-infected cells, and it is concluded that these proteins play diverging roles in mediating apoptosis during infection, and are themselves modulated

possibly by components of upstream signalling pathways, such as those arising from ER stress response.

3.2 RESULTS

3.2.1 Affymetrix array analysis of Bcl-2 family genes reveals up-regulation of Bak and Mcl-1 and down-regulation of Bcl-2 variant α at the mRNA level in IBV-infected Vero cells

IBV-infection of human and animal cells induces apoptosis in cultured cells at late stages of the infection cycle between 24 and 48 hours post infection (Li, Tam, and Liu, 2007; Liu, Xu, and Liu, 2001). To study the involvement of Bcl-2 family genes in the regulation of IBV-induced apoptosis and viral pathogenesis, global gene expression profiles were determined in Vero cells infected with IBV at an MOI of approximately 1 at 24 hours post-infection using Affymetrix array analysis, where approximately 4500 genes were found to be affected by IBV infection. As shown in Table 3-1, the expression of 11 Bcl-2-related genes at the mRNA level was up-regulated and 2 down-regulated. Among them, a 5.28-fold induction of both Bak and Mcl-1 and a 2.3-fold reduction of Bcl-2 variant α were detected (Table 3-1). No detectable change was observed for other Bcl-2-related genes in this screen.

3.2.2 IBV infection of Vero cells, chicken embryos and chicken fibroblast cells up-regulates Bak and Mcl-1

Western blot analysis of IBV-infected cells, followed by densitometry measurements, was then carried out to study the expression of Bak, Mcl-1, Bax and Bcl-2 in IBV-infected Vero cells at the protein level. In Vero cells infected with IBV at an MOI of 1, significant up-regulation of both Bak and Mcl-1 was observed at 16 and 24 hours post-infection with an increase in IBV-N protein expression as an indication

of infection (Fig. 3-1A). In contrast, constant levels of both Bax and Bcl-2 were detected throughout the time-course experiments (Fig. 3-1A). Quantification of the corresponding bands by densitometry measurement showed a 1.11-3.66-fold and a 1.10-2.82-fold induction of Bak and Mcl-1 from 8-24 hours post-infection, respectively (Fig. 3-1A). These results demonstrate that both Bak and Mcl-1 are up-regulated at the translational level in IBV-infected Vero cells.

In chicken fibroblast DF1 cells infected with IBV an MOI of 1, moderate up-regulation of both Bak (1.39-2.09-fold) and Mcl-1 (1.14-1.30-fold) at the transcriptional level were also observed by RT-PCR analysis at 8 and 16 hours post-infection (Fig. 3-1B). The increase – after normalization against GAPDH – in the expression levels of Bak (2.37-fold) and Mcl-1 (1.92-fold) in IBV-infected chicken embryos was observed as well (Fig. 3-1C). This increase was also quantified by real-time PCR, which, after normalization to mock-infected chicken embryos, showed a 6.41- and 6.43-fold increase in Bak and Mcl-1 induction, respectively, at 48 hours post-infection (Fig. 3-1D).

Table 3-1 Affymetrix array analysis of the expression of BCL-2-related genes in IBV-infected Vero cells at 24 hours post-infection. The genes shown are classified in a sequential order of decreasing fold in induction.

Gene	Accession Number	Induction fold	Description
BAK1	NM_001188.1	5.28	BCL-2-antagonist/killer 1
MCL1	NM_021960.1	5.28	Myeloid cell leukaemia sequence 1 (BCL-2-related), transcript variant 1
BNIP1	U15172	1.87	BCL-2/adenovirus E1B 19kD-interacting protein 1
BCL-2L1	NM_001191.1	1.74	BCL-2-like 1, nuclear gene encoding mitochondrial protein, transcript variant 2
BECN1	AF139131.1	1.62	Beclin 1
BAG1	AF116273.1	1.62	BCL-2-associated athanogene 1 protein variant
BAG-2	AF095192.1	1.62	BCL-2-associated athanogene-family molecular chaperone regulator-2
BAG4	NM_004874.1	1.52	BCL-2-associated athanogene 4
BAX	NM_004324.1	1.32	BCL-2-associated X protein
BAG3	NM_004281.1	1.23	BCL-2-associated athanogene 3
BAX	U19599.1	1.23	BCL-2-associated X delta
BNIP3L	AF060922.1	0.9	BCL-2/adenovirus E1B 19kDa interacting protein 3-like
BCL-2	NM_000633.2	0.8	B-cell CLL/lymphoma 2 nuclear gene encoding mitochondrial protein transcript variant α

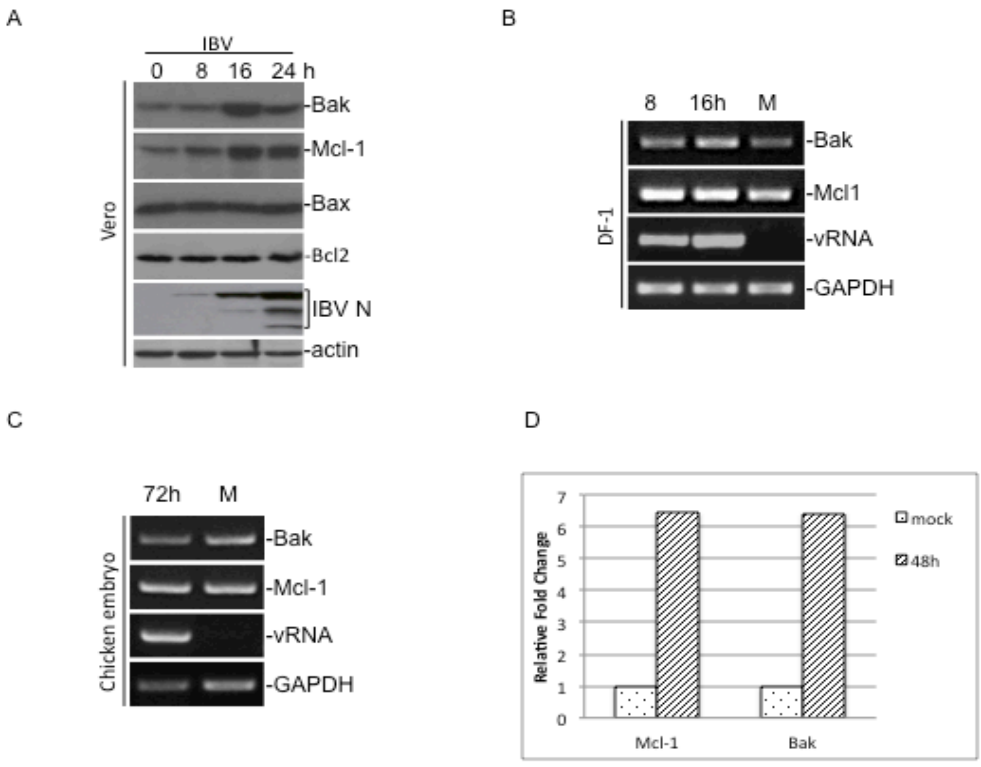

Figure 3-1

Analysis of the expression of BCL-2-related proteins in IBV-infected Vero cells, chicken fibroblast DF1 cells and chicken embryos.

(A) Vero cells were infected with IBV, harvested at 0, 8, 16 and 24 hours post-infection, and lysates prepared. Western blot analysis was performed with the indicated specific antibodies, and probed with anti-actin as a loading control.

(B) Chicken fibroblast DF1 cells were infected with IBV, harvested at 8 and 16 hours post-infection and RNA extracted. RT-PCR analysis was carried out using specific primers for the indicated genes, with GAPDH as a loading control.

(C) 10-day-old chicken embryos were inoculated with either mock virus (M) or IBV (1000 pfu per egg) in a 37^0C incubator for 72 hours. Total RNA was extracted from homogenized tissues and used for RT-PCR using specific primers as above (B).

(D) Total RNA was extracted from (C) was used for real time PCR using specific primers for the indicated genes, with GAPDH as a loading control.

3.2.3 Active viral replication is required for up-regulation of Mcl-1 and Bak at the transcriptional and translational levels in IBV-infected Vero, H1299 and Huh7 cells

To further confirm the up-regulation of Bak and Mcl-1 expression during IBV infection and to study if this up-regulation is cell type-specific, Vero, H1299 and Huh7 cells were infected with IBV at an MOI of 1 and harvested at 0, 8, 12, 16 and 24 hours post-infection, respectively. Northern blot analysis, followed by densitometry measurements, of all three IBV-infected mammalian cell lines showed an induction of both *Bak* and *Mcl-1* transcripts at the mRNA level from 12 hours post-infection (Fig. 3-2A). Quantification of the corresponding bands by densitometry measurement showed a 1.04-4.66-fold and a 0.85-3.92-fold induction of Bak and Mcl-1 In IBV-infected Vero cells from 8-24 hours post-infection, respectively. In IBV-infected H1299 cells, significant induction of *Mcl-1* (1.67-9.51-fold) was detected from 12-24 hours post-infection; however, relatively less efficient induction of *Bak* (1.09-2.83-fold) was observed as the basal level of *Bak* is much higher in this cell line. In IBV-infected Huh7 cells, a 1.28-2.06-fold and a 1.17-2.06-fold induction of *Bak* and *Mcl-1* from 8-20 hours post-infection was observed. It was also noted that the total mRNA of sufficient concentration could not be extracted for IBV-infected Huh7 cells at 24 hours post-infection due to the death and detachment of the infected cells (Fig. 3-2A). It reflects a much faster rate of viral infection in this cell line.

To investigate if viral replication and synthesis of structural proteins are required for the up-regulation of *Bak* and *Mcl-1* transcripts, same amounts of UV-inactivated IBV were incubated with the three cell lines and cells were harvested at the same time points as the cells infected with live IBV shown in Fig. 3-2A. Northern blotting analysis showed that the up-regulation trend at the transcriptional levels previously

observed in live IBV-infected cells was abolished for both Bak and Mcl-1 (Fig. 3-2A), confirming that active viral replication is required for induction of the two genes. The induction of Mcl-1 and Bak was also examined quantitatively by real-time RT-PCR, which, after normalization to UV-inactivated IBV-infected cells, showed significant induction in Vero, H1299 and Huh7 cells infected with live IBV at 16 hours post-infection. Specifically, Mcl-1 induction showed a 4.96-, 5.97- and 9.75-fold increase, and Bak induction saw a 7.00-, 10.66- and 4.04-fold increase in IBV-infected Vero, H1299 and Huh7 cells, respectively.

The induction kinetics of Mcl-1 and Bak at the protein level in IBV-infected Vero, H1299 and Huh7 cells were then characterized. Cells were infected with IBV at an MOI of 1, and harvested at 0, 8, 12, 16 and 20 hours post-infection, respectively. Immunoblotting was carried out, followed by densitometry measurements. Virus infection efficiency was monitored by Western blot analysis of the same cell lysates with anti-IBV S antibodies, showing efficient detection of the S protein expression in these cells from 12 hours post-infection (Fig. 3-2B). Moderate up-regulation of Mcl-1_L protein (40 kDa) was observed in all three cell lines infected with IBV (Fig. 3-2B). Densitometry measurements of the corresponding bands showed a 1.26-2.59-fold induction of Mcl-1 In IBV-infected Vero cells from 8-20 hours post-infection. Up-regulation of Mcl-1 protein expression was also observed in IBV-infected H1299 (1.1-1.97-fold) and Huh7 (2.35-2.98-fold) cells. However, down-regulation of the protein expression was consistently observed in IBV-infected H1299 cells at 20 hours post-infection (Fig. 3-2B). This could be due to the fact that Mcl-1 has a short half-life and is subjected to constitutive polyubiquitination and subsequent proteasome degradation (Adams and Cooper, 2007), which might account for the decline in its expression in some, but not all, virus-infected human cells in the later stages of

infection (Cuconati et al., 2003).

In normal, healthy cells, Bak is localized to the mitochondrial outer membrane as an inactive monomer. After appropriate apoptotic stimuli, Bak undergoes an activating conformational change that results in the formation of higher-order multimers (Wei et al., 2000). Analysis of Bak monomer (24 kDa) expression showed an up-regulation trend in IBV-infected Vero, H1299 and Huh7 cells (Fig. 3-2B). Densitometry measurements of the corresponding bands showed 1.02-1.79-, 1.37-1.48- and 1.84-2.63-fold induction of Bak in IBV-infected Vero, H1299 and Huh7 cells from 8-20 hours post-infection, respectively.

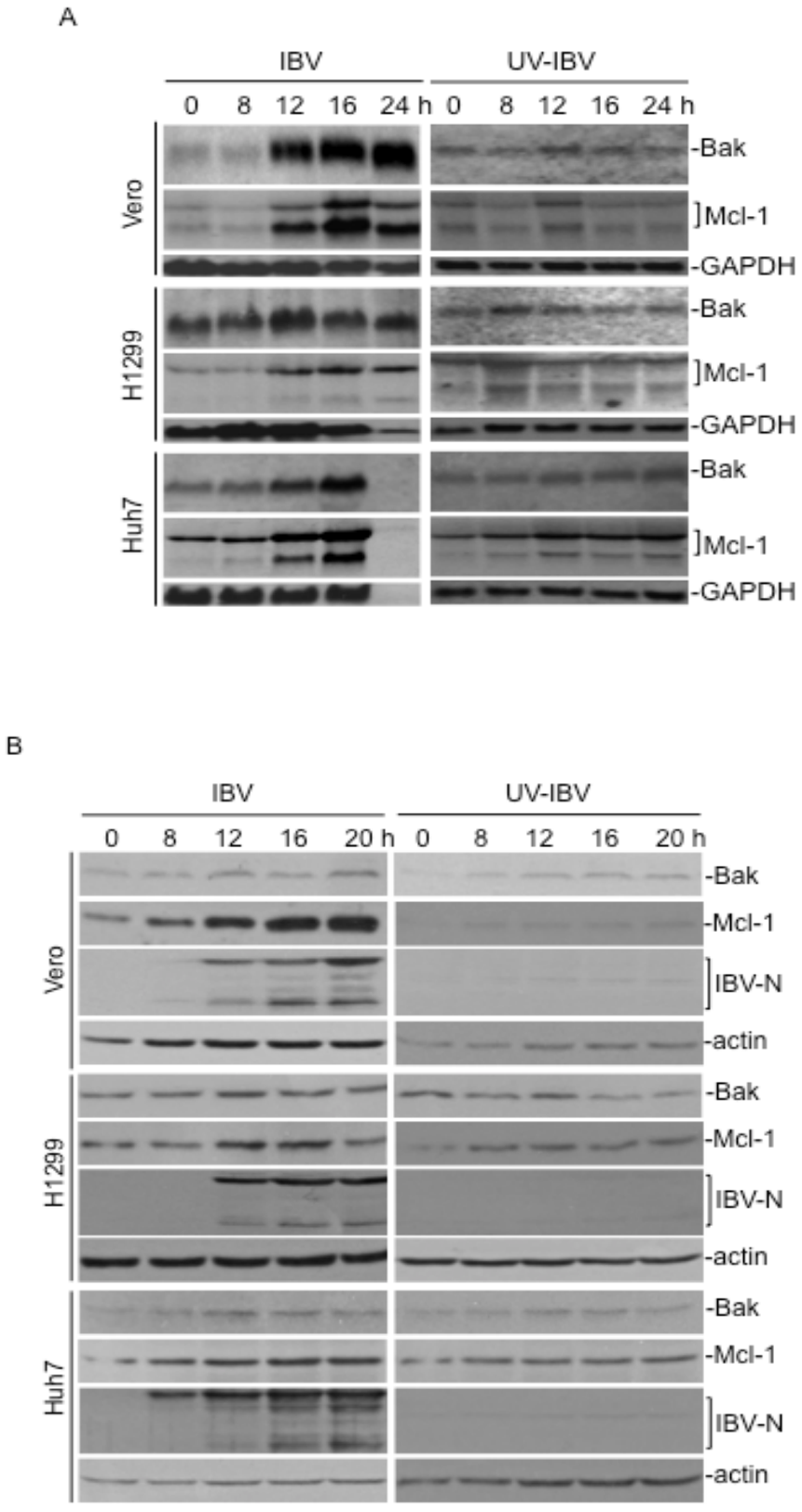
A
IBV
UV-IBV
0 8 12 16 24 h 0 8 12 16 24 h
Vero
H1299
Huh7
-Bak
]Mcl-1
-GAPDH
B
IBV
UV-IBV
0 8 12 16 20 h 0 8 12 16 20 h
Vero
H1299
Huh7
-Bak
-Mcl-1
IBV-N
-actin

Figure 3-2

Analysis of Bak and Mcl-1 expression at the mRNA and protein levels in IBV-infected mammalian cells

(A) Northern blot analysis of Bak and Mcl-1 expression at the mRNA level in IBV-infected mammalian cells. Vero, H1299 and Huh7 cells infected with IBV or UV-IBV were harvested at 0, 8, 12, 16 and 24 hours post-infection, respectively, and total RNA was extracted. Northern blot analysis was carried out with specific probes for Bak and Mcl-1. The same membrane was also probed with a GAPDH probe as a loading control.

(B) Western blot analysis of Bak and Mcl-1 expression at the protein level in mammalian cells. Vero, H1299 and Huh7 cells infected with IBV were harvested at 0, 8, 12, 16, 24 and 36 hours post-infection, respectively, and cell lysates prepared. Western blot analysis was performed using specific antibodies as indicated, with anti-actin as a loading control. M, mock infection.

3.2.4 Manipulation of the expression of Mcl-1 and Bak regulates IBV-induced apoptosis

The effects of Mcl-1 and Bak knockdown on IBV-induced apoptosis was first assessed by using the TUNEL assay. H1299 cells were transfected with siRNA duplexes targeting Mcl-1 (siMcl-1), Bak (siBak) or EGFP (siEGFP), respectively, and either mock-infected or infected with IBV at an MOI of 1 at 72 hours post-transfection. At 20 and 24 hours post-infection, cells were fixed and permeabilized before overlaying with the TUNEL reaction mixture, which labels apoptotic cells such that samples with the incorporated fluorescein can be visualized under a fluorescence microscope (Fig. 3-3A). Significantly more apoptotic cells were observed in Mcl-1 knockdown cells infected with IBV compared to the control cells transfected with siEGFP, or with Bak-knockdown cells at both 20 and 24 hours post-infection, whereas little or no apoptotic cells were observed in mock-infected cells (Fig. 3-3A). These results demonstrate that knockdown of Mcl-1 appears to speed up the onset of IBV-induced apoptosis, whereas silencing of Bak causes a slight delay.

The specific regulatory roles of Bak and Mcl-1 in IBV-induced apoptosis were further studied by examining the cleavage kinetics of PARP (116 kDa). This zinc-dependent eukaryotic DNA-binding protein specifically recognizes DNA strand breaks produced by genotoxic agents, and is normally involved in DNA repair, DNA stability and other cellular events. It is one of the substrates cleaved by members of the caspase family during early apoptosis, and detection of the caspase cleavage fragment (85 kDa) of PARP has long been considered to be a hallmark of apoptosis (Boulares et al., 1999). Using siEGFP as a negative control, Western blot analysis, followed by densitometry measurements, of H1299 and Huh7 cells infected with IBV showed that Mcl-1 and Bak expression were specifically decreased by siMcl-1 and siBak,

respectively, in both H1299 and Huh7 cells (Fig. 3-3B). Interestingly, the detection of the 85 kDa PARP cleavage fragment in both cell lines appeared to be inversely correlated with Mcl-1 expression levels. As shown in Fig. 3-3B, a significantly more amount of the cleavage product was detected in IBV-infected, Mcl-1 knockdown H1299 (29%) and Huh7 (30%) cells at 20 hours post-infection, compared to the same infected cell lines treated with either siBak (0% in both cell lines) or siEGFP (23% in H1299 and 0% in Huh7). The same trend was also observed at 24 hours post-infection, although more cleavage product was detected in siEGFP-treated Huh7 cells (Fig. 3-3B). As no significant amount of Mcl-1 was observed in siEGFP-transfected H1299 and Huh7 cells at 24 hours post-infection (Fig. 3-3B), it may suggest rapid proteasome degradation of the protein as observed previously.

In contrast, PARP cleavage was not observed in IBV-infected, siBak-transfected H1299 and Huh7 cells at 20 hours post-infection, and in H1299 cells at 24 hours post-infection (Fig. 3-3B). The appearance of the PARP cleavage fragment in Bak-silenced Huh7 cells at 24 hours post-infection, albeit at lower levels as those in similarly infected Mcl-1 and EGFP knockdown Huh7 cells, could be attributed to a slight decrease in Mcl-1 expression in the Bak knockdown cells (Fig. 3-3B). Taken together, these results confirm that Mcl-1 may play a part in the regulation of IBV-induced apoptosis, and a decrease in the Mcl-1 expression in cells could enhance IBV-induced apoptosis at earlier stages of infection.

The differential regulatory effects of Mcl-1 and Bak on IBV-induced apoptosis were further studied by over-expression of Mcl-1 and Bak in mammalian cells. For this purpose, Myc-tagged Mcl-1 and a similarly-tagged Bak were constructed and transfected into H1299 and Huh7 separately, using an empty vector as a negative transfection control. The cells were then infected with IBV at an MOI of 1. At 24

hours post-infection, a significant increase in PARP cleavage was observed in both H1299 (3.25-fold) and Huh7 (2.73-fold) cells transfected with Myc-Bak (Fig. 3-3C). In contrast, the full-length PARP was not significantly cleaved in both IBV-infected H1299 and Huh7 transfected with Myc-Mcl-1 (Fig. 3-3C). It was noted that a significant increase (2.88-fold) in PARP cleavage was observed in IBV-infected H1299 cells transfected with siEGFP, reflecting a high level of viral replication in these cells as described in a later section. These results further confirm the respective roles Mcl-1 and Bak may play in regulating the onset and rate of IBV-induced apoptosis.

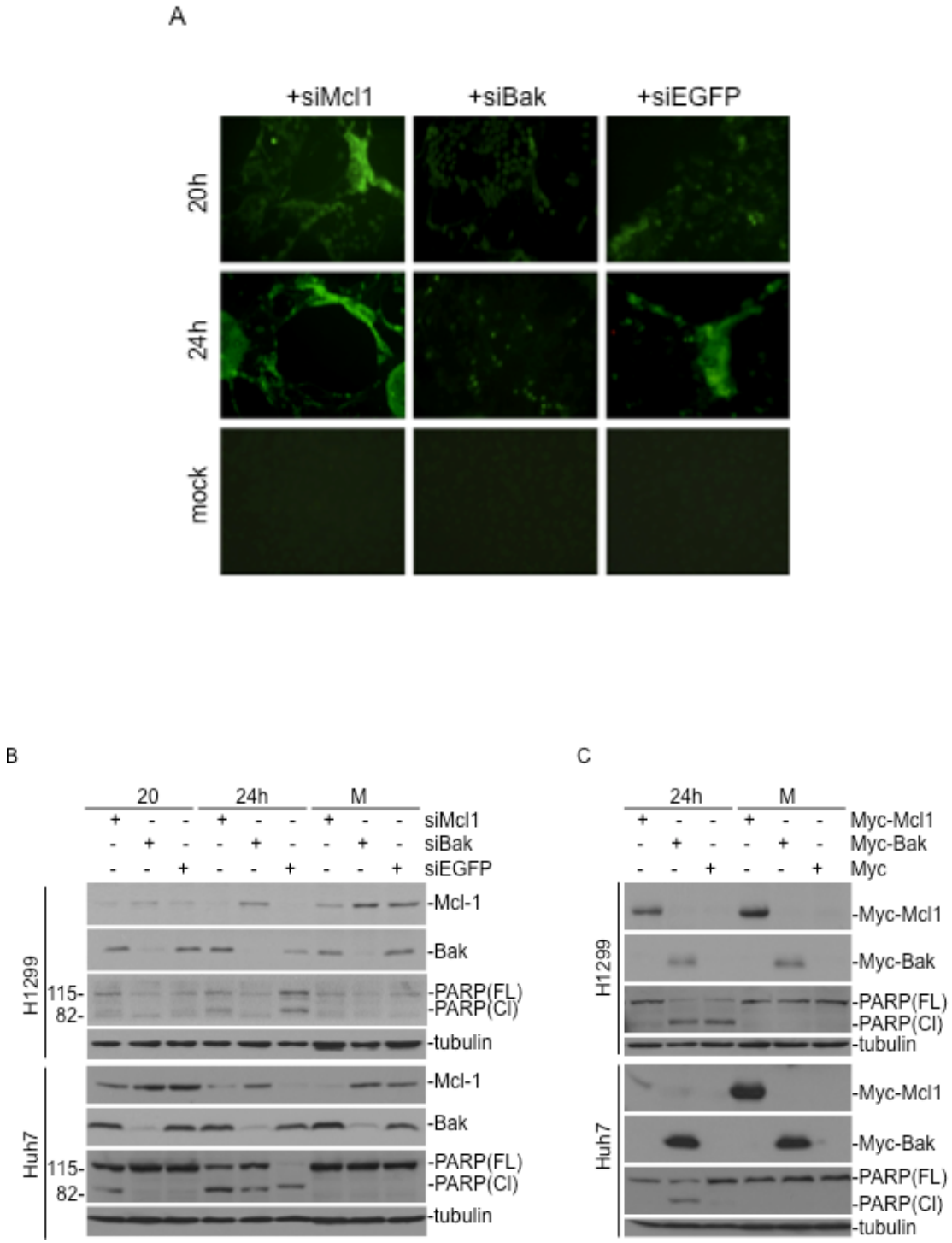
A
+siMcl1
+siBak
+siEGFP
20h
24h
mock
B
20
24h
M
siMcl1
siBak
siEGFP
H1299
Huh7
-Mcl-1
-Bak
115-
82-
-PARP(FL)
-PARP(Cl)
-tubulin
C
Myc-Mcl1
Myc-Bak
Myc

Figure 3-3

The effects of manipulation of the expression of Bak and Mcl-1 in mammalian cells on IBV-induced apoptosis and PARP cleavage.

(A) TUNEL assay of the effects of down-regulation of Bak and Mcl-1 by RNA interference in mammalian cells on IBV-induced apoptosis. H1299 cells were transfected with siRNA duplexes targeting Mcl-1, Bak or EGFP, respectively. At 72 hours post-transfection, cells were either mock-infected, or infected with IBV, then fixed and permeabilized at 20 and 24 hours post-infection. Cells were stained with the TUNEL reaction mixture and images taken at an excitation wavelength of 488 nm.

(B) Western blot analysis of the effects of down-regulation of Bak and Mcl-1 by RNA interference in mammalian cells on IBV-induced apoptosis and PARP cleavage. H1299 (upper panel) and Huh7 cells (lower panel) were transfected with siRNA duplexes targeting Mcl-1, Bak or EGFP. At 72 hours post-transfection, cells were infected with IBV and harvested at 20 and 24 hours post-infection. M, mock infection. Western blot analysis was performed using the indicated specific antibodies, with anti-tubulin as a loading control.

(C) The effects of the transient expression of Mcl-1 and Bak in mammalian cells on IBV-induced apoptosis and PARP cleavage. H1299 (upper panel) and Huh7 cells (lower panel) were transfected with pXJ40-myc-Mcl-1, pXJ40-myc-Bak or pXJ40-myc empty vector and either mock-infected (M) or infected with IBV at 16 hours post-transfection. Cells were harvested 24 hours post-infection and western blot analysis was performed using the indicated specific antibodies, with anti-tubulin as a loading control.

3.2.5 IBV-mediated Mcl-1 induction is reduced by inhibition of both ERK and PI3K pathways, and by silencing of GADD153

We then checked the upstream signalling pathways that may play a role in regulating the induction of Mcl-1 in IBV-infected cells. Recent reports suggested that ER stress response, in particular the downstream activation of MEK/ERK and PI3K/Akt signalling pathways, may be involved in the regulation of Mcl-1 and other Bcl-2 family of proteins (Kim, Xu, and Reed, 2008). The involvement of MAP/ERK and PI3K kinase pathways in IBV-induced Mcl-1 regulation was first studied by infection of Vero and H1299 cells with IBV at an MOI of 2 in the presence or absence of either 20 mM of MAP/ERK kinase MEK-1 inhibitor U0126 or 40 mM of PI3K inhibitor LY294002. Mcl-1 induction was quantitatively defined by real-time RT-PCR at 16 hours post-infection, showing that both U0126 and LY294002 significantly reduced the Mcl-1 induction in both cell lines, compared to the control cells treated with DMSO alone (Fig. 3-4A). As U0126, and not LY294002, was also able to inhibit IBV infection at the same concentration (data not shown), the inhibitory effect observed was probably due to the reduced viral replication.

The inhibitory effects of U0126 on virus infection warranted a closer look of the upstream signals that may regulate the MAP/ERK pathway. GADD153, also known as C/EBP homologous protein (CHOP), is a pro-apoptotic transcription factor and well-known component of several ER stress-mediated pathways, including the MAP/ERK pathway (Ariyama et al., 2008; Kim, Xu, and Reed, 2008; Oyadomari and Mori, 2004). Induction of GADD153 has been found to regulate different members of the Bcl-2 family (McCullough et al., 2001; Puthalakath et al., 2007). Downstream of the ER stress–mediated up-regulation of GADD153 expression is a correlated suppression of Akt signalling (Wang et al., 2008). The activation of the latter is, in turn,

known to up-regulate Mcl-1 through its Akt kinase (Longo et al., 2008). We first looked at the expression and induction of GADD153 in IBV-infected H1299 and observed its up-regulation (0.84-9.91-fold) from 2-20 hours post-infection (Fig. 3-4B). The same up-regulation was obliterated upon infection with UV-inactivated IBV at the same time points, indicating the involvement of virus replication in regulating GADD153 expression (Fig. 3-4B).

To elucidate the regulatory roles, if any, for GADD153 in the induction of Mcl-1, H1299 cells transfected with either siRNA duplexes targeting GADD153 (siGADD153) or a non-targeting control (siControl) were infected with IBV at an M.O.I of 1 for 16-20 hours and harvested for Western blot analysis, followed by densitometry measurements. We observed a corresponding reduction in the expression of Mcl-1 (40-73% down-regulation) with a decreased GADD153 expression (21-27% knockdown efficiencies) in IBV-infected cells, alongside a 66-98% reduction in viral replication efficiency, compared to that in infected control cells (Fig. 3-4C). These results suggest the possible involvement of many signalling pathways in the modulation of Mcl-1 induction, including MAP/ERK and ER stress response, leading to the regulation of virus-induced apoptosis.

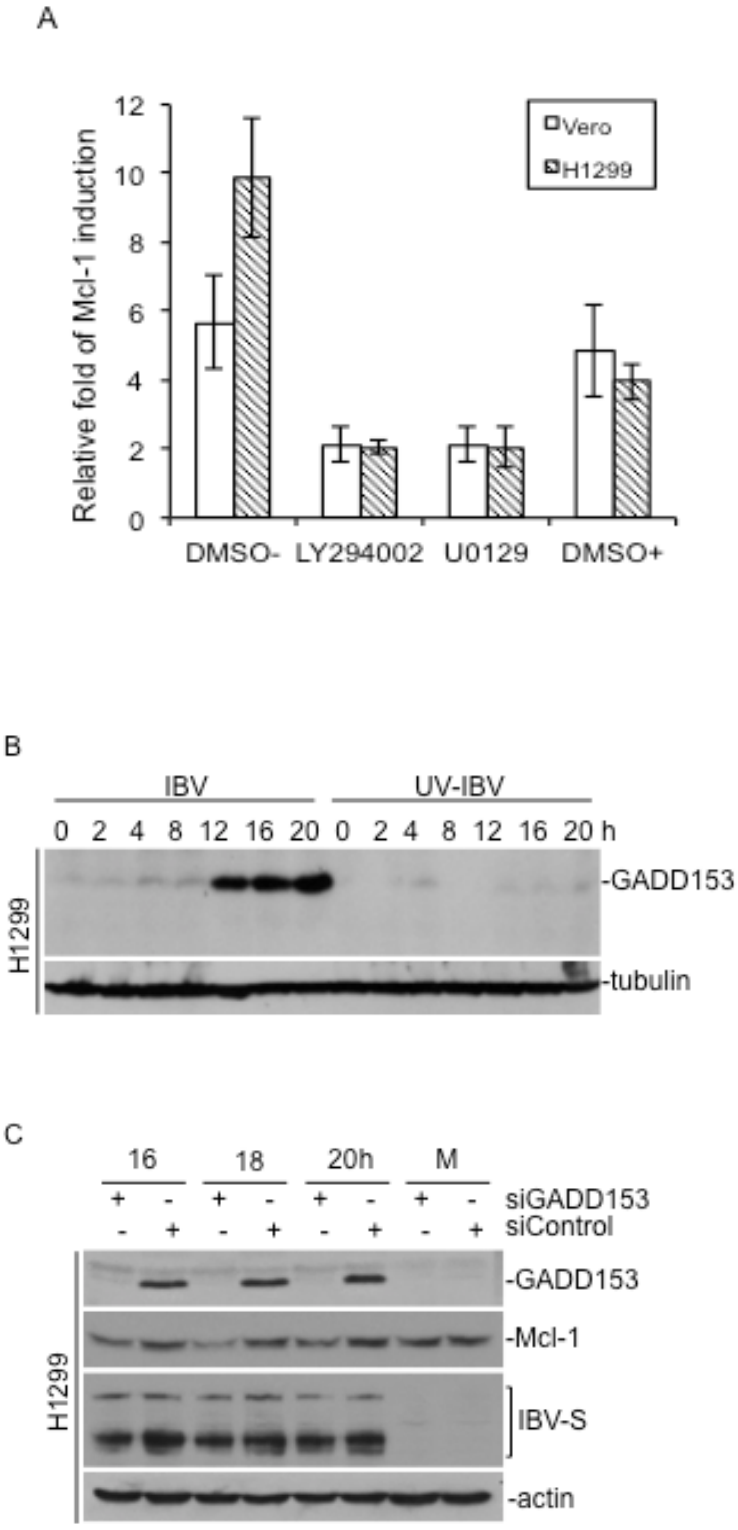
A
Relative fold of Mcl-1 induction
12
10
8
6
4
2
0
Vero
H1299
DMSO-
LY294002
U0129
DMSO+
B
IBV
UV-IBV
0 2 4 8 12 16 20 0 2 4 8 12 16 20 h
H1299
-GADD153
-tubulin
C
16
18
20h
M
siGADD153
siControl
H1299
-GADD153
-Mcl-1
IBV-S
-actin

Figure 3-4

Induction of Mcl-1 in mammalian cells in the presence or absence of either 20 mM of MEK-1 inhibitor U0126, 40 mM of PI3K inhibitor LY294002, or the pro-apoptotic transcription factor GADD153.

(A) Vero, and H1299 cells were incubated with normal medium (DMSO-), LY294002 in DMSO, U0129 in DMSO and DMSO only (DMSO+) for 1 hour, and then infected with IBV at a multiplicity of infection of approximately 2 in the presence or absence of the inhibitors. Cells were harvested at 16 hours post-infection, and total RNA extracted. The relative amounts of Mcl-1 transcripts were determined by quantitative RT-PCR and normalized against GAPDH. The relative fold of Mcl-1 induction in IBV-infected cells was determined by comparing with mock-infected cells.

(B) H1299 cells were infected with either IBV or UV-IBV for 0-20 hours and harvested for western blot analysis using specific GADD153 antibody, with anti-tubulin as a loading control.

(C) H1299 cells were transfected with either siGADD153 or a non-targeting control for 72 hours and subsequently infected with IBV. Cells were harvested at 16, 18 and 20 hours post-infection for western blot analysis using specific antibodies against the indicated proteins, with anti-actin as a loading control. M, mock infection.

3.2.6 Knockdown of Mcl-1 and Bak by RNA interference regulates virus activity and virus titres at late stages of the infection cycle

The effects of Mcl-1 and Bak knockdown, respectively, on virus activity were also studied using a virus luciferase assay, which showed a slight increase in virus activity in Mcl-1 knockdown cells infected with IBV. Luciferase activity was monitored by infecting Mcl-1, Bak and EGFP knockdown cells with recombinant IBV stably carrying and expressing luciferase (Fig. 3-5A). An increase in luciferase activity was observed in Mcl-1 knockdown cells infected with IBV-luc at 12, 16 and 24 hours post-infection, and a slight decrease was observed in Bak knockdown cells at 12 and 16 hours post-infection, as compared with control EGFP knockdown cells.

Plaque assays were performed to determine infectious virus titre in the knockdown cells. A representative plate for the comparison of the virus titre among the knockdown cells at 24 hours post-infection is shown in Fig. 3-5B, while the virus growth kinetics are calculated on a logarithmic scale (Fig. 3-5C). The virus titre in Mcl-1 knockdown cells at 20 hours post-infection was 6.67×10^4 pfu/ml, compared to 1.58×10^4 pfu/ml in siEGFP control cells, and 7.34×10^4 pfu/ml at 24 hours post-infection, compared to 3.17×10^4 pfu/ml in siEGFP control cells. This corresponds to a 4.22- and 2.32-fold increase, respectively, over control cells. Virus titres in Bak knockdown cells are 1.3×10^4 pfu/ml and 1.17×10^4 pfu/ml at 20 and 24 hours post-infection, respectively. This corresponds to a 1.22- and 2.71-fold decrease, respectively, over control cells.

While these results together suggest the possible roles Mcl-1 might play in enhancing the rate of progeny production and virus release, virus titration may not be the most ideal method for the analysis of viral activity and progeny production in siRNA-treated cells. Instead, Western blotting analysis of viral proteins in total cell

lysates and culture medium may be a more realistic method over viral titration, as the viability of IBV was heavily influenced by the transfection reagents as well as DMSO used in some experiments. Measurements of viral protein synthesis and release would more accurately reflect the effects of apoptosis and its regulation on IBV replication.

A

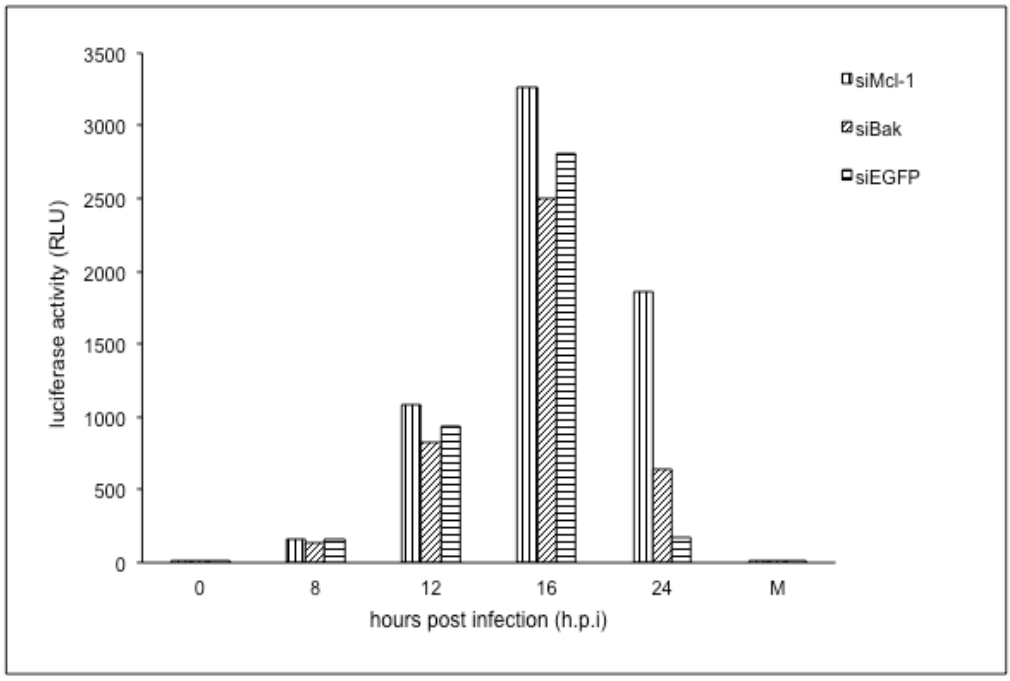
3500
3000
2500
2000
1500
1000
500
0
luciferase activity (RLU)
0
8
12
16
24
M
hours post infection (h.p.i)
siMcl-1
siBak
siEGFP

B

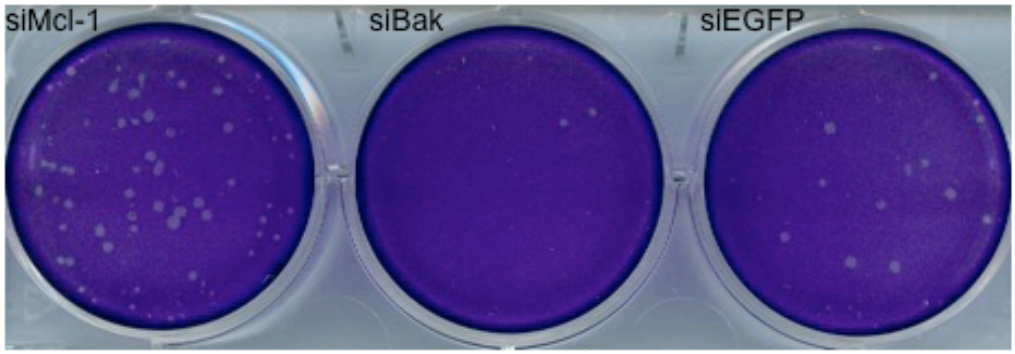
siMcl-1
siBak
siEGFP

C

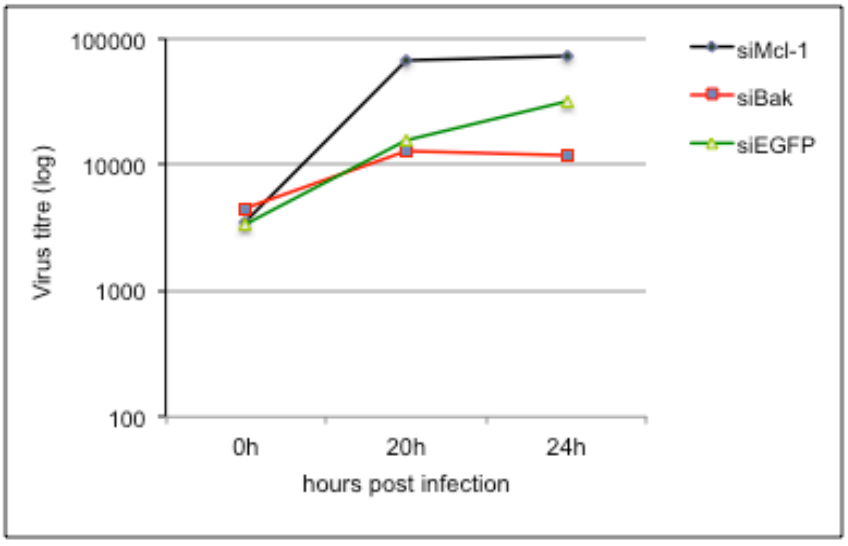
100000
10000
1000
100
Virus titre (log)
0h
20h
24h
hours post infection
siMcl-1
siBak
siEGFP

Figure 3-5

The effects of down-regulation of Mcl-1 and Bak by RNA interference in mammalian cells on virus activity and the production of progeny viruses.

(A) Luciferase assay. H1299 cells were transfected with siRNA duplexes targeting Mcl-1, Bak and EGFP for 72 hours and subsequently either mock-infected (M) or infected with IBV-luc. The cells were lysed at 0, 8, 12, 16 and 24 hours post-infection and subsequently checked for luciferase activity.

(B) Comparison of virus growth kinetics in siMcl-1-, siBak- and siEGFP-infected cells. H1299 cells were transfected with siMcl-1, siBak and siEGFP respectively. At 72 hours post-transfection, cells were infected with IBV, frozen down at 0, 20 and 24 hours post-infection, and subsequently freeze-thawed three times. These were used to infect confluent monolayers of Vero cells grown on 6-well plates in the presence of 0.5% carboxymethyl cellulose for 3 days, after which the cells were fixed with 4% formaldehyde and stained with 0.1% toluidine blue for the visualization of viral plaques and calculation of plaque forming units.

(C) A representative comparison of the plaque numbers between siMcl-1-, siBak and siEGFP-infected cells, respectively, at 24h post-infection.

3.2.7 Knockdown of Mcl-1 and Bak by RNA interference regulates the replication and release of IBV at late stages of the infection cycle

For a more relevant examination of the effects of Mcl-1 and Bak knockdown on IBV replication and release, Western blot analysis and densitometry measurements of IBV S and N proteins in total cell lysates and in culture medium were performed. While the release of viral protein/particles were enhanced with decreased expression levels of Mcl-1, compared to that in Bak knockdown and control cells, IBV S and N protein expression levels in total cell lysates were only slightly higher in Mcl-1 knockdown cells at 20 hours post-infection, and largely comparable with siEGFP-transfected cells at 24 hours post-infection (Fig. 3-6A). Bak knockdown H1299 cells, on the other hand, showed a decrease in viral replication efficiency, although slightly less so in similarly knocked down Huh7 cells (Fig. 3-6A).

The effects of Bak and Mcl-1 knockdown by RNA interference on IBV RNA replication were checked. Bak and Mcl-1 knockdown and control H1299 cells infected with IBV at an MOI of 1, harvested at various time points from 0 to 20 hours post-infection, and total RNA was extracted for Northern blot analysis, followed by densitometry measurements. The data presented here showed that knockdown of either Bak or Mcl-1 renders minimal, if any, effects on the replication and transcription of IBV RNA. As shown in Fig. 3-6B, no consistent trends of increase/decrease of viral RNA were observed in Bak and Mcl-1 knockdown cells infected with IBV compared to the siEGFP control cells. The observed variations among different samples may be caused by experimental factors. These results suggest that, as would be expected, manipulation of the Bak and Mcl-1 expression renders little effort on IBV replication at these early stages of the infection cycle. It may also reflect the sensitivity of the assays used.

The effects of over-expression of Mcl-1 and Bak in mammalian cells shown in Fig. 3-6C on IBV replication and release were analyzed by Western blot analysis of IBV S and N proteins in total cell lysates and culture media. While the expression of IBV-S protein in total cell lysates showed little or no increase in IBV infected H1299 (96%) and Huh 7 (90%) cells over-expressing Bak as compared to similarly infected control cells, an increase in the release of virus proteins/particles was observed, as is evident in the increase in IBV-S and -N protein expression levels in the culture medium of infected H1299 (2.1-fold for S protein and 2.3-fold for N protein) and Huh7 (1.43-fold for S protein and 1.54-fold for N protein cells) transfected with Myc-Bak (Fig. 3-6C). The contrary was observed in the culture medium of infected cells over-expressing Mcl-1 (Fig. 3-6C). It was also noted that transient expression of Myc-Mcl-1 significantly inhibited the replication of IBV in H1299 cells (Fig. 3-6C). Taken together, these results further confirm the respective roles Mcl-1 and Bak play in regulating the rate of both IBV-induced apoptosis and viral progeny release.

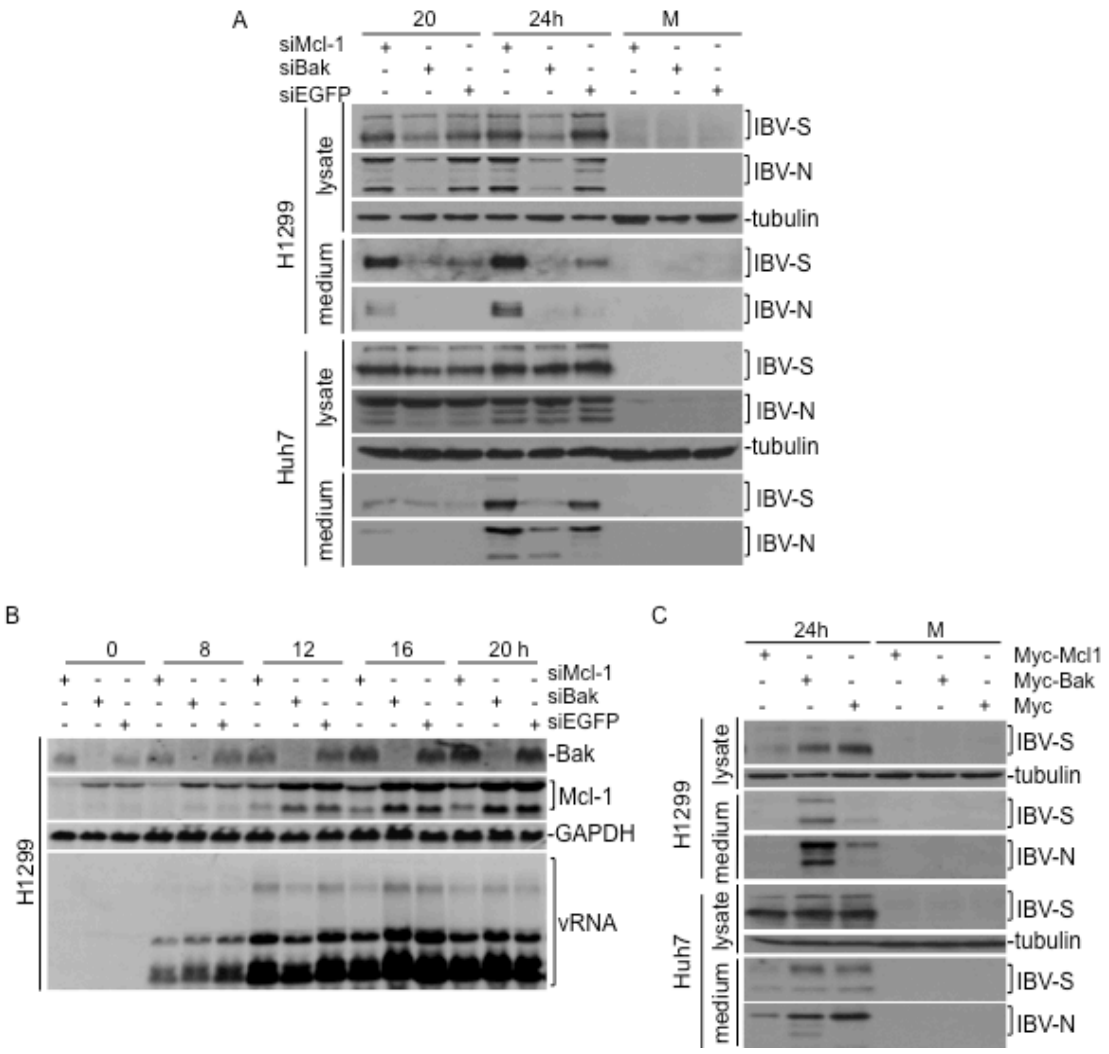
A
20
24h
M
siMcl-1
siBak
siEGFP
H1299
lysate
medium
Huh7
IBV-S
IBV-N
-tubulin
B
0
8
12
16
20 h
siMcl-1
siBak
siEGFP
-Bak
Mcl-1
-GAPDH
vRNA
H1299
C
24h
M
Myc-Mcl1
Myc-Bak
Myc
H1299
Huh7
lysate
medium
IBV-S
-tubulin
IBV-N

Figure 3-6

The effects of manipulation of the expression of Bak and Mcl-1 on the replication and transcription of IBV RNA and the synthesis of IBV proteins in mammalian cells.

(A) The effects of down-regulation of Bak and Mcl-1 by RNA interference on the synthesis of IBV proteins in mammalian cells. H1299 cells were transfected with siRNA duplexes targeting Mcl-1, Bak and EGFP, and infected with IBV at 72 hours post-transfection. The culture medium and cells were harvested separately for Western blot analysis, using specific antibodies for IBV-S and IBV-N and anti-tubulin as a loading control. M, mock infection.

(B) The effects of down-regulation of Bak and Mcl-1 by RNA interference on the replication and transcription of IBV RNA in mammalian cells. Cells were harvested for Northern blot analysis, using specific probes for Bak, Mcl-1 and the 3'-UTR of IBV, with a GAPDH probe as loading control.

(C) The effects of over-expression of Bak and Mcl-1 on the synthesis of IBV proteins in mammalian cells. H1299 (upper panel) and Huh7 cells (lower panel) were transfected with pXJ40-myc-Mcl-1, pXJ40-myc-Bak or pXJ40-myc empty vector and either mock-infected (M) or infected with IBV at 16 hours post-transfection. The culture medium and cells were harvested separately 24 hours post-infection, and western blot analysis was performed using the indicated specific antibodies, with anti-tubulin as a loading control.

3.3 DISCUSSION

In this study, global gene expression profiles have been first determined in IBV-infected Vero cells at 24 hours post-infection by Affymetrix array, revealing an up-regulation at the transcriptional level of both pro-apoptotic Bak and pro-survival Mcl-1. These results were further confirmed in IBV-infected chicken embryos and chicken fibroblast DF1 cells, as well as in mammalian cells such as H1299, Vero and Huh7 cells. As apoptosis is influenced, both positively and negatively, by a variety of genes including various members of the Bcl-2 gene family (Kim et al., 2006), up-regulation of Bak and Mcl-1 may play essential roles in maintaining the intricate balance between life and death of infected cells to ensure a successful infection cycle.

The data presented here show that IBV viral protein release was increased in cells with knockdown of the anti-apoptotic Mcl-1 protein, and in cells over-expressing the pro-apoptotic Bak protein. Likewise, PARP cleavage occurs earlier in cells depleted of Mcl-1, and in cells with elevated levels of Bak. This points to the importance of these two members of the Bcl-2 family in regulating IBV-induced apoptosis, especially at an early stage of infection. Mcl-1 and Bak also appear to be involved in regulating viral replication efficiency at late stages of infection, as a decrease in Mcl-1 expression levels and an increase in that of Bak promote virus progeny release. A tricky balance between the two may therefore be a key requisite in first maintaining the integrity of the host cell environment during infection before the conclusion of a triumphant infection cycle.

The expression profiles of Mcl-1 and Bak at the protein level demonstrated in this study appear to be differentially regulated by the efficiency of IBV replication in different host cells. In IBV-infected H1299 and Huh7 cells, Mcl-1 was shown to be gradually decreased at late time points. As explained earlier, Mcl-1 has a short half-life

as it undergoes polyubiquitination and subsequent proteasome degradation. The down-regulation observed during late stages of virus infection may be due to the rapid degradation of the protein. It also suggests that, unlike in Chlamydia trachomatis-infected cells (Rajalingam et al., 2008), IBV infection does not stabilize Mcl-1 protein, particularly in human cells. Another reason is that more efficient viral replication and infection are usually observed in these two cell lines, especially in Huh7 cells, compared to that in Vero cells, leading to the destruction of the monolayers and degradation of cellular RNAs.

Attempts to identify the viral component(s) that is responsible for up-regulation of Bak and Mcl-1 were made but without success. It is apparent that viral replication is required for the up-regulation of these two genes at the transcriptional level. As the UV-inactivated virus fails to induce the expression of the two proteins, it suggests that IBV structural proteins, at least at low concentration, do not play a direct role. In fact, transfection of individual IBV proteins into cells did not induce the expression of these two proteins (unpublished observations).

The complex of Mcl-1 and Bak in an otherwise healthy cell can be disrupted by various factors, including mitochondrial p53 (Ren et al., 2005) and other members of the Bcl-2 family (Pearce and Lyles, 2009). Mcl-1 activation can also be triggered by many signalling events, including MAPK pathways, PI3K/AKT pathway, growth factors and cell stress (Kim, Xu, and Reed, 2008; Li, Lee, and Lee, 2006; Puthalakath et al., 2007; Rajalingam et al., 2008). From the data presented here, it appears that the induction of Mcl-1 protein in IBV-infected cells is indeed affected by the activation of MEK and/or PI3K pathways, as well as by upstream activators such as the transcriptional regulator of ER-stress mediated apoptosis, GADD153. In a previous study, it has been shown that IBV infection induced the expression of GADD34 (Wang

et al., 2009), indicating activation of the double-stranded RNA- activated protein kinase-like ER kinase (PERK) branch of the unfolded protein response (UPR) in IBV-infected cells. The observed up-regulation of GADD153 in IBV-infected cells in this study would lend further support to this conclusion. ER stress also activates the inositol-requiring enzyme 1 (IRE1) branch of the UPR, which, other than its role in the cleavage and degradation of misfolded proteins, serves to transcriptionally up-regulate Mcl-1 through its downstream activation of the PI3k/Akt pathway (Dong et al., 2011; Jiang et al., 2008). The induction of Mcl-1, likely the consequence of a combination of viral RNA replication, protein synthesis and cellular signal cascades triggered by all these events, would then attenuate Bak activation and subsequent apoptosis.

CHAPTER 4. FUNCTIONAL CHARACTERIZATION OF MDA5, RIG-I AND MAVS IN IBV-INDUCED INNATE IMMUNITY AND APOPTOSIS

4.1 INTRODUCTION

Antiviral innate immunity begins with the recognition of conserved microbial 'non-self' motif products – PAMPs – by certain host proteins hailing from various pathogen recognition receptor families (Takeuchi and Akira, 2009; Wilkins and Gale, 2010). Among the different families of PRRs, the best studied are the Toll-like receptor family and the RNA helicase family (Kumar, Kawai, and Akira, 2009; Loo and Gale, 2011), although recent insights into the NOD-like receptor family and the IFIT family of proteins have also surfaced (Pichlmair et al., 2011; Werts et al., 2011).

The association between a PAMP and a PRR triggers PRR-dependent signalling pathways that eventually lead to the downstream activation of type I IFN, as well as of other inflammatory cytokines and chemokines (Takeuchi and Akira, 2010). As discussed previously in Chapter 1, Toll-like receptors are capable of recognizing and binding diverse viral sequence patterns at the cellular surface or in other organelle compartments such as the endosome. On the other hand, RIG-I-like receptors from the RNA helicase family of proteins are known to intervene in the recognition of pathogens in the cytosol. Either way, the recognition of viral DNA and/or RNA results in a structural modification of the PRR that leads to its activation, thereby driving the expression of type I IFNs (Garcia-Sastre and Biron, 2006), as well as the subsequent production of multiple ISGs (de Veer et al., 2001).

RNA viruses encompass at least four-fifths of all identified viruses and are known causations of a wide variety of infectious diseases (Lai and Holmes, 2001). While vastly diverse in terms of genome structure, infectivity and/or replicative tactics, RNA viruses exhibit conventional molecular patterns that can be recognized by members of the RIG-I-like receptor family, namely MDA5, RIG-I and LGP2 (Takeuchi and Akira, 2008; Yoneyama and Fujita, 2009). Briefly, the initial activation

of MDA5 and RIG-I through the binding of viral ligands lead to their interaction with the downstream adaptor protein MAVS via their respective CARD domains, and ultimately trigger the activation of transcription factors, IRF3 and NFκB, through the recruitment of signalling complexes (Takeuchi and Akira, 2008). Conflicting reports have arisen with regards to the function of LGP2. As it lacks a signalling CARD domain, it was initially proposed to be a repressor of antiviral signalling through the inhibition of RIG-I activation (Rothenfusser et al., 2005). However, recent reports have highlighted the ability of LGP2 to positively regulate viral RNA recognition through MDA5 and RIG-I signalling (Satoh et al., 2010). The function of LGP2 therefore remains controversial.

Other than the well-studied MHV, a group 2 coronavirus, little is known about the roles MDA5 and RIG-I might play in the recognition of the other coronaviruses. Although both PRRs have been indicated through transient RNA interference experiments to activate IRF3 and NFκB through the RLH signalling pathway in MHV (Li, Liu, and Zhang, 2010), Roth-Cross *et al.* has shown, with knockout mouse models, that MDA5 is the sole PRR that is responsible for the induction of type I IFN response in MHV-infected murine brain cells (Roth-Cross, Bender, and Weiss, 2008). Moreover, MDA5 and RIG-I have also been demonstrated to be involved in apoptotic signalling pathways that is independent of type I IFN response (Besch et al., 2009). As such, the potentiality of these two proteins in playing dual roles in both anti-coronaviral response and coronavirus-induced apoptosis is worth looking into.

In this study, the roles of MDA5 and RIG-I in IBV infection were examined through the characterization of MDA5 and RIG-I expression at both transcriptional and translational levels, as well as through RNAi knockdown and transient expression experiments, in IBV-infected cells. The role of their downstream adaptor, MAVS, was

also investigated through similar experiments, for a clearer understanding of the activation of RLH signalling components during IBV infection. While the data presented here is still fairly inconclusive with regards to the actual recognition of IBV by RIG-like helicase PRRs, perhaps due to the ability of coronaviruses to evade general recognition by host PRRs, the unveiling of RLH proteins as potentially divergent modulators of coronavirus-induced apoptosis was a surprising discovery. The cleavage of MAVS, too, has been found to concomitant with PARP cleavage during coronavirus-induced apoptosis in a caspase-dependent manner, and appears to be capable of modulation by members of the Bcl-2 family. Attempts to identify viral component(s) responsible for the modification of RLH signalling also highlighted the ability of IBV nsp15 to inhibit MAVS-mediated phosphoactivation of IRF3, which may explain the lack of significant interferon response initiated during IBV infection.

4.2 RESULTS

4.2.1 Affymetrix array analysis of innate immunity genes reveals up-regulation of MDA5 at the mRNA level in IBV-infected Vero cells

To explore the possible involvement, if any, of RLH signalling proteins in the regulation of IBV-induced apoptosis and viral pathogenesis, global gene expression profiles were first determined in Vero cells infected with IBV at an MOI of approximately 1 at 24 hours post-infection using Affymetrix array analysis, as described previously in Section 3.2.1 of Chapter 3. Highlighted in Table 4-2 is the up-regulated expression of various innate immunity genes detected in the array screen. In particular, a 3.4-fold induction of MDA5 was detected, while the apparent induction of RIG-I was not observed (Table 4-1).

Table 4-1 Affymetrix array analysis of the induction of various innate immunity genes in IBV-infected Vero cells at 24 hours post-infection.

Gene	**Accession Number**	**Induction fold**	**Description**
ISG20	NM_002201.2	64	Homo sapiens interferon stimulated gene (20kD)
DUSP6	BC003562.1	36.8	Dual specificity phosphatase 6
H174	AF002985.1	27.9	Homo sapiens putative alpha chemokine (H174)
SCYA3	NM_002983.1	19.7	Homo sapiens small inducible cytokine A3
MDA5	NM_022168.1	10.6	Homo sapiens melanoma differentiation associated protein-5
ISG15	NM_005101.1	6.5	Homo sapiens interferon-stimulated protein, 15 kDa
IL6	NM_000600.1	5.7	Homo sapiens interleukin 6 (interferon, beta 2)
DUSP1	NM_004417.2	5.7	Homo sapiens dual specificity phosphatase 1
IL12A	NM_000882.1	5.7	Homo sapiens interleukin 12A
IRF1	NM_002198.1	4	Homo sapiens interferon regulatory factor 1
IL8	NM_000584.1	4	Homo sapiens interleukin 8

4.2.2 IBV infection induces the expression of MDA5 and RIG-I in Vero and H1299 cells, and up-regulates only MDA5 in RIG-I deficient chicken embryos and chicken fibroblast cells

RT-PCR analysis of IBV-infected cells, followed by densitometry measurements, was carried out to study the expression of MDA5, RIG-I and IFNβ in IBV-infected cells at the transcriptional level. In Vero and H1299 cells infected with IBV at an MOI of 1, a significant increase in the expression of both MDA5 and RIG-I was observed at 16 and 24 hours post-infection with an increase in viral RNA expression as an indication of infection (Fig. 4-1A-B). The expression of IFNβ was also checked, and an increase was observed in infected H1299 cells (Fig. 4-1A). Vero cells lack functional IFNβ and thus do no exhibit IFNβ induction. Quantification of the corresponding bands by densitometry measurement showed a 1.93-1.83-fold, a 2.74-1.77-fold induction and a 1.92-1.95-fold induction of MDA5, RIG-I and IFNβ from 16-24 hours post-infection, respectively, in H1299 cells (Fig. 4-1A), and a 2.55-3.89-fold and a 6.89-11.28-fold induction of MDA5 and RIG-I from 16-24 hours post-infection, respectively, in Vero cells (Fig 4-1B). These results demonstrate that both MDA5 and RIG-I are up-regulated at the transcriptional level in IBV-infected Vero and H1299 cells. As such, although RIG-I induction was not observed in the Affymetrix array analysis (Table 4-1), this could be a case of false negatives.

In chicken fibroblast DF1 cells infected with IBV an MOI of 1, significant up-regulation of both MDA5 (3.40-22.26-fold) and IFNβ (2.53-48.62-fold) at the transcriptional level were also observed by RT-PCR analysis at 16 and 24 hours post-infection (Fig. 4-1C). The increase in expression levels of MDA5 (43.57-fold) and IFNβ (3.5-fold) in IBV-infected chicken embryos was observed as well (Fig. 4-1D). As the difference in GAPDH was quite significant (Fig. 4-1D), this increase

was also quantified by real-time PCR, which, after normalization to mock-infected chicken embryos, showed a 14.52- and 1.86-fold increase in MDA5 and IFNβ induction, respectively, at 72 hours post-infection. The expression of RIG-I was not detected in chicken cells, as was similarly reported by Barber *et al*., although RIG-I appears to be present in other fowl, such as ducks, as a natural form of innate immunity and confers pathological resistance in these animals (Barber et al., 2010).

The protein expression levels of MDA5 and RIG-I were also examined in H1299 cells infected with IBV at an MOI of 1. As the commercial antibodies for MDA5 and RIG-I purchased for this study detects only human proteins, Vero (monkey) cells were not tested in this experiment. Infected H1299 cells were harvested at 16, 20 and 24 hours post-infection, respectively, and the lysates obtained were subjected to Western blot analysis, followed by densitometry measurements. An increase in the expression of both MDA5 (1.35-1.18-fold) and RIG-I (1.19-1.36-fold) was observed from 16 to 20 hours post-infection (Fig 4-1E). However, the expression of both proteins declined at 24 hours post-infection with a corresponding decrease in IBV-S expression (Fig 4-1E). This could be due to a higher rate of infectivity that led to the death of infected cells, as evidenced by a slight decrease in the expression of the tubulin loading control (Fig 4-1E). It is also likely that full-length MDA5 might have undergone cleavage during virus infection, as shown by Barral *et al.*, although the commercial MDA5 antibody purchased for this study was unable to detect any of the smaller cleavage bands (Barral et al., 2007).

Together, these results confirm the up-regulation of MDA5 and RIG-I during coronavirus infection.

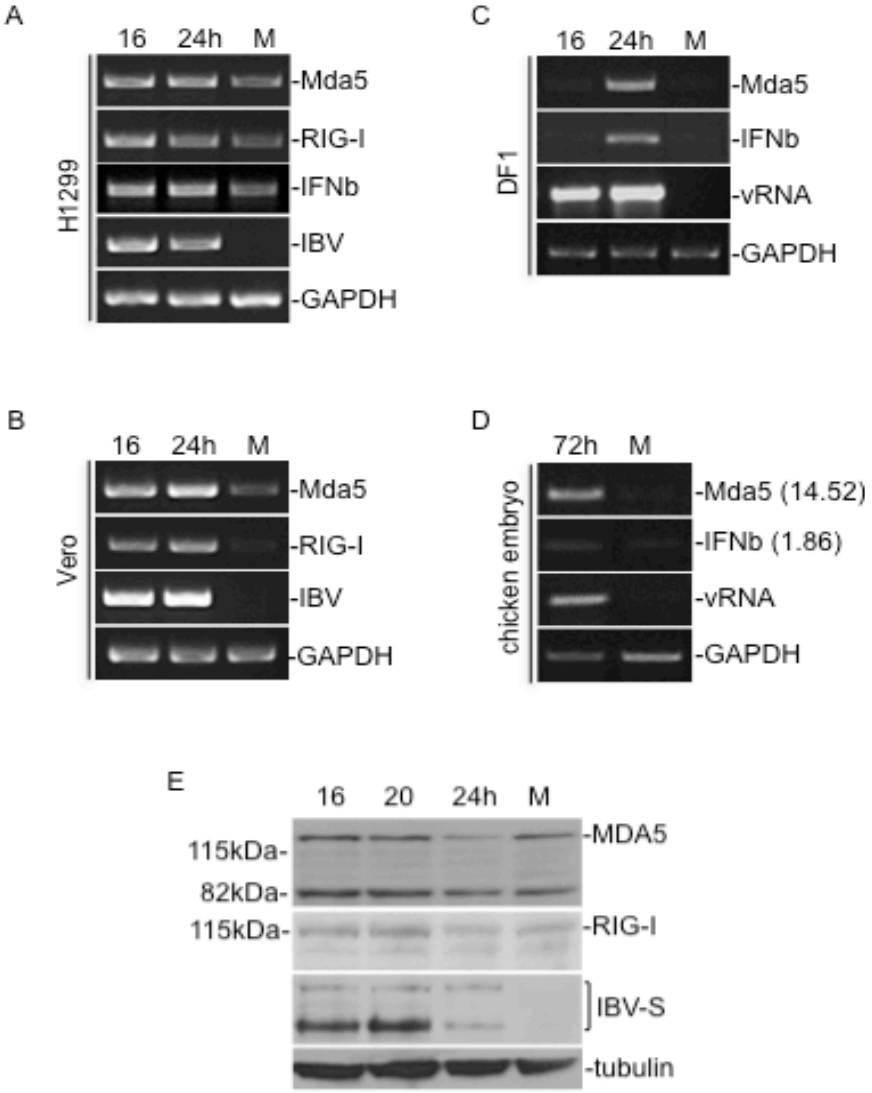
A
16
24h
M
H1299
-Mda5
-RIG-I
-IFNb
-IBV
-GAPDH
C
16
24h
M
DF1
-Mda5
-IFNb
-vRNA
-GAPDH
B
16
24h
M
Vero
-Mda5
-RIG-I
-IBV
-GAPDH
D
72h
M
chicken embryo
-Mda5 (14.52)
-IFNb (1.86)
-vRNA
-GAPDH
E
16
20
24h
M
115kDa-
82kDa-
-MDA5
115kDa-
-RIG-I
IBV-S
-tubulin

Figure 4-1

Analysis of the expression of MDA5, RIG-I and IFNβ in IBV-infected Vero and H1299 cells, chicken fibroblast DF1 cells and chicken embryos.

(A) H1299 cells were infected with IBV, harvested at 16 and 24 hours post-infection, and RNA extracted with TRIzol. RT-PCR analysis was performed with the indicated specific primers, with GAPDH as a loading control. M, mock.

(B) Vero cells were infected with IBV, harvested at 16 and 24 hours post-infection, and RNA extracted. RT-PCR analysis was performed with the indicated specific primers, with GAPDH as a loading control.

(C) Chicken fibroblast DF1 cells were infected with IBV, harvested at 16 and 24 hours post-infection and RNA extracted. RT-PCR analysis was carried out using specific primers for the indicated genes, with GAPDH as a loading control.

(D) 10-day-old chicken embryos were inoculated with either mock virus (M) or IBV (1000 plaque-forming units per egg) and kept in a 37^0C incubator for 72 hours. Total RNA was extracted from homogenized tissues and used for RT-PCR using specific primers as above (C).

(E) Western blot analysis of MDA5 and RIG-I expression at the translational level in IBV-infected mammalian cells. H1299 cells infected with IBV were harvested at 16, 20 and 24 hours post-infection, respectively, and cell lysates prepared. Western blot analysis was performed using specific antibodies as indicated, with anti-tubulin as a loading control. M, mock infection.

4.2.3 Manipulation of MDA5 and RIG-I by RNA interference regulates the expression of RLH signalling pathway downstream components during IBV infection in mammalian cells

To further investigate the roles, if any, MDA5 and RIG-I may play during IBV infection, these two genes were subjected to RNA interference with their respective siRNAs and the expression levels of various RLH signalling pathway components were checked, at both translational and transcriptional levels, in IBV-infected H1299 cells at 20 and 24 hours post-infection. The genes checked at the transcriptional level include LGP2, IFNβ and ISG56. A marked increase in the mRNA levels of RIG-I, LGP2 and ISG56 was observed with a corresponding decrease in MDA5 mRNA expression after its knockdown with siMDA5 interference (Fig. 4-2A, upper panels). Densitometry measurements showed a 1.13-1.74-fold increase in RIG-I, a 1.31-8.91-fold increase in LGP2, and a 1.05-4.29-fold increase in ISG56 mRNA levels, respectively. This also corresponded with a slightly lower expression of viral RNA (2.22-2.27-fold decrease) and a slightly higher IFNβ expression (0.89-1.36-fold increase) at 20 and 24 hours post-infection (Fig. 4-2A).

In IBV-infected RIG-I knockdown cells, the mRNA levels of MDA5, LGP2 and ISG56 were reduced (Fig. 4-2A). Densitometry measurements showed a 1.37-2.56-fold decrease in MDA5, a 1.22-3.13-fold decrease in LGP2 and a 1.52-7.69-fold decrease in IGS56, respectively. This corresponded with a slightly higher expression of viral RNA (0.99-1.32-fold increase) and declined levels of IFNβ mRNA (1.54-2.17-fold decrease) obtained at 20 and 24 hours post-infection. To confirm the results obtained for ISG56 and IFNβ, the relative mRNA expression of these two genes were checked quantitatively using real time PCR (Fig 4-2B). In IBV-infected H1299 cells, relative to mock-infected cells, a 1.52-fold increase in

ISG56 mRNA expression was observed in MDA5 knockdown cells at 20 hours post-infection, while a 6.10-fold and a 20-fold decrease were observed in RIG-I knockdown and control cells, respectively. At 24 hours post-infection, a 3.08-fold increase was observed in MDA5 knockdown cells, while a 11.1-fold and a 7.09-fold increase was observed in RIG-I knockdown and control cells, respectively. In the case of IFNβ, a 1.95-fold and 5.90-fold increase were observed in MDA5 knockdown cells at 20 and 24 hours post-infection, respectively, while a 3.09-fold decrease and a 1.34-fold increase, respectively, were observed in RIG-I knockdown cells at the same infection time points (Fig. 4-2C). A 1.34-fold decrease and 3.64-fold increase, respectively, in IFNβ expression was also observed in infected control cells at the same time points, compared to mock-infected cells (Fig. 4-2C). This implied that, while ISG56 mRNA expression levels were observed to increase at late stages of the infection, the rate of increase was greater in infected MDA5 knockdown cells, and lower in infected RIG-I knockdown cells, compared to infected control cells.

The efficiency of MDA5 and RIG-I knockdown by RNA interference at the translational level was also checked. Cells were transfected with siMDA5, siRIG-I or the control siEGFP for 72 hours, mock-infected or infected with IBV, and harvested at 20 and 24 hours post-infection for Western blot analysis. Only ISG56 was examined at the translational level; the commercial LGP2 and IFNβ antibodies bought for this study did not appear to work as no bands were obtained. Densitometry measurements showed a 43-99% knockdown efficiency in MDA5 and a 76-87% knockdown efficiency was obtained for RIG-I (Fig. 4-2A, lower panels). ISG56 expression was low across the board, although a marginal increase in ISG56 was observed in both MDA5 (0.87-1.53-fold) and RIG-I (0.68-1.67-fold) knockdown cells (Fig. 4-2A, lower panels). No significant difference was observed in the production of viral proteins

among the different knockdown cells. Specifically, a 1.02-1.28-fold increase and a 1.16-1.23-fold increase in IBV-S were observed in MDA5 knockdown and RIG-I knockdown cells, respectively (Fig. 4-2A, lower panels).

These results together appear to imply a more significant regulation of downstream components of the RLH signalling pathway, by MDA5 and RIG-I, at the transcriptional level. A decrease in MDA5 expression saw a corresponding increase in the levels of RIG-I, LGP2 and ISG56 expression, which concomitantly act to augment the antiviral response induced against IBV infection and consequently reduced viral RNA expression levels. In contrast, a decrease in RIG-I expression resulted in a corresponding decrease in MDA5, LGP2 and ISG56 expression levels, which subsequently failed to keep IBV infection at bay and resulted in a greater amount of viral RNA production. However, despite a high efficiency of MDA5 and RIG-I knockdown at the protein level, no variable differences were observed in ISG56 protein expression as well as the production of IBV-S protein. This is probably due in part to the indiscernible difference in MDA5 expression between infected siRIG-I knockdown cells and control cells, as well as in RIG-I expression between infected siMDA5 knockdown and control cells. As such, the induction of an antiviral reaction in response to IBV infection, at least on a transcriptional level, appears to be largely dependent on the up-regulation of either MDA5 or RIG-I.

A

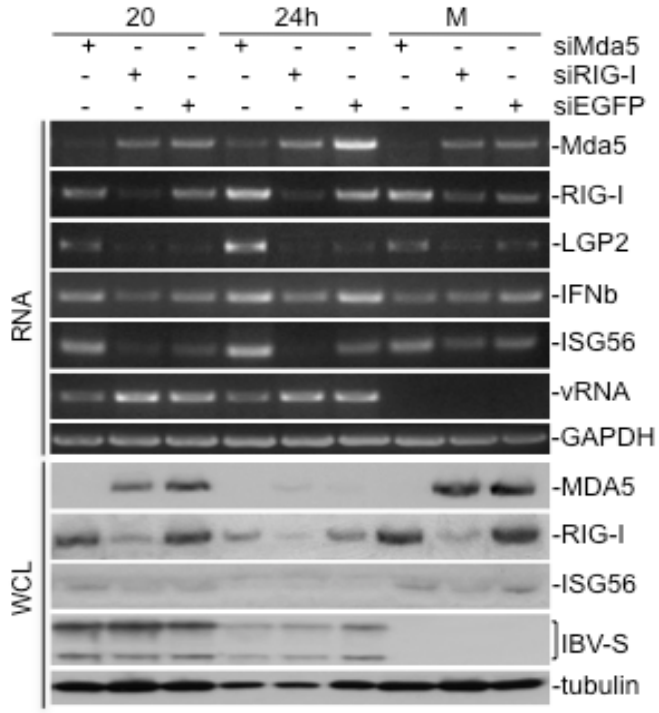
20
24h
M
siMda5
siRIG-I
siEGFP
RNA
-Mda5
-RIG-I
-LGP2
-IFNb
-ISG56
-vRNA
-GAPDH
WCL
-MDA5
-RIG-I
-ISG56
IBV-S
-tubulin

B

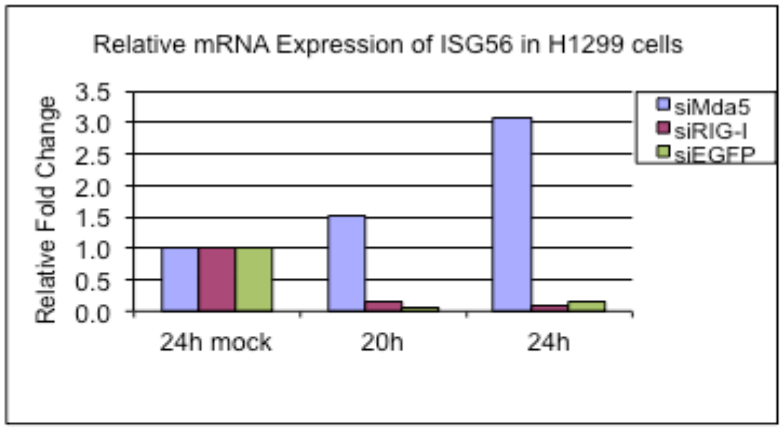
Relative mRNA Expression of ISG56 in H1299 cells
Relative Fold Change
3.5
3.0
2.5
2.0
1.5
1.0
0.5
0.0
24h mock
20h
24h
siMda5
siRIG-I
siEGFP

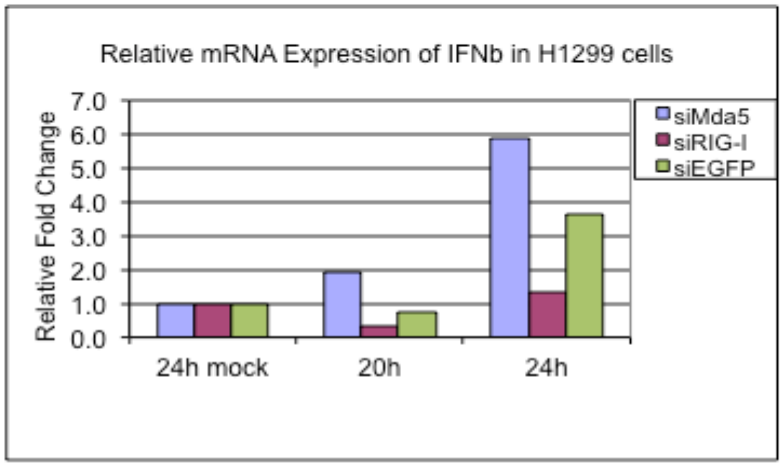
Relative mRNA Expression of IFNb in H1299 cells
Relative Fold Change
7.0
6.0
5.0
4.0
3.0
2.0
1.0
0.0
24h mock
20h
24h
siMda5
siRIG-I
siEGFP

Figure 4-2

The effects of manipulation of the expression of MDA5 and RIG-I in mammalian cells on the regulation of downstream RLH signalling pathway components.

(A) RT-PCR analysis (upper panels) and Western blot analysis (lower panels) of the effects of down-regulation of MDA5 and RIG-I by RNA interference in mammalian cells on the regulation of RLH signalling pathway. H1299 cells were transfected with siRNA duplexes targeting MDA5, RIG-I or control EGFP. At 72 hours post-transfection, cells were infected with IBV and total RNA, or total cell lysates, was extracted at 20 and 24 hours post-infection for RT-PCR and Western blot analyses, respectively. RT-PCR analysis was performed with specific primers for the indicated different genes, with GAPDH as a loading control. Western blot analysis was performed using the indicated specific antibodies, with anti-tubulin as a loading control. M, mock infection.

(B) Quantitative real-time PCR analysis of the effects of down-regulation of MDA5 and RIG by RNA interference in mammalian cells on the regulation of ISG56 and IFNβ. H1299 cells were transfected with siRNA duplexes targeting MDA5, RIG-I or control EGFP. At 72 hours post-transfection, cells were infected with IBV and RNA extracted at 20 and 24 hours post-infection for real-time PCR using specific primers for the indicated genes. Results are normalized to mock-infected (24h mock) cells.

4.2.4 Manipulation of MDA5 by RNA interference in the absence of IFNβ regulates the expression of RLH signalling pathway downstream component ISG56 during IBV infection in IFNβ-null mammalian cells

To investigate the roles, if any, that MDA5 and RIG-I may play in the activation of downstream IFN responses during IBV infection, the effect of a decrease in MDA5 and/or RIG-I levels in the absence of functional IFNβ was also examined. MDA5 and RIG-I were subjected to RNA interference with their respective siRNAs and ISG56 expression was checked at the transcriptional level, in mock infected or IBV-infected IFNβ-null Vero cells at 24 hours post-infection. LGP2 could not be detected despite multiple attempts. The knockdown efficiency of MDA5 was 78% and 92%, while that of RIG-I knockdown was between 28% and 30% (Fig. 4-3A). While there was no discernible difference in the expression level of ISG56 between infected RIG-I knockdown and control cells, a significant 0.93-fold decrease in ISG56 mRNA level was observed in infected siMDA5 cells (Fig. 4-3A). Despite numerous attempts, ISG56 was not detected at the protein level, as the commercial ISG56 antibody appeared to detect only human ISG56 protein. As such, a more quantitative measurement of the relative fold change in ISG56 mRNA was performed via real time PCR analysis. Compared to infected RIG-I knockdown cells (147-fold increase) and infected control cells (100-fold increase), only a marginal increase in ISG56 mRNA expression was observed (17.7-fold increase) in MDA5 knockdown cells (Fig 4-3B). The knockdown efficiencies of MDA5 (83%-98%) and RIG-I (21%-24%) were also quantitatively checked (Fig. 4-3C).

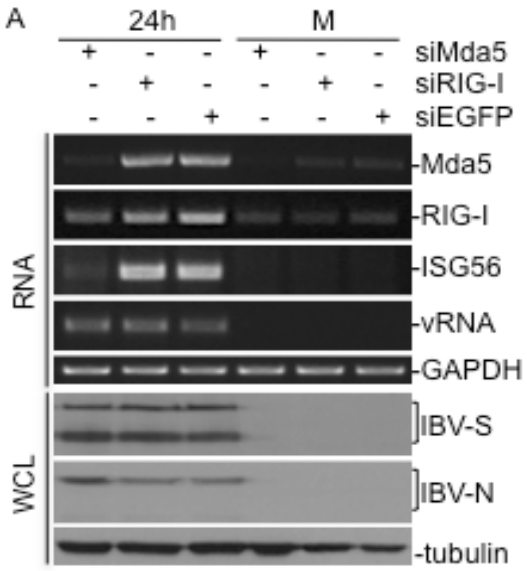
A
24h
M
+ - - + - - siMda5
- + - - + - siRIG-I
- - + - - + siEGFP
RNA
Mda5
RIG-I
ISG56
vRNA
GAPDH
WCL
IBV-S
IBV-N
-tubulin

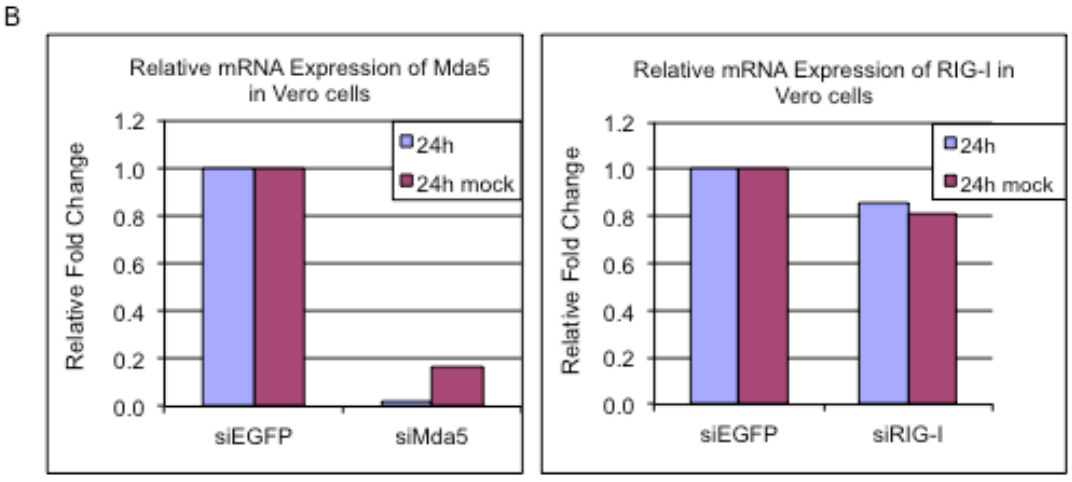
B
Relative mRNA Expression of Mda5 in Vero cells
Relative Fold Change
1.2
1.0
0.8
0.6
0.4
0.2
0.0
24h
24h mock
siEGFP
siMda5
Relative mRNA Expression of RIG-I in Vero cells
Relative Fold Change
1.2
1.0
0.8
0.6
0.4
0.2
0.0
24h
24h mock
siEGFP
siRIG-I

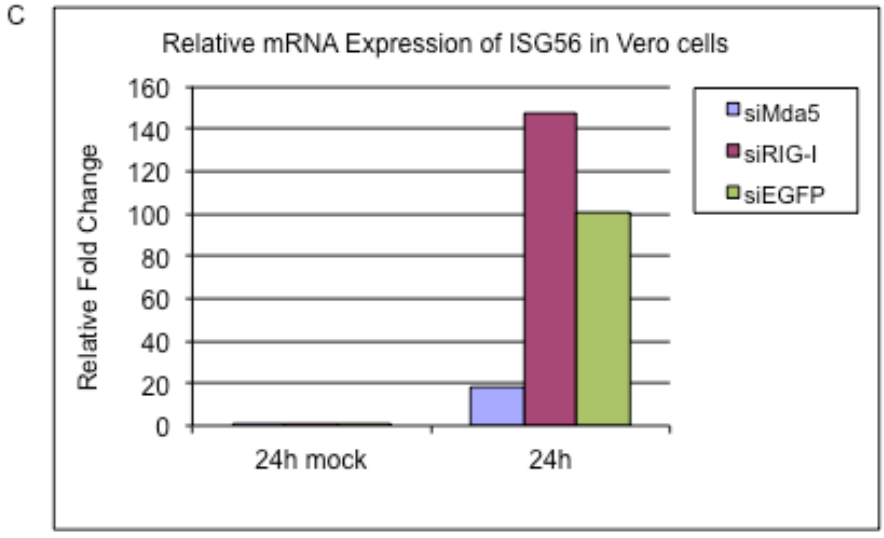
C
Relative mRNA Expression of ISG56 in Vero cells
Relative Fold Change
160
140
120
100
80
60
40
20
0
siMda5
siRIG-I
siEGFP
24h mock
24h

Figure 4-3

The effects of manipulation of the expression of MDA5 and RIG-I in mammalian cells on the regulation of downstream RLH signalling pathway component IGS56 in the absence of functional IFNβ.

(A) RT-PCR analysis of the effects of down-regulation of MDA5 and RIG-I by RNA interference in Vero cells on the regulation of ISG56. Vero cells were transfected with siRNA duplexes targeting MDA5, RIG-I or control EGFP. At 72 hours post-transfection, cells were either mock-infected, or infected with IBV. Total RNA was extracted at 24 hours post-infection for RT-PCR analysis. RT-PCR analysis was performed with specific primers for the indicated different genes, with GAPDH as a loading control. M, mock infection.

(B) Quantitative real-time PCR analysis of the effects of down-regulation of MDA5 and RIG by RNA interference in Vero cells on the regulation of ISG56. Vero cells were transfected with siRNA duplexes targeting MDA5, RIG-I or control EGFP. Total RNA extracted in (A) was used for qRT-PCR, using specific primers for ISG56. Results are normalized to mock-infected (24h mock) cells.

(C) Quantitative real-time PCR analysis of knockdown efficiencies of MDA5 and RIG by RNA interference in Vero cells. Vero cells were transfected with siRNA duplexes targeting MDA5, RIG-I or control EGFP. Total RNA extracted in (A) was used for qRT-PCR using specific primers for MDA5 and RIG-I, respectively. Results are normalized to mock-infected (24h mock) cells.

4.2.5 MDA5 and RIG-I may have opposing roles in the regulation of coronavirus replication and viral progeny release during the late stages of infection

The effects of MDA5 and RIG-I knockdown by RNA interference on IBV RNA replication were checked. MDA5 and RIG-I knockdown, as well as control EGFP knockdown H1299 cells infected with IBV at an MOI of 1 and harvested at various time points from 0 to 20 hours post-infection. Total RNA was extracted for Northern blot analysis, followed by densitometry measurements. No consistent trends of viral RNA regulation was observed in MDA5 and RIG-I knockdown cells infected with IBV compared to siEGFP control cells (Fig. 4-4A) at 0-12 hours post-infection, an indication that neither MDA5 nor RIG-I instigated much effect on the replication and transcription of IBV RNA during the early stages of infection. The observed minor variations among different samples may be caused by experimental factors. Surprisingly, however, MDA5 knockdown cells exhibited a slightly lower rate of virus replication compared to control cells at 16 and 20 hours post-infection, while the opposite was observed in RIG-I knockdown cells at the same infection time points, where a higher rate of virus replication was observed compared to infected control cells (Fig. 4-4A, mRNA2).

To confirm these results, the respective effects of MDA5 and RIG-I knockdown on virus activity were also studied through a virus luciferase assay, where viral luciferase activity was monitored by infecting MDA5, RIG-I and EGFP knockdown cells with recombinant IBV stably carrying and expressing luciferase. An decrease in luciferase activity was observed in MDA5 knockdown cells infected with IBV-luc at 12, 16 and 24 hours post-infection, and an increase in luciferase activity was similarly observed in RIG-I knockdown cells at the same infection time points, as compared with control cells (Fig 4-4B).

Plaque assays were also performed to determine infectious virus titre in the knockdown cells. A representative plate for the comparison of the virus titre among the knockdown cells at 24 hours post-infection is shown in Fig. 4-4C, while the virus growth kinetics are calculated on a logarithmic scale (Fig. 4-4D). The virus titre in MDA5 knockdown cells at 20 hours post-infection was 8.0 x 10^4 pfu/ml, compared to 1.13 x 10^5 pfu/ml in siEGFP control cells, and 4.0 x 10^4 pfu/ml at 24 hours post-infection, compared to 6.6 x 10^4 pfu/ml in siEGFP control cells. This corresponds to a 1.41-and 1.65-fold decrease, respectively, over control cells. Virus titres in RIG-I knockdown cells are 1.87 x 10^5 pfu/ml and 1.07 x 10^5 pfu/ml at 20 and 24 hours post-infection, respectively. This corresponds to a 1.65- and 1.62-fold increase, respectively, over control cells.

For the examination of the effects of MDA5 and RIG-I knockdown on IBV replication and release, Western blot analysis and densitometry measurements of IBV S protein in total cell lysates and IBV S and IBV N proteins in culture medium were performed. While the release of viral protein/particles were enhanced with a decrease in levels of RIG-I at 20 hours post-infection, the release of viral protein/particles decreased with decreased expression levels of MDA5 and RIG-I at 24 hours post-infection, compared to that in control cells. IBV S protein expression level in total cell lysates in MDA5 and RIGPI knockdown cells were also largely comparable with siEGFP-transfected cells at 20 and 24 hours post-infection (Fig. 4-4E).

While these results show that MDA5 and RIG-I may possess opposing roles in the control of virus activity and the production and release of viral progeny, it is more plausible that other factors may participate in this complex network of virus regulation, and as such may tilt the scales in favour of either better host survival or enhanced virus replication, depending the balance of the involved constituents.

A

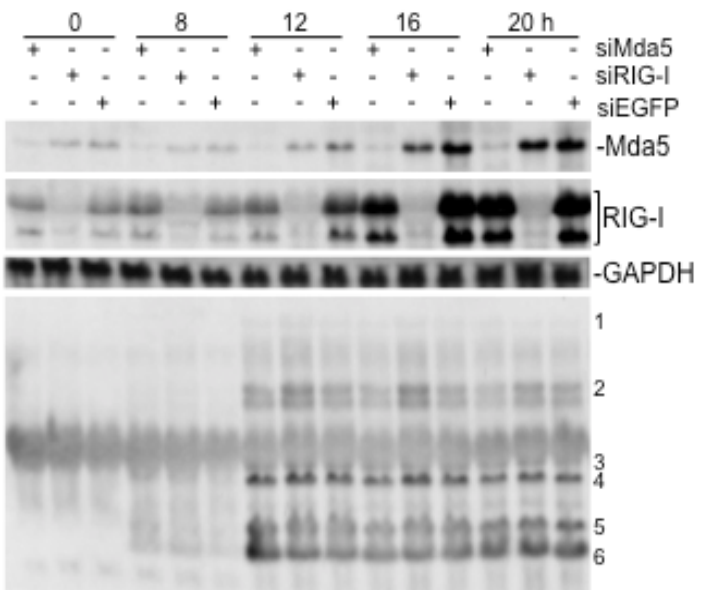
0
8
12
16
20 h
siMda5
siRIG-I
siEGFP
-Mda5
RIG-I
-GAPDH
1
2
3
4
5
6

B

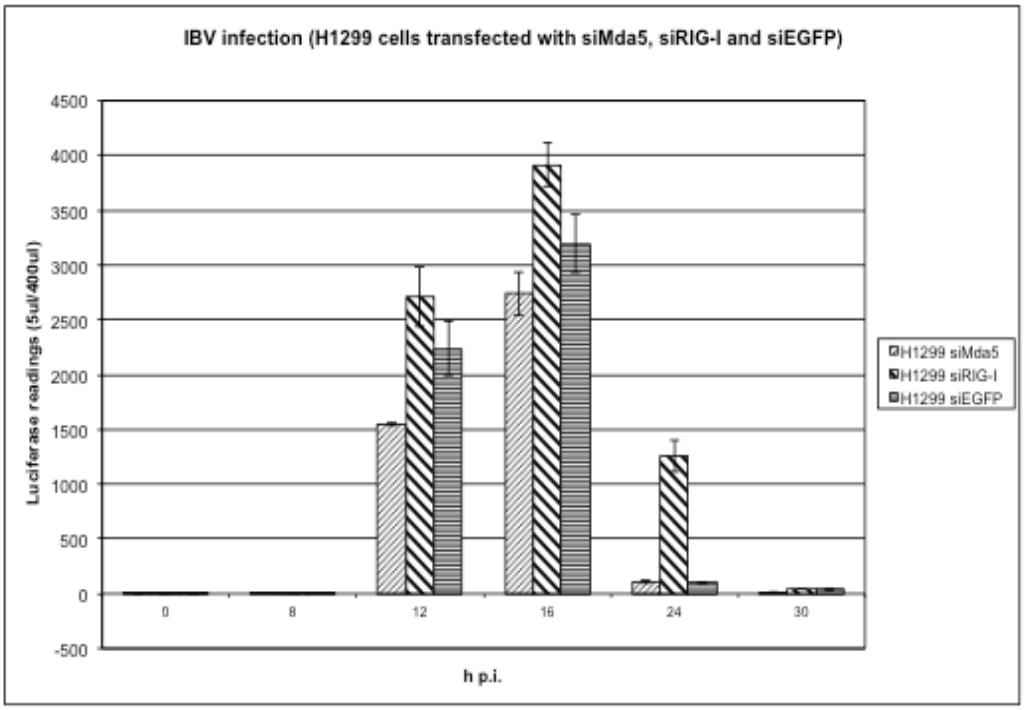
IBV infection (H1299 cells transfected with siMda5, siRIG-I and siEGFP)
Luciferase readings (5ul/400ul)
4500
4000
3500
3000
2500
2000
1500
1000
500
0
-500
0
8
12
16
24
30
h p.i.
H1299 siMda5
H1299 siRIG-I
H1299 siEGFP

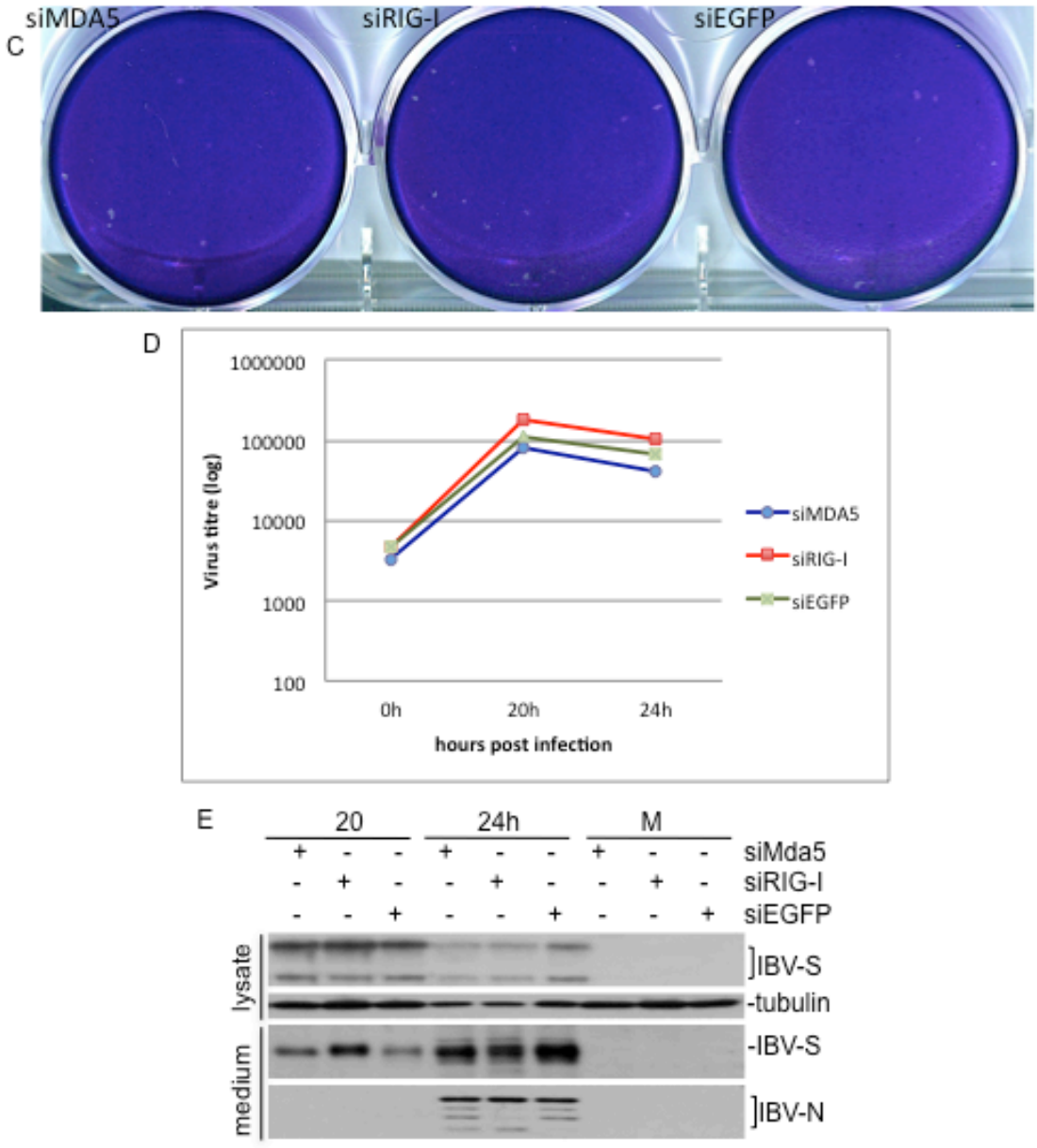

Figure 4-4

The effects of down-regulation of MDA5 and RIG-I by RNA interference in mammalian cells on virus activity, the production of progeny viruses and the production of viral proteins.

(A) The effects of down-regulation of MDA5 and RIG-I by RNA interference on the replication and transcription of IBV RNA in mammalian cells. H1299 cells were harvested for Northern blot analysis, using specific probes for MDA5, RIG-I and the 3'-UTR of IBV, with a GAPDH probe as loading control.

(B) Luciferase assay. H1299 cells were transfected with siRNA duplexes targeting MDA5, RIG-I and EGFP for 72 hours and subsequently either mock-infected (M), or infected with IBV-luc. The cells were lysed at 0, 8, 12, 16, 24 and 30 hours post-infection and checked for luciferase activity.

(C) A representative comparison of the plaque numbers between siMDA5-, siRIG-I- and siEGFP-infected H1299 cells, respectively, at 20h post-infection. At 72 hours post-transfection, cells were infected with IBV, frozen down at 0, 20 and 24 hours post-infection, and subsequently freeze-thawed three times. These were used to infect confluent monolayers of Vero cells grown on 6-well plates in the presence of 0.5% CMC for 3 days, after which the cells were fixed with 4% formaldehyde and stained with 0.1% toluidine blue for the visualization of viral plaques and calculation of plaque forming units.

(D) Comparison of virus growth kinetics (in logarithmic scale) in siMDA5-, siRIG-I- and siEGFP-infected H1299 cells, respectively.

(E) The effects of down-regulation of MDA5 and RIG-I by RNA interference on the synthesis of IBV proteins in mammalian cells. H1299 cells were transfected with siRNA duplexes targeting MDA5, RIG-I and EGFP, and infected with IBV at 72 hours post-transfection. The culture medium and cells were harvested separately for Western blot analysis, using specific antibodies for IBV-S and IBV-N and anti-tubulin as a loading control. M, mock infection.

4.2.6 Transient expression of MDA5 and RIG-I regulates the expression of ISG56 during IBV infection

The regulatory effects of MDA5 and RIG-I on IBV-induced apoptosis were further studied by transient expression of MDA5 and RIG-I in mammalian cells. For this purpose, both Flag-tagged MDA5 and Flag-tagged RIG-I were constructed and transfected into H1299, using an empty vector (pXJ40-Flag) as a negative transfection control. The cells were then infected with IBV at an MOI of 1. At 24 hours post-infection, ISG56 protein levels in infected cells transiently expressing MDA5 (1.11-fold decrease) was similar to that in infected control cells (Fig. 4-5). On the other hand, ISG56 protein levels in infected cells transiently expressing RIG-I were slightly higher (1.34-fold increase) than that in infected control cells (Fig. 4-5). This also could be due in part to an increase in MDA5 expression (3.47-fold increase) in cells transiently expressing RIG-I (Fig. 4-5). Taken together, this suggests a concerted effort by both MDA5 and RIG-I in activating their downstream IFN-induced genes like ISG56.

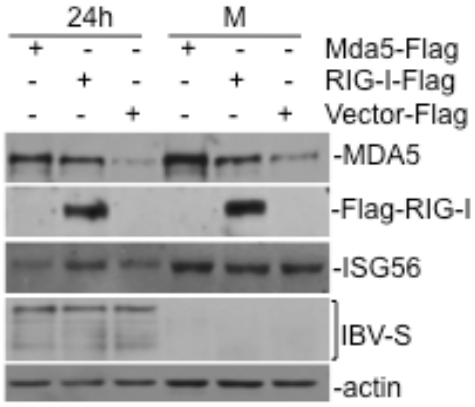

Figure 4-5

The effects of transient MDA5 and/or RIG-I expression in mammalian cells on IBV-induced ISG56 expression. H1299 cells were transfected with pXJ40-Flag-MDA5, pXJ40-Flag-RIG-I or pXJ40-Flag empty vector and either mock-infected (M) or infected with IBV at 16 hours post-transfection. Cells were harvested 24 hours post-infection and western blot analysis was performed using the indicated specific antibodies, with anti-actin as a loading control.

4.2.7 Identification of MDA5 or RIG-I PAMP RNAs in IBV-infected H1299 cells through IFNβ reporter assay

As previous protein and RNA analyses did not yield clear indications whether MDA5 or RIG-I sufficiently recognizes IBV to induce downstream IFN responses, an attempt was made to identify MDA5 or RIG-I PAMPs, if any, in IBV RNA, through a modified IFNβ reporter assay devised from an earlier report by Saito *et al*. (Saito et al., 2008). The induction of IFNβ promoter was first examined in H1299-R-luc cells transiently expressing either MDA5, RIG-I or control empty vector pXJ40 that is co-transfected with an IFNβ firefly reporter, and further transfected 16 hours later, individually, with: (i) 5 different IBV RNA fragments, obtained from *in vitro* transcription and labelled IBV A-E according to their respective positions in the IBV RNA genome; (ii) purified full-length IBV RNA, obtained from sucrose cushion centrifugation; (iii) IBV 3'UTR RNA, in both single strand and double strand forms; and (iv) poly(I:C) as a positive control for IFNβ induction. The nucleotide numbers of the IBV fragments, together with their respective protein coding regions, are presented in Table 4-2. IFNβ induction was examined by dual luciferase assay using a plate reader, and the results were normalized to renilla luciferase readings for cell number control. Surprisingly, the same trend was observed in H1299 cells transiently expressing either MDA5 and RIG-I; little or no IFNβ induction was observed in IBV fragments IBV-A, -B and -D, as well as in total IBV RNA, while higher levels of IFNβ induction were observed in IBV RNA constructs IBV-C and IBV-E, as well as in the 3'UTR (Fig. 4-6A). While poly(I:C) was initially thought to induce downstream IFN response through MDA5, a shorter length of poly(I:C) is able to switch allegiance from MDA5 to RIG-I as its preferred PRR (Kato et al., 2008), which may account for the higher levels of IFN activity observed in cells co-expressing RIG-I than in those

co-expressing MDA5 (Fig. 4-6A). These results were further confirmed in qRT-PCR (Fig. 4-6B) and RT-PCR (Fig. 4-6C) assays. In particular, IBV-D and total IBV RNA appeared to be able to 'evade' recognition by either MDA5 or RIG-I, exhibiting 11.1-50-fold decrease in IFNβ induction when compared to positive control poly(I:C) in the qRT-PCR assay (Fig. 4-6B), and showing a fold decrease of between 1.67-fold (transient RIG-I expression) and 2-fold (transient MDA5 expression) in the induction of IFNβ for IBV-D, and a 5-fold decrease in the same for total IBV RNA in the RT-PCR assay (Fig. 4-6C).

Taken together, these data suggest the possibility that both MDA5 and RIG-I may be capable of recognizing IBV RNA through the identification of certain PAMPs that may be present in various segments of the virus genome, specifically in the regions of IBV-C and IBV-E, that ultimately results in IFNβ induction. The evidence presented also supports the strong likelihood of certain IBV viral proteins, especially those from the IBV-D segment of the virus genome, in possessing the ability to evolve evasion strategies to escape recognition by PRRs.

Table 4-2 A list of IBV RNA constructs with the name of their respective vectors, respective nucleotide sizes and individual protein coding regions used in the IFNβ reporter assay.

IBV RNA construct	Fragment region	Non-structural/Structural/ Accessory proteins (in order of sequence)
pKTO-IBV-A	1 - 5752	5'UTR; Nsp2; Nsp3
pGEM-IBV-B	5748 - 8694	Nsps-3; -4; -5
pXL-IBV-C	8689 - 15532	Nsps-5; -6; -7; -8; -9; -10; -12; -13
pGEM-IBV-D	15511 - 20930	Nsps-13; -14; -15; -16; IBV-S
pXL-IBV-E	20887 - 27614	IBV-S; 3a3b (accessory); IBV-E; IBV-M; 5a5b (accessory); IBV-N; 3'UTR
3'UTR ssRNA	27102 - 27614	3’UTR
3'UTR dsRNA	1 - 63 + 27109 - 27614	3’UTR with leader sequence
Viral RNA (full length)	1 - 27611	

A

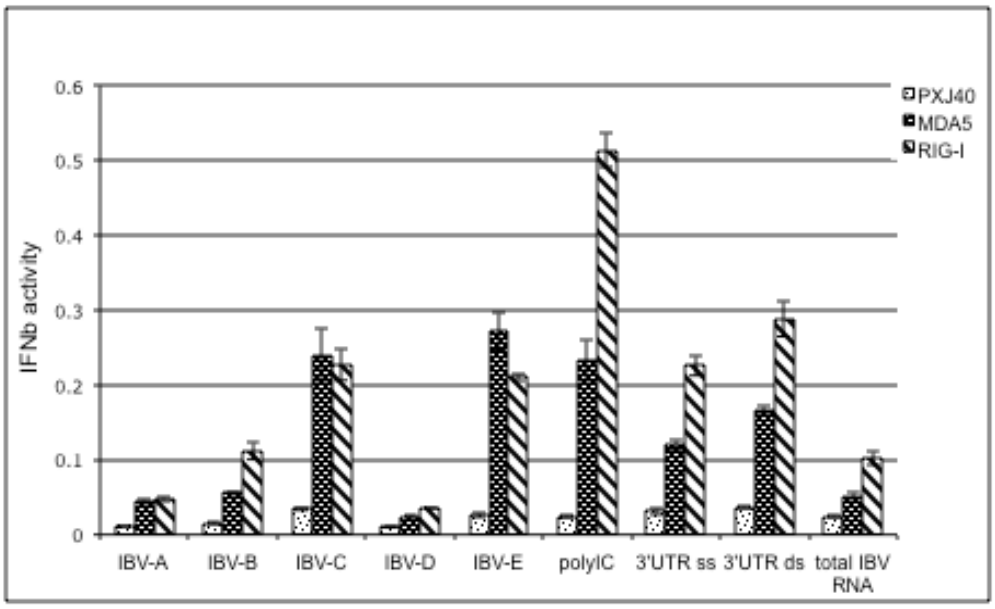

B

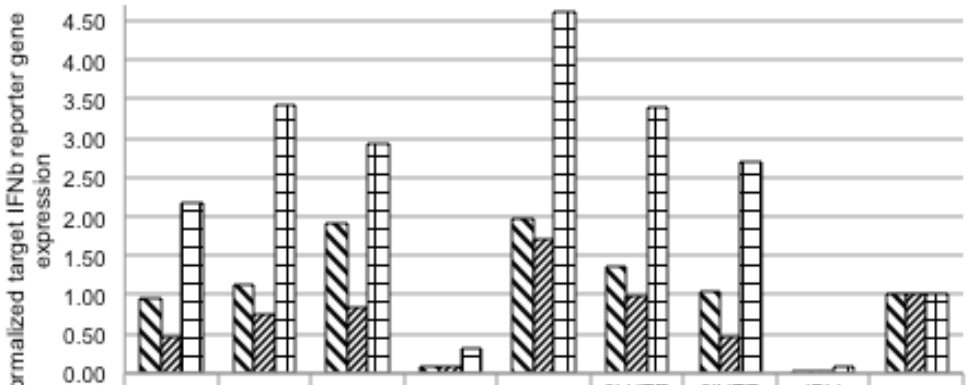

	IBV A	IBV B	IBV C	IBV D	IBV E	3' UTR SS	3'UTR DS	IBV vRNA	poly:IC
MDA5	0.97	1.14	1.91	0.08	1.97	1.36	1.03	0.02	1
RIG-I	0.46	0.74	0.83	0.09	1.71	0.99	0.47	0.03	1
PXJ	2.19	3.41	2.93	0.33	4.61	3.40	2.69	0.07	1

C

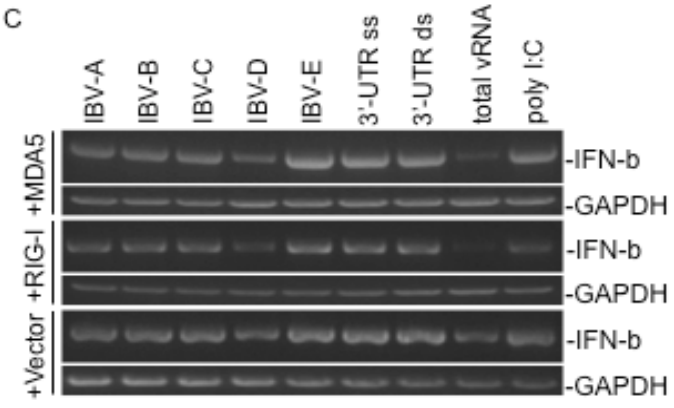

Figure 4-6

The identification of PAMP RNA in IBV RNA constructs.

(A) RNA-induced IFNβ promoter firefly luciferase activity in H1299-R-luc cells, shown as mean fold induction normalized to renilla luciferase activity in H1299-R-luc cells. H1299-R-luc cells were first co-transfected with 0.1ug of IFNβ reporter and 0.1ug of either MDA5, RIG-I or control constructs, then subsequently transfected with either 0.3ug (1 pmol) of total IBV RNA, 0.3ug of poly(I:C) RNA (positive control) or with 0.3ug of the indicated IBV RNA constructs 16 h later, and harvested for dual luciferase assay the next day.

(B) RNA-induced IFNβ gene expression in H1299 cells, shown as relative fold change normalized to loading control GAPDH and positive control poly(I:C). H1299 cells were transfected with the respective constructs as in (A), and harvested for RNA extraction and subsequent reverse transcriptase for qRT-PCR analysis with specific primers for IFNβ.

(C) RNA-induced IFNβ gene expression in H1299 cells, shown as semi-quantitative PCR bands. H1299 cells were transfected with the indicated constructs as in (A), and harvested for RNA extraction and subsequent RT-PCR with specific primers for IFNβ and GAPDH (loading control).

4.2.8 Transient expression of RLH signalling pathway downstream adaptor MAVS inhibits viral protein expression

While the transient expression of MDA5 and RIG-I did not appear to have significant effects on the expression of viral proteins (Fig. 4-5) or the recognition of total viral RNA (Fig. 4-6), it is not known whether their downstream signalling adaptor MAVS would have a similar effect on IBV-infected cells. Many reports, however, have highlighted the role of MAVS in controlling infection by viruses such as West Nile virus (Suthar et al., 2010) and HCV (Meylan et al., 2005). To confirm if this is the case in IBV, H1299 cells were transfected either with MDA5, RIG-I or MAVS constructs, and mock- or IBV-infected 16 hours post-transfection. Cells were harvested 16 hours post-infection for Western blot analysis. The results obtained showed a significant decrease in IBV-S protein expression with an increased expression of MAVS in IBV-infected H1299 cells, although the production of IBV-S protein in infected cells transiently expressing MDA5 and RIG-I were not notably affected (Fig. 4-7A).

H1299 cells transiently expressing MDA5, RIG-I or MAVS were also infected with IBV-luc and harvested at 16h post-infection for luciferase assay to check virus activity. Infected cells transiently expressing the negative control pXJ40-empty vector, MDA5 or RIG-I, respectively, were observed under the microscope to exhibit obvious CPE typical of an IBV infection (Fig. 4-8B), while no CPE was observed in infected cells transiently expressing positive control poly(I:C) or MAVS, respectively (Fig. 4-7B). The luciferase assay performed was normalized to the negative control pXJ40 vector (100%). Cells transiently expressing RIG-I showed an increase in IBV activity (1.1-fold increase) and viral activity was slightly decreased in cells transiently expressing MDA5 (1.11-fold decrease), and little or no viral activity was observed in

infected cells transiently expressing either poly(I:C) or MAVS (Fig. 4-7C).

Together, this implies an essential role MAVS plays in regulating anti-coronaviral innate immune responses, although the virus possibly has devised certain strategies to thwart recognition by MDA5 and RIG-I, as shown in section 4.2.7.

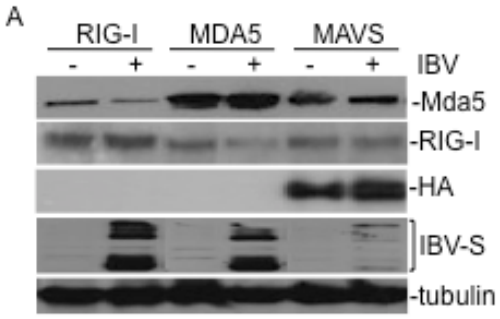
A
RIG-I
MDA5
MAVS
- + - + - +
IBV
-Mda5
-RIG-I
-HA
IBV-S
-tubulin

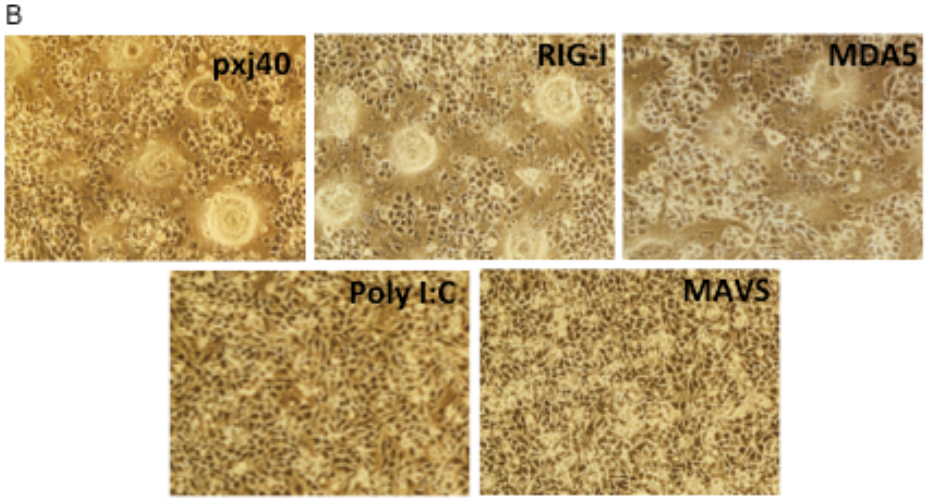
B
pxj40
RIG-I
MDA5
Poly I:C
MAVS

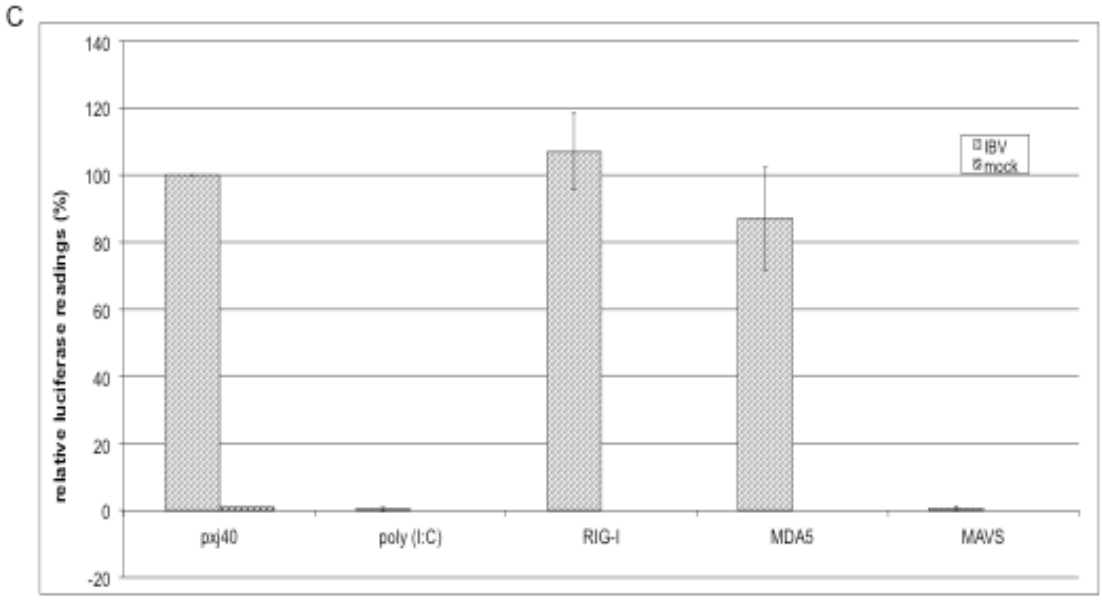
C
relative luciferase readings (%)
140
120
100
80
60
40
20
0
-20
IBV
mock
pxj40
poly (I:C)
RIG-I
MDA5
MAVS

Figure 4-7

The effects of the transient expression of MDA5, RIG-I and MAVS in mammalian cells on IBV protein expression.

(A) H1299 cells were transfected with pXJ40-Flag-MDA5, pXJ40-Flag-RIG-I or pXJ40-HA-MAVS and either mock-infected (-) or infected with IBV (+) at 16 hours post-transfection. Cells were harvested 16 hours post-infection and western blot analysis was performed using the indicated specific antibodies, with anti-HA tag as a positive identification of HA-MAVS expression and anti-tubulin as a loading control.

(B) H1299 cells were transfected with pXJ40-empty vector, pXJ40-Flag-MDA5, pXJ40-Flag-RIG-I, pjx40-HA-MAVS, or poly(I:C) and infected with IBV-luc at 16 hours post-transfection. Cells were observed under a phase-contrast microscope at 16 hours post-infection.

(C) Transfected and infected H1299 cells as above in (B) were harvested at 16 hours post-infection with 1x passive lysis buffer and subjected to luciferase assay using a single luciferase kit from Promega, according to the manufacturer's instructions. Experiments were repeated thrice, and the data obtained presented as mean relative luciferase readings normalized to the negative control pXJ40 vector.

4.2.9 Manipulation of MAVS through stable and transient knockdown regulates downstream components of the RLH signalling pathway at the transcriptional level

Given the significant antiviral innate immune response MAVS is capable of triggering during IBV infection, one would expect to see the contrary with decreased MAVS expression. MAVS was first stably knocked down in A549 cells through the introduction of an shMAVS (small hairpin RNA) vector into these cells, according to manufacturer instructions by Ambion. Stably transfected cells displaying long-term silencing of MAVS were selected with antibiotics (G418), and these were seeded in experimental plates for infection with mock virus, IBV, or UV-inactivated IBV, respectively, alongside wildtype A549 cells over a 12-20 hour period, after which the cells were harvested for RNA extraction and subsequent RT-PCR analyses. In cells stably expressing shMAVS, expression of ISG56, a downstream component of the RLH signalling pathway, was reduced significantly along with a corresponding decrease in MAVS (1.10-14.3-fold decrease) (Fig. 4-8A, upper panels). Transcriptional levels of IFNβ in shMAVS cells also registered a slight decrease (1.43-fold decrease) at 16 and 20 hours post-infection (Fig. 4-8A, upper panels). Surprisingly, these infected MAVS knockdown cells also saw a decrease in IBV mRNA levels (3.23-7.69-fold decrease), indicating the presence of other signalling pathways in the regulation of IBV replication.

Infection of shMAVS cells with UV-IBV abolished the expression of viral RNA, as expected, and resulted in little or no expression of ISG56 as well, although no discernable trend was observed in the transcriptional levels of IFNβ (1.64-fold decrease – 4.61-fold increase) (Fig. 4-8A, lower panels). In agreement with the observations of Li *et al*., whose report highlighted the role of ISG56 in the negative

feedback regulation of virus-induced IFN signalling and host cellular antiviral responses (Li et al., 2009), this indicated the necessity of viral replication for the regulation of ISG56.

To confirm these results, a different set of complementary siRNAs custom designed to transiently knockdown MAVS was transfected into H1299 cells for 72 hours, after which the cells were infected for a 12-20 hour period and the RNA was harvested for subsequent RT-PCR analysis. Similarly to the results obtained in stably transfected shMAVS A549 cells, a knockdown in MAVS (1.72-fold decrease) corresponded with reduced transcriptional levels of IFNβ (1.34-fold decrease), and ISG56 (3.33-fold decrease) at 20 hours post-infection (Fig. 4-8B). However, an increase in ISG56 (1.20-2.16-fold increase) was observed at 12 and 16 hours post-infection with a corresponding decrease in MAVS (1.35-2.70-fold decrease), and a reduction in viral RNA was observed (1.23-1.92-fold decrease) throughout the time course (Fig. 4-8B).

Taken together, these results suggest that while the role of MAVS in inducing antiviral responses is unambiguous, the control of downstream components of the RLH signalling pathway, in which it is an important antiviral adaptor protein, possibly requires other regulatory proteins that aid in both the positive and negative regulation of this pathway, depending on the stage of virus infection and the differential regulation of viral replication by the former.

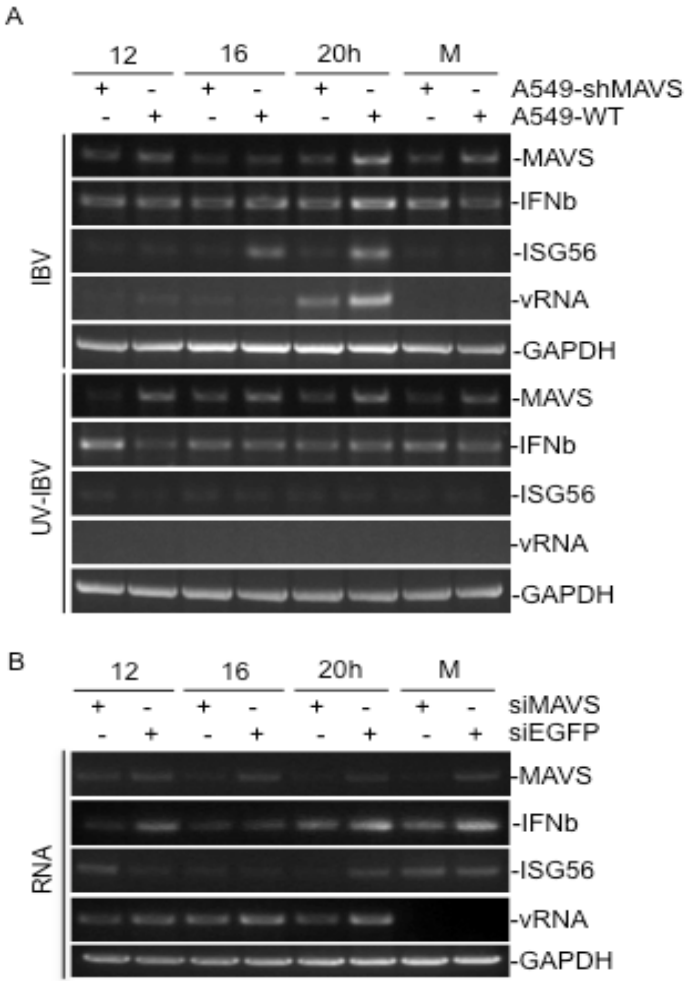

Figure 4-8

MAVS knockdown regulates the transcriptional levels of ISG56 during IBV infection.

(A) Regulation of RLH-signalling components in UV-IBV- or IBV-infected shMAVS stable cells. Stably transfected shMAVS A549 stable cells (A549-shMAVS) and wild type A549 were infected with either IBV or UV-IBV for 12-20 hours before harvesting for RNA extraction and subsequent RT-PCR analysis with specific primers for the indicated genes. GAPDH, loading control. M, mock infection.

(B) Regulation of RLH-signalling components in IBV-infected siMAVS transfected H1299 cells. H1299 cells were transfected with either siMAVS or siEGFP for 72 hours before infection with IBV from 12-20 hours. Cells were harvested for RNA extraction and subsequent RT-PCR analysis with specific primers for the indicated genes. GAPDH, loading control. M, mock infection.

4.2.10 Manipulation of MAVS through transient knockdown regulates virus-induced apoptosis

An examination of the total cell lysates obtained from MAVS knockdown cells after a time course infection period from 12-20 hours yielded surprising results in the Western blot analysis. MAVS was observed to undergo cleavage at 20 hours post-infection (Fig. 4-9A). The cleaved MAVS fragment was present in both siMAVS and siEGFP infected cells, and was marked by a decreased expression in full-length MAVS protein as well. An increased rate of MAVS cleavage, measured as the amount of full-length protein over cleaved product, was observed in infected MAVS knockdown cells compared to control cells (0.42- vs. 0.09-fold, respectively) (Fig. 4-9A). As a cleavage in MAVS protein has been previously reported in cells undergoing apoptosis (Scott and Norris, 2008), PARP cleavage – a standard hallmark of apoptosis – was checked in the same samples as well. Interestingly, PARP was also cleaved in MAVS knockdown cells at 20 hours post-infection (2.31-fold) in correspondence to MAVS cleavage observed at the same time point. A decrease in MAVS protein also saw a slight decrease in the production of IBV-S protein (1.23-4.17-fold decrease) from 12-20 hours post-infection, in comparison to infected control cells (Fig. 4-9A).

MAVS cleavage is an anti-host immunity strategy employed by a number of viruses to evade host innate immune responses and facilitate persistent infection (Meylan et al., 2005). The cleavage of MAVS dissociates the protein from the mitochondria, thus impeding the RLH antiviral signalling pathway, as its ability to activate downstream factors such as IRF3 leading to IFNβ production is dependent on its localization to the outer mitochondrial membrane (Yang et al., 2007). Upstream of MAVS, the RNA helicase, MDA5, has also be reported to undergo cleavage during

virus infection (Barral et al., 2007). To confirm this, the protein levels of MDA5, RIG-I, PARP and MAVS were first checked in wildtype H1299 cells infected with IBV over a time course period from 16-24 hours. While the expression level of RIG-I registered a gradual increment from 16 to 24 hours post-infection (0.73-1.30-fold increase), the expression level of full length MDA5 was observed to increase at 16 and 20 hours post-infection (1.94-2.07-fold increase), but decreased sharply at 24 hours post-infection (3.45-fold decrease) (Fig. 4-9B). However, the hypothesized cleavage bands were not observed despite lengthier exposure times; this could be due to the limitations of the commercial MDA5 antibody purchased for this study. The significant decline in full length MDA5 protein expression coincided with a cleavage in both PARP and MAVS at 24 hours post-infection (Fig. 4-9B).

As the transfection of synthetic dsRNA such as poly(I:C) has been shown to induce MAVS cleavage in HeLa cells (Scott and Norris, 2008), the possibility of this occurring in H1299 cells was also checked. Different concentrations of poly(I:C) from 0-3ug were transfected into H1299 cells for 12 hours and cells were harvested for Western blot analysis. Both PARP and MAVS showed significant cleavage at a poly(I:C) concentration of 2-3 ug, while smaller bands were observed below full-length MDA (Fig. 4-9C). To confirm if these observed cleavage bands were due to the induction of apoptosis, staurosporine, an apoptosis inducer, was also introduced to cells from 0-5 hours before cells were harvested for Western blot analysis. Both PARP and MAVS were also observed to undergo cleavage at 2-5 hours post addition of staurosporine, while smaller bands, albeit slightly weak, were also visible beneath full-length MDA5 (Fig. 4-9D).

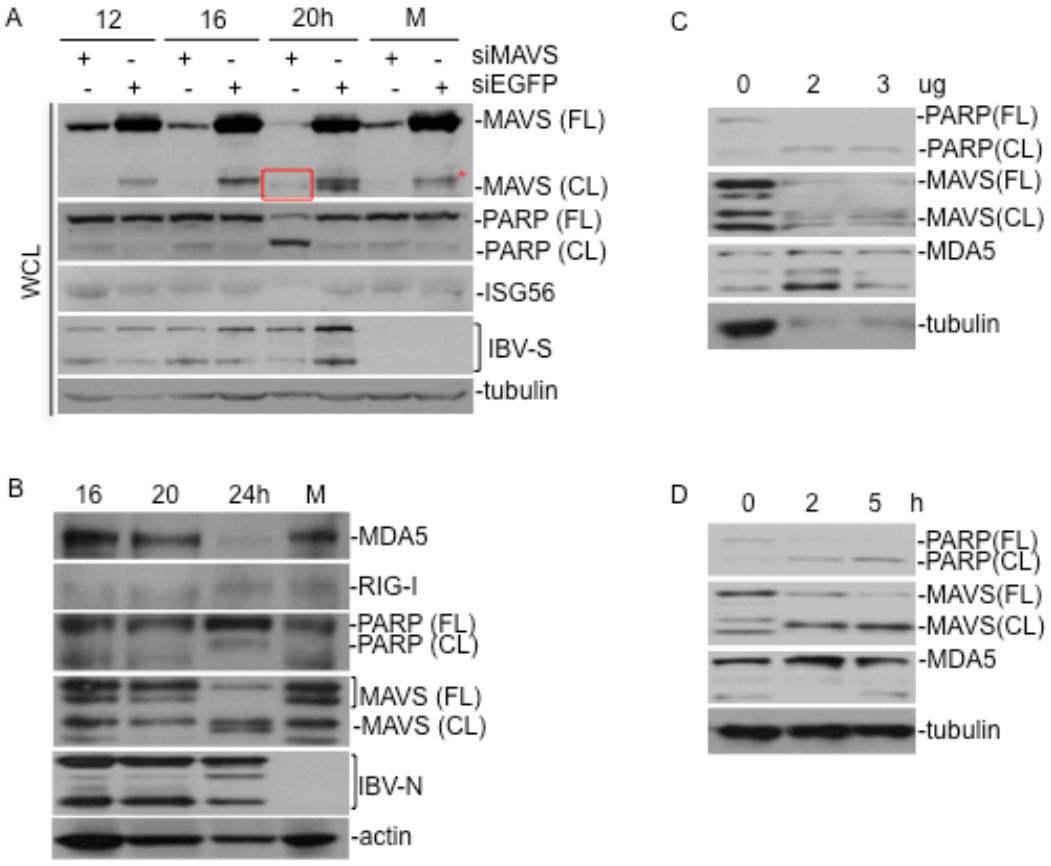

Figure 4-9

Regulation of virus-induced apoptosis and MAVS cleavage through the infection of H1299 cells.

(A) Regulation of virus-induced apoptosis and MAVS cleavage through the infection of siMAVS-silenced H1299 cells. H1299 cells were transfected with siMAVS or siEGFP for 72 hours, after which cells were either infected with IBV for 12-20 hours. Cells were harvested for Western blot analysis with appropriate antibodies for specified proteins, using tubulin as a loading control. M, mock infection. Red box, MAVS cleavage band. Red asterisk (*), full length MAVS bands as detected by anti-MAVS.

(B) Analysis of specific protein endogenous levels in IBV-infected wild type H1299 cells. H1299 cells were infected with IBV for 16-24 hours before they were harvested for Western blot analysis with the appropriate antibodies for the specified proteins, using actin as a loading control and IBV-N as an marker for infection. M, mock infection.

(C) Poly(I:C) transfection in H1299 cells lead to apoptosis. H1299 cells were first transfected with poly(I:C) at a concentration between 0 and 3ug for 12 hours before they were harvested for Western blot analysis with the appropriate antibodies for the specified proteins, using tubulin as a loading control.

(D) Addition of staurosporine in H1299 cells lead to apoptosis. 1uM of staurosporine were added to H1299 cells from 0-5 hours before the cells were harvested for Western blot analysis with the appropriate antibodies for the specified proteins, using tubulin as a loading control.

4.2.11 Manipulation of MDA5 and RIG-I through RNA interference regulates apoptosis and the rate of MAVS cleavage

The results obtained in Fig. 4-9 imply the possible regulation of apoptosis by the RLH signalling pathway. To examine this possibility, manipulation of MDA5 and RIG-I through RNA interference with their respective siRNAs was undertaken in H1299 cells, and infection of these same cells with IBV was carried out 72 hours post-(siRNA) transfection. Cells were harvested at 20 and 24 hours post-infection, respectively, for Western blot analysis. Surprisingly, a faster rate of apoptosis, as shown by a greater rate of PARP cleavage, was observed in infected MDA5 knockdown cells (4.11-fold) as compared to infected control cells (0.31-fold). In contrast, a slower rate of apoptosis was observed in infected RIG-I cells (0.03-fold) in comparison to that in infected control cells (Fig. 4-10A). Likewise, a similar trend was observed in the cleavage of MAVS; a greater rate of cleavage was observed in the same infected MDA5 cells (2.16-fold) as compared to infected control cells (0.32-fold), while no cleavage bands were observed in infected RIG-I cells (Fig. 4-10A).

To confirm the results obtained in Fig. 4-10A, TUNEL assay was carried out in H1299 cells transfected with siMDA5, siRIG-I or siEGFP either mock-infected or infected with IBV, according to the manufacturer's instructions. At 20 and 24 hours post-infection, cells were fixed and permeabilized before overlaying with the TUNEL reaction mixture, and subsequently labelled apoptotic cells were visualized under a fluorescence microscope (Fig. 4-10B). Significantly more apoptotic cells were observed in MDA5 knockdown cells infected with IBV compared to the siEGFP control cells, or with RIG-I-knockdown cells, at both 20 and 24 hours post-infection, whereas little or no apoptotic cells were observed in mock-infected cells, as exemplified by the lack of florescence observed (Fig. 4-10B). These results

demonstrate that a decrease in MDA5 levels appear to speed up the onset of IBV-induced apoptosis, whereas silencing of RIG-I causes a slight delay.

As IBV-induced apoptosis has previously been reported to be caspase-dependent (Liu, Xu, and Liu, 2001), it was possible that the cleavage of MAVS during virus-induced apoptosis might also be dependent on caspases. To examine this possibility, the cell permanent pan-caspase inhibitor, Z-VAD-FMK, was added to siRNA-transfected cells prior to infection with IBV (or mock). Cells were harvested at 24 hours post-infection and subjected to Western blot analysis. The results obtained showed no cleavage of either PARP or MAVS at 24 hours post-infection in siMDA5-, siRIG- or siEGFP-transfected cells (Fig. 4-10C).

The differential regulatory effects of MDA5 and RIG-I on IBV-induced apoptosis were further studied by transient expression of MDA5 and RIG-I in mammalian cells. For this purpose, both Flag-tagged MDA5 and Flag-tagged RIG-I were constructed and transfected into H1299, using a Flag-tagged empty vector as a negative transfection control. The cells were then infected with IBV at an MOI of 1. At 24 hours post-infection, a significant increase in PARP cleavage was observed in infected H1299 cells transfected with empty-vector (2.36-fold), RIG-I (1.64-fold) and MDA5 (1.12-fold) at 24 hours post-infection (Fig. 4-10D). MAVS cleavage, too, was observed in H1299 cells transfected with empty-vector (1.20-fold), RIG-I (0.86-fold) and MDA5 (0.45-fold) at the same time point. This corresponded with an increase in IBV-S (1.96-fold increase) and IBV-N (2.24-fold increase) production cells transiently expressing MDA5 while that in cells transiently expressing RIG-I were on par with control cells (Fig. 4-10D).

Taken together, these results confirm the cleavage of MAVS as a result of caspase-dependent, IBV- or chemically-induced apoptosis induction, and the rate of

apoptosis is dependent on the balance between MDA5 and RIG-I expression.

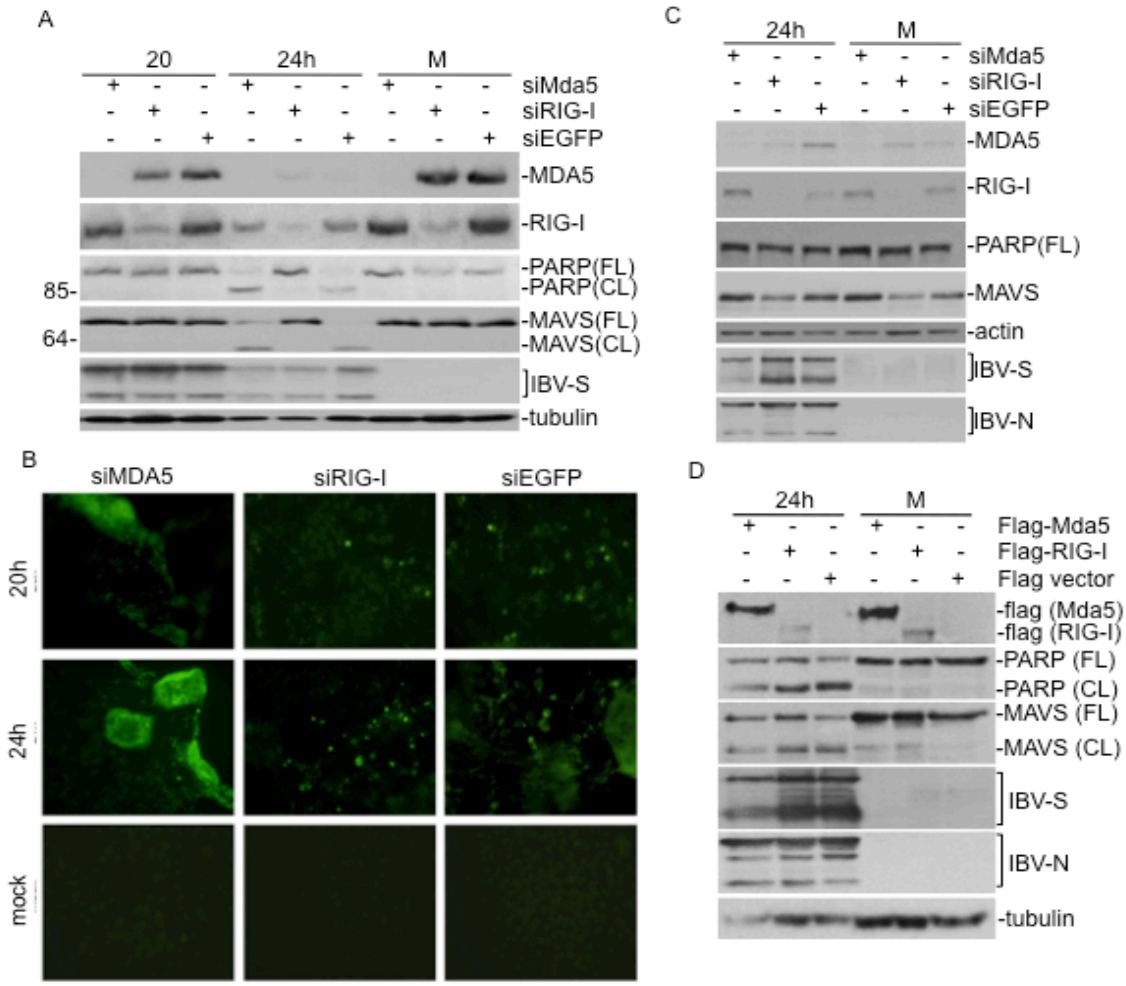

Figure 4-10

The effects of manipulation of the expression of MDA5 and RIG-I in mammalian cells on IBV-induced apoptosis and MAVS cleavage.

(A) Western blot analysis of the effects of down-regulation of MDA5 and RIG-I by RNA interference in mammalian cells on IBV-induced apoptosis (PARP cleavage) and MAVS cleavage. H1299 cells were transfected with siRNA duplexes targeting MDA5, RIG-I or EGFP. At 72 hours post-transfection, cells were infected with IBV and harvested at 20 and 24 hours post-infection. M, mock infection. Western blot analysis was performed using the indicated specific antibodies, with anti-tubulin as a loading control.

(B) TUNEL assay of the effects of down-regulation of MDA5 and RIG-I by RNA interference in mammalian cells on IBV-induced apoptosis. H1299 cells were transfected with siRNA duplexes targeting MDA5, RIG-I or EGFP, respectively. At 72 hours post-transfection, cells were either mock-infected, or infected with IBV, then fixed and permeabilized at 20 and 24 hours post-infection. Cells were then stained with the TUNEL reaction mixture and images were taken with a fluorescence microscope at an excitation wavelength of 488 nm.

(C) The effect of pan-caspase inhibitor Z-VAD-FMK on the induction of apoptosis during IBV infection. H1299 cells were transfected with siRNA duplexes targeting MDA5, RIG-I or EGFP. At 72 hours post-transfection, 20uM of Z-VAD-FMK was first added to the cells and incubated for 1 hour, before the cells were either mock-infected or infected with IBV and harvested at 24 hours post-infection. Western blot analysis was performed using the indicated specific antibodies, with anti-actin as a loading control.

(D) The effects of transient MDA5 and RIG-I expression in mammalian cells on IBV-induced apoptosis and PARP cleavage. H1299 cells were transfected with pXJ40-Flag-MDA5, pXJ40-Flag-RIG-I or pXJ40-Flag empty vector and either mock-infected (M) or infected with IBV at 72 hours post-transfection. Cells were harvested 24 hours post-infection and Western blot analysis was performed using the indicated specific antibodies, with anti-tubulin as a loading control.

4.2.12 Virus-induced apoptosis and MAVS cleavage is also dependent on the expression of Bcl-2 family proteins

As a link between coronavirus-induced apoptosis and Bcl-2 family proteins has been previously highlighted in Chapter 3, a possible link between MAVS cleavage and the expression of Bcl-2 family proteins could exist. To examine this, H1299 and Huh7 cells were transfected with Myc-tagged Mcl-1 and Myc-tagged Bak constructs separately, with an empty vector as a negative transfection control. The cells were then either mock infected or infected with IBV at an MOI of 1. At 24 hours post-infection, a significant increase in PARP cleavage was observed in both H1299 (13.89-fold; Fig. 4-11A) and Huh7 (1.13-fold; Fig. 4-11B) cells transfected with Myc-Bak. A significant increase in MAVS cleavage was also observed in H1299 (4.81-fold; Fig. 4-11A) and less so in Huh7 (0.80-fold; Fig. 4-11B), respectively. In contrast, the full-length PARP and full-length MAVS were not significantly cleaved in both IBV-infected H1299 (Fig. 4-11A) and Huh7 (Fig. 4-11B) transfected with Myc-Mcl-1, or in control cells.

Together, these results signify the involvement of pro-apoptotic Bak and anti-apoptotic Mcl-1 in the differential regulation of both PARP and MAVS cleavage in the onset of apoptosis induced through virus infection.

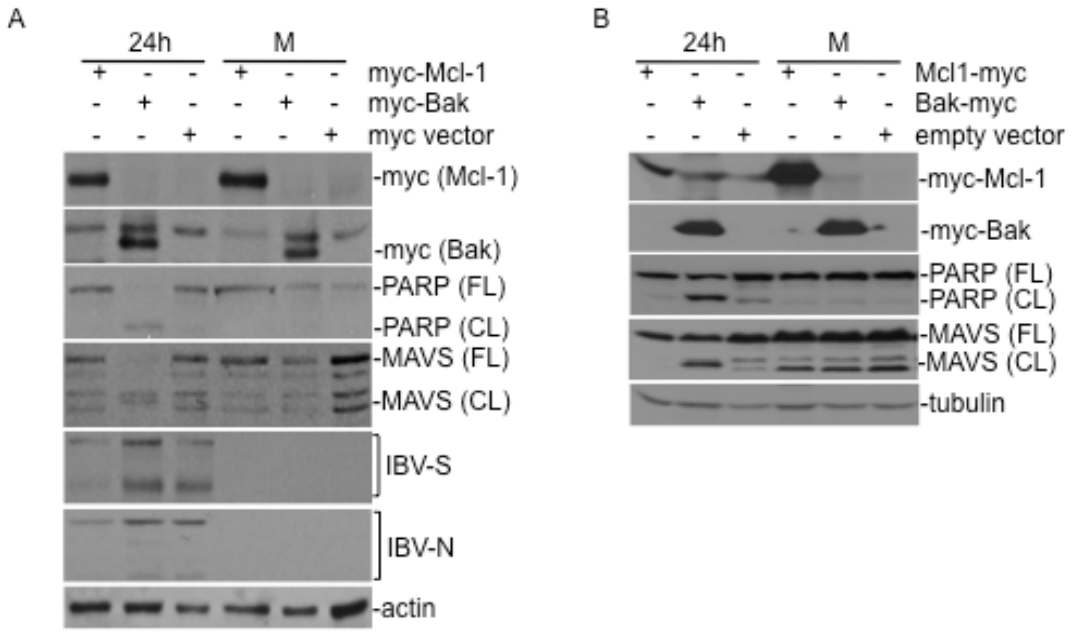

Figure 4-11

The effects of transient Mcl-1 and Bak expression in mammalian cells on IBV-induced apoptosis and PARP cleavage.

(A) H1299 cells were transfected with pXJ40-myc-Mcl-1, pXJ40-myc-Bak or pXJ40-myc empty vector and either mock-infected (M) or infected with IBV at 72 hours post-transfection. Cells were harvested 24 hours post-infection and western blot analysis was performed using the indicated specific antibodies, with anti-actin as a loading control.

(B) Huh7 cells were transfected with pXJ40-myc-Mcl-1, pXJ40-myc-Bak or pXJ40-myc empty vector and either mock-infected (M) or infected with IBV at 72 hours post-transfection. Cells were harvested 24 hours post-infection and western blot analysis was performed using the indicated specific antibodies, with anti-tubulin as a loading control.

4.2.13 IBV non-structural protein 15 inhibits MAVS-induced IRF3 phosphoactivation and may potentially regulate host apoptotic responses

As described earlier in Chapter 3, many hosts adopt antiviral strategies through the elicitation of apoptotic responses, while viruses, in turn, have evolved diverse mechanisms to thwart these host responses or manipulate them to the viruses' advantage. In this instance, coronavirus proteins may serve as potential modulators of cell death during virus infection. Lei *et al.* also highlighted this possibility in a recent paper, in which SARS-CoV was observed to be able to interfere with host antiviral apoptotic responses by targeting MAVS (Lei et al., 2009). In particular, SARS-CoV non-structural protein 15 was discovered to be able to completely abolish MAVS-induced apoptosis (Lei et al., 2009). To examine the link between IBV proteins and MAVS in the hindrance of cell death during infection, a number of IBV genes coding for structural and non-structural proteins mainly from the IBV-D fragment, including nsps 12-16, IBV-N and IBV-S, were cloned in expression vectors containing a Flag-tag and co-expressed with HA-tagged MAVS in H1299 cells for Western blot and FACS analysis. Surprisingly, MAVS and PARP cleavage bands were not detected in any of the IBV structural or non-structural proteins co-expressed with MAVS, nor were they observed in the positive control (MAVS co-expressed with empty vector) or in the negative control (empty vector) cells, although IBV-nsp15 (4.78-fold increase) and the empty vector negative control (6.02-fold increase) both displayed higher expression levels of full length PARP as compared to the positive control transiently expressing MAVS (Fig. 4-12A).

MAVS may also present an attractive target for viral defence against host innate immune signalling, as exemplified in the case of HCV NS3/4A protease which is able to cleave MAVS to prevent its oligomerization and subsequent activation of

downstream IFN pathways (Baril et al., 2009). In this study, IBV nsp 15 was shown to abrogate both MAVS oligomerization and MAVS-induced IRF3 phosphoactivation (Fig. 4-12A, lane 4). With the exception of IBV-S, which was expressed in an expression vector with no tag, the expression of the various IBV proteins and MAVS were checked using anti-Flag and anti-HA, respectively, and the expression of IBV nsps12, nsp13 and nsp14 were found to be relatively low (Fig. 4-12B). These were finally expressed on a second blot with a higher concentration of protein lysate and overnight exposure time, as evidenced by a very strong expression of Flag-tagged IBV-N as a positive comparison (Fig. 4-12C).

To further examine the possible effects of the co-expression of MAVS and IBV nsp15 in the intervention of apoptosis during infection, a simplified FACS analysis was performed with H1299 cells co-expressing nsp15 and MAVS, together with a positive control (cells co-expressing MAVS and an empty vector) and a negative control (cells expressing empty vector). Cells were harvested after 48 hours, washed, and fixed with 70% ethanol and RNase A before the addition of propidium iodide prior to analysis. The data obtained showed a higher percentage of apoptotic cells (11.4%) in cells transiently expressing MAVS (Fig. 4-12D), compared to cells co-expressing nsp15 and MAVS (6.1%), and negative control cells expressing just the empty vector (6.5%), thus indicating a possible delay in the onset of apoptosis as mediated by nsp15.

These results collectively highlight a possible coronavirus strategy in combating host responses through nsp15, which act to thwart the MAVS phosphoactivation of IRF3 and apoptosis to prevent downstream IFN responses and premature host cell death.

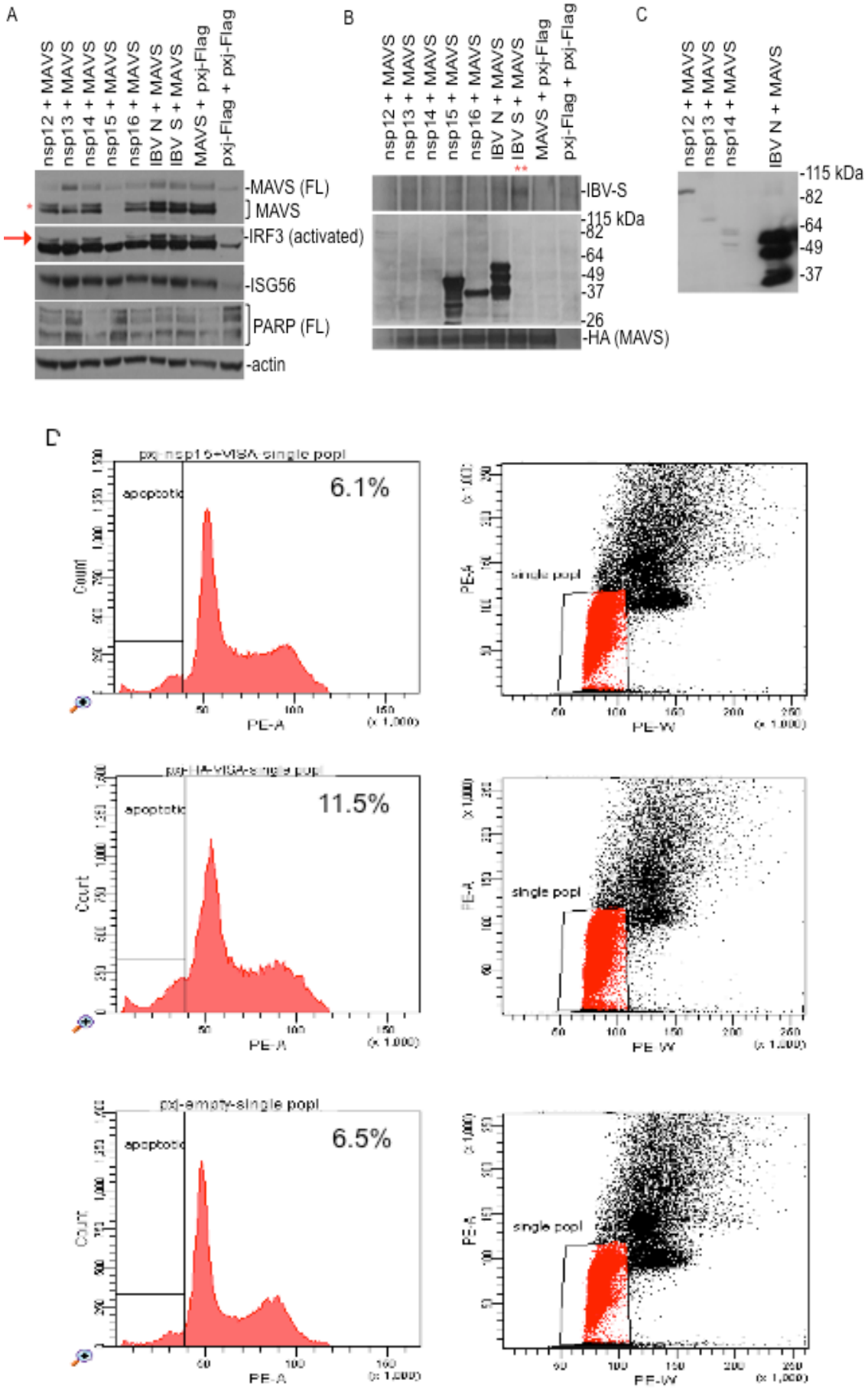
A
nsp12 + MAVS
nsp13 + MAVS
nsp14 + MAVS
nsp15 + MAVS
nsp16 + MAVS
IBV N + MAVS
IBV S + MAVS
MAVS + pxj-Flag
pxj-Flag + pxj-Flag
-MAVS (FL)
MAVS
-IRF3 (activated)
-ISG56
PARP (FL)
-actin
B
-IBV-S
-115 kDa
-82
-64
-49
-37
-26
-HA (MAVS)
C
-115 kDa
-82
-64
-49
-37
D
6.1%
11.5%
6.5%
apoptotic
single popl
Count
PE-A
PE-W
PE-H

Figure 4-12

IBV nsp15 inhibits MAVS-induced IRF3 phosphoactivation and potentially modulates apoptosis.

(A) Co-expression of IBV structural and non-structural proteins with MAVS. IBV nsps12-16, IBV S and IBV N proteins were individually co-expressed with MAVS in H1299 cells with cells co-expressing MAVS and empty vector as a positive control and cells expressing empty vector alone as a negative control. Cells were harvested 48 hours post-transfection for Western blot analysis with the specific indicated antibodies, with anti-actin as a loading control. Full length MAVS bands, as detected by anti-MAVS, is denoted as *; →, phosphoactivated IRF3.

(B) Expression of IBV structural, non-structural proteins and MAVS in H1299. Transient expression of Flag-tagged IBV structural and non-structural proteins were detected with anti-Flag antibody, HA-tagged MAVS with anti-HA antibody, and IBV S protein with anti-IBV S antibody (denoted as **).

(C) Expression of IBV nsps 12-14 in comparison with IBV N structural protein. Transient expression of Flag-tagged IBV nsps 12-14 and IBV N structural protein were detected with anti-Flag antibody after overnight exposure of the blot.

(D) FACS analysis of the inhibitory effects of IBV nsp 15 on MAVS-induced apoptosis. MAVS was co-expressed with IBV nsp15 (top panel) or empty vector as a positive control (middle panel), with cells expressing empty vector as a negative control (lower panel), and harvested at 48 hours post-transfection for FACS analysis using propidium iodide according to a standard staining protocol.

4.3 DISCUSSION

The results of this study underline the immense significance of MAVS, a downstream regulator of intracellular RNA helicases MDA5 and RIG-I, in activating downstream host innate immune signals in response to IBV infection. This comes as no surprise, as MAVS is also an important requisite in the induction of innate immune response to a variety of RNA viruses (Loo et al., 2008).

Global gene expression profiles have been determined in IBV-infected Vero cells at 24 hours post-infection by Affymetrix array analyses to show an up-regulation at the transcriptional level of MDA5. These results were further confirmed in IBV-infected chicken embryos and chicken fibroblast DF1 cells, as well as in mammalian cells such as H1299 and Vero cells. In the event that it was erroneously recognized as a false negative in the Affymetrix array, the expression of RIG-I, being the most closely related to MDA5 (Yoneyama et al., 2005), was also checked in these cells and found to be up-regulated as well, at the transcriptional level in H1299 and Vero infected cells. However, RIG-I was not detected in chicken cells or chick embryos, as corroborated by Barber *et al*. in a report that suggests the presence of RIG-I in ducks but not chickens, which confers innate immunity protection to the former (Barber et al., 2010).

While the up-regulation of both MDA5 and RIG-I expression can be confirmed at both transcriptional and, to a lesser extent, translational levels, in mammalian cells during IBV infection, the silencing of MDA5 or RIG-I through RNA interference did not particularly present conclusive evidence strongly supporting the ability of one or the other RLH in the recognition of IBV. Unexpectedly, a knockdown in MDA5 levels was accompanied by an increase in RIG-I and another RLH, LGP2, which resulted in

an increase in the expression of IFNβ and ISG56. In contrast, a knockdown in RIG-I levels resulted in a corresponding decrease in MDA5, LGP2, IFNβ and ISG56 levels, respectively. It appears that LGP2, which has recently been shown to be important in the upstream activation of RIG-I- and MDA5-mediated signalling pathways (Satoh et al., 2010), may be able to positively regulate RIG-I expression for the subsequent activation of IFN responses in times of low MDA5 levels. Knockdown of RIG-I levels in cells, however, leads to a corresponding decrease in MDA5. This was observed in different sets of RIG-I siRNAs (unpublished observations), as well as in RIG-I knockdown dengue infected cells (Nasirudeen et al., 2011). The corresponding decrease in MDA5 levels was coupled with a decrease in LGP2, and resulted in little or no IFN response. This also suggests the fact that MDA5 may play a supplementary role in boosting innate immune signalling initiated by RIG-I during IBV infection. It must also be noted that significant IFNβ expression was observed only in cells treated with siRNA prior to infection, perhaps due to additional cell stress; expression of IFNβ and downstream ISGs was minimally observed in infected wildtype cells.

To examine the effects of MDA5 and RIG-I signalling in the absence of functional IFN, Vero cells were silenced with siRNAs targeting MDA5 and RIG-I, respectively. Surprisingly, a significant level of ISG56 was observed in infected siRIG-I knockdown Vero cells but not in infected MDA5 knockdown Vero cells. As ISG56 is a negative feedback regulator of virus-activated MDA5 and RIG-I signalling and type I IFN responses (Li et al., 2009), the differential ISG56 expression levels observed in the absence of functional IFN suggests an IFN-dependent regulation of ISG56 during IBV infection.

While a moderate enhancement of IBV activity and viral protein release was observed in RIG-I knockdown cells, this is likely indirectly due to a more efficient rate

of virus replication in these cells, as the virus titres obtained from siMDA5, siRIG-I and control knockdown cells were similar, as were the production of virus proteins in total cell lysates. As such, the effect of transient MDA5, RIG-I and MAVS expression on IBV activity and viral protein production was also checked. Surprisingly, while the transient expression of MAVS in cells was able to almost completely abolish virus infection, this was not observed in cells transiently expressing MDA5 or RIG-I. Indeed, when the five different IBV fragments were each co-transfected with either MDA5 or RIG-I and IFN reporter, respectively, IFN activity was not observed in cells co-expressing MDA5/RIG-I and IBV-D fragment, as well as in cells co-expressing MDA5/RIG-I and total IBV RNA, thus suggesting the fact that IBV may escape immune surveillance, possibly through certain viral mechanisms that allow for evasion from virus recognition by MDA5 or RIG-I.

Stable and transient knockdown of MAVS showed a tight regulation of downstream IFN responses at the transcriptional level. A decrease in MAVS expression was also shown to regulate caspase-dependent apoptosis at the translational level, especially during the later stages of infection, and full-length MAVS was duly cleaved together with the apoptosis marker PARP. This activity is in turn maintained by RIG-I and MDA5, as decreased levels of MDA5 and increased levels of RIG-I result in both PARP and MAVS cleavage. Members of the Bcl-2 family proteins can also mediate MAVS-induced apoptosis; an increase in pro-apoptotic Bak results in the cleavage of both MAVS and PARP in human H1299 and Huh7 cells.

Screening of selected IBV structural and non-structural proteins from the IBV-D fragment eliminated all but one – nsp 15 – with the ability to inhibit MAVS-mediated IRF3 phosphoactivation, which could possibly explain the lack of significant IFN response during IBV infection, despite substantial production of chemokines (Versteeg

et al., 2007). IBV nsp15, like its SARS-CoV counterpart (Lei et al., 2009), was also shown through FACS analysis to be able to slightly reduce MAVS-induced apoptosis when co-expressed with MAVS, although this could not be observed at the protein level and as such may require further verification.

The data presented in this study suggest that the attenuation of IFN response, together with the regulation of RLH related proteins through the manipulation of virus-induced apoptosis, might be two crucial characteristics in prolifically abundant IBV-infected cells and utilized as a clever strategy to thwart the actions of cellular antiviral proteins.

CHAPTER 5. GENERAL DISCUSSION AND FUTURE DIRECTIONS

The main focus of the work presented in this thesis is the investigation of host-virus interactions using the avian coronavirus IBV as a model for the study. In this chapter, results of all the research work done so far are summarized and discussed, and suggestions for future directions are put across as well.

5.1 VIRUS-INDUCED APOPTOSIS AND ITS REGULATION BY BCL-2 FAMILY PROTEINS

5.1.1 Main conclusions

The following conclusions have been drawn in Chapter 3:

- IBV infection up-regulates Bak and Mcl-1 at both transcriptional and translational levels in mammalian cells.
- A similar up-regulation trend for Bak and Mcl-1 expression levels is confirmed in IBV-infected chicken embryos and chicken fibroblast cells at the transcriptional level.
- Targeted Bak and Mcl-1 down-regulation by siRNA reveals an enhancement in IBV progeny production in cells depleted of the pro-survival Mcl-1 protein, and a decrease in IBV progeny production in that of the pro-apoptotic Bak protein.
- IBV-induced apoptosis also appeared earlier in Mcl-1 knockdown cells, and later in Bak knockdown cells.
- The upstream signalling pathways leading to infection-mediated Mcl-1 induction were studied, and components of the MAP/ERK, PI3K/Akt and GADD153 in the endoplasmic reticulum (ER) stress pathways were identified as potential modulators.

5.1.2 General discussion and future directions

Viral regulation of programmed cell death is a sophisticated process (Hay and

Kannourakis, 2002). It is also a complex aspect of viral pathogenesis. In the past few decades, numerous viruses have been shown to manipulate various apoptotic pathways to their own advantage (Shen and Shenk, 1995). Viruses may inhibit apoptosis during the initial stages of infection so as to garner enough time to multiply and disperse rapidly from the plasma membrane to infect other cells (Kurokawa et al., 1999). Yet, viruses may just as easily infect a cell, elicit apoptosis, and spread to neighbouring cells through phagocytosis of the resulting apoptotic bodies while cleverly minimizing an immune response at the same time (Mi et al., 2001). It has also been previously reported that SARS-CoV induces apoptosis as well, both *in vitro* and *in vivo*, which might account for the destruction of lung epithelial cells in infected patients (Yan et al., 2004). IBV infection has also been shown to trigger cell cycle arrest at the S (synthesis) and G2/M (interphase/mitosis) phases at the early stages, and apoptosis at late stages, of the viral infection cycle on cultured mammalian cells (Li, Tam, and Liu, 2007).

5.1.2.1 Mcl-1 and Bak are up-regulated in IBV-infected cells

Various members of the Bcl-2 family proteins in the mitochondria have been shown to mediate the onset of apoptosis (Kim et al., 2006). In this study, elevated levels of both anti-apoptotic Mcl-1 and pro-apoptotic Bak have been confirmed in mammalian and chicken cells infected with IBV. The regulated expression of these Bcl-2 family proteins may therefore be fundamental to the preservation of the tricky equilibrium between life and death of infected cells to allow for the completion of an infection cycle.

5.1.2.2 The regulation of IBV-induced apoptosis by Mcl-1 and Bak

PARP cleavage occurred earlier in cells transiently expressing siRNA targeting Mcl-1 down-regulation, and was delayed in cells depleted of pro-apoptotic Bak during

infection. In contrast, PARP cleavage occurred at a slower rate in cells transiently expressing Mcl-1, and faster in cells transiently expressing Bak. This implies an increased rate of IBV-induced apoptosis in Mcl-1 knockdown cells, and a decreased rate of the same in Bak knockdown cells, indicating the fact that Mcl-1 and Bak play diverging roles in the regulation of coronavirus-induced apoptosis at different stages of infection.

5.1.2.3 Targeted Mcl-1 down-regulation by siRNA reveals an enhancement in IBV progeny production was in cells depleted of the pro-survival Mcl-1 protein

A moderate enhancement effect on viral protein synthesis and the release of viral particles was observed in Mcl-1 knockdown cells infected with IBV in the late stages of infection. As Mcl-1 is unlikely to be directly involved in viral RNA replication and protein synthesis, the detection of more viral protein expression in Mcl-1 knockdown cells than that in the control cells at these time points would be due to the fact that more infectious viral particles were released from the primary infection. Subsequently, these viruses could infect more neighbouring cells during secondary and tertiary infections, resulting in the detection of more viral proteins. In fact, minor, if any, differences in viral RNA replication and protein synthesis were observed during the earlier stages of infection, lending support to this conclusion.

On the other hand, the minimal to moderate regulatory effect observed in Mcl-1 knockdown cells may not truthfully reflect the actual impact of Mcl-1 up-regulation on viral replication and pathogenesis in the infected animals. As all siRNA transfection experiments require at least 72 hours' incubation period in addition to a requisite reduced serum environment for the experimental cells, this inadvertently compounds additional cell stress on these knockdown cells, and may not veraciously reflect the actual effect of Mcl-1 and/or Bak down-regulation on viral replication and

pathogenesis in infected hosts. This is a complication that can only be tackled in Mcl-1 and/or Bak knockout mouse or other suitable animal models. Nevertheless, it appears that up-regulation of Mcl-1 in IBV-infected cells, as characterized here, may represent an effective host anti-coronavirus response that regulates viral infectivity and productivity.

5.1.2.4 Possible viral mechanisms that may be involved in Bak and Mcl-1 regulation

While the requirement for viral replication in the up-regulation of Bak and Mcl-1 at the transcriptional level has been confirmed, attempts to identify viral proteins that may be responsible for up-regulation of these two genes were made but in vain. It has recently been shown, however, that poly(I:C), a dsRNA synthetic analogue that resembles dsRNA intermediates derived from infectious viruses, was able induce apoptosis, through the activation of TLR- and mitochondrial-mediated pathways, in both mammalian cancer cells (Shen et al., 2011) and in chicken fibroblast cells (Lv and Bao, 2009). The dsRNA-dependent PKR, itself activated during viral infections and also in response to cellular stress signals, has also been reported to trigger apoptosis through both extrinsic and intrinsic pathways (Garcia, Meurs, and Esteban, 2007). As such, it is possible that viral dsRNA intermediates, and not viral proteins, may ultimately be responsible for triggering the production of enhanced levels of Bak and Mcl-1 during avian IBV-induced apoptosis in both mammalian cells and chicken cells.

5.1.2.5 Mediators of the mitochondrial apoptotic pathway

While components of the ER stress response have also been highlighted in this study as probable mediators in Mcl-1-induced apoptosis in the mitochondrial apoptotic pathway, it is still unclear just how dependent mitochondria-initiated apoptosis is on ER stress-induced apoptotic signalling *in vivo*. ER stress response brings about

complex consequences on a number of crucial metabolic processes such as cell cycle arrest and autophagy, among others; this may also account for cell death arising from ER stress response in normal cells (Wang et al., 2011a).

BH3 mimetics, designed to mimic the functional properties of BH3-only proteins, have been shown to both inhibit, or antagonize, more than one anti-apoptotic protein – including Mcl-1 – and trigger the activation of pro-apoptotic instigators to significantly bring about the onset of apoptosis (Albershardt et al., 2011). As highlighted in Chapter 1, certain BH3-only proteins have previously also been identified as being activated by ER stress response to induce Bak/Bax-mediated apoptosis in the mitochondria in a p53-dependent manner (Li, Lee, and Lee, 2006).

Pro-apoptotic Bcl-2 proteins such as Bak and Bax are also able to regulate ER membrane permeability to the release of ER luminal proteins during ER-stress activation of apoptosis; this takes place in a manner similar to the Bak/Bax regulation of MOMP during the onset of the intrinsic death pathway, and both of these processes are purported to occur in tandem (Wang et al., 2011b).

As IBV has previously been reported to induce apoptosis independently of p53 (Li, Tam, and Liu, 2007), molecular components, such as the multi-functional BH3-only proteins, that could be involved in mediating the plausible connections between ER stress response and initiation of the intrinsic (mitochondrial) apoptotic pathways in a p53-independent manner can also be examined for future work. As reiterated in an earlier paragraph, however, the ER stress response observed here may be caused by amino acid starvation during the long, serum-free incubation period after RNAi transfection and not activated by unfolded proteins in the ER resulting in ER stress induction of eIF2α (alpha subunit of eukaryotic translation initiation factor 2) phosphorylation (Harding et al., 2003). The establishment of shRNA cell lines stably

expressing decreased expression levels of various proteins involved in related ER stress responses would provide more credible insights into the dual functions of Bcl-2 proteins in regulating both ER stress-associated and mitochondria-related intrinsic death responses during virus infection.

5.1.2.6 Practical applications of this study

In addition to understanding the general overview of virus-host cell interactions and viral pathogenesis, the further progression of this study would have several potential practical applications, especially in relation to virus-induced cancers and with oncolytic viruses that target virus-mediated lysis of tumour cells. Several small molecular mimetics, constructed particularly to imitate the binding specificity of BH3-only proteins to the hydrophobic groove of their respective anti-apoptotic proteins, have been hailed as effective drugs in targeted therapeutic treatments of diseases where Mcl-1 confers resistance to apoptosis (Nguyen et al., 2007). As such, potential BH3 mimetics with suitable hydrophobic properties that may also be able to demonstrate formidable inhibition of the constitutive interactions between Mcl-1 and Bak within the mitochondrial outer membrane would be equally useful as well.

The circumvention of apoptosis in tumour cells has been long regarded as a distinctive feature of cancer (Danial and Korsmeyer, 2004). With the ability of viruses to behave as oncolytic, apoptosis-inducing agents (Mi et al., 2001) and the rapid advances in molecular biology, apoptotic viral genes can be harnessed as vectors and targeted to tumour cells as a potential anti-cancer therapeutic benefit (Liu et al., 2005). Degenerative diseases such as Alzheimer's disease and Huntingdon's disease may also be similarly treated with anti-apoptotic viral genes (Hay and Kannourakis, 2002). Investigating the relationship between Bcl-2 family proteins and IBV-induced apoptosis may therefore lead to further refinement of the virotherapy concept (Cao et

al., 2011) to develop safer, virally-derived gene therapies that could target cancer cells with more discrimination.

5.2 HOST INNATE IMMUNE RESPONSES AGAINST IBV INFECTION

5.2.1 Main conclusions

The following conclusions are observed in Chapter 4:

- Up-regulation in the transcriptional levels of both MDA5 and RIG-I in avian coronavirus IBV infected mammalian cells was observed.
- An increase in the mRNA levels of MDA5 was also observed in IBV infected chick embryos and chicken fibroblasts, both of which have been previously shown to be naturally deficient in RIG-I (Barber et al., 2010), and corresponded with a significant increase in IFNβ levels.
- Targeted MDA5 and RIG-I down-regulation by RNA interference in mammalian cells revealed a regulatory role for another RLH, LGP2, which participated in the upstream positive regulation of RIG-I in infected MDA5 down-regulated cells. Both IFNβ and ISG production were subsequently enhanced, and the down-regulation of MDA5 in infected RIG-I knockdown cells to decrease both IFNβ induction and ISGs production.
- MAVS, an essential adaptor protein in the RLR signalling pathway, was observed to be crucial in the antiviral activation of IFN responses, and its transient expression was able to completely abolish IBV infection.
- MDA5 and RIG-I were unable to recognize full length IBV RNA to induce IFNβ activity, although individual segments of the IBV genome – with the primary exception of IBV-D fragment that encompasses the region of IBV genome from 15511-20930 and encodes IBV S protein and non-structural proteins 13-16 –

could be detected by these PRRs.

- Transient RNAi experiments also presented an interesting link between antiviral innate immunity and virus-induced apoptosis; the latter appeared earlier in both MAVS and MDA5 knockdown cells and faster in RIG-I knockdown cells during infection.
- Virus-induced apoptosis resulted in the caspase-dependent cleavage of full length MAVS, indicating the possibility that the tight regulation of apoptosis during IBV infection, either to the virus' advantage or as yet another line of host defence.
- The pro-apoptotic branch of the Bcl-2 family of proteins, such as Bak, could also cleave full length MAVS during the induction of apoptosis at the mitochondria, thus reiterating the importance of the mitochondria as an ideological battlefield for the survival struggle between virus and host.
- IBV nsp15 was identified as a potential inhibitor of MAVS induction of apoptosis as well as a likely inhibitor of IRF3 phosphoactivation, thus allowing for partial immune evasion of the virus from host antiviral defences. It could also explain the lack of significant Type I interferon response observed during IBV infection.

5.2.2 General discussion and future directions

Interferon genes are best known as early-onset transcriptional responses to virus infection of host mammalian cells (Fensterl and Sen, 2009). Interferons are secreted as ligands from specific cell surface receptors involved in innate immune signalling, and their secretion evoke the transcription of interferon-stimulated genes, which are in turn translated into protein products with antiviral defences and immunomodulatory consequences (de Veer et al., 2001). Type I IFN expression is induced in host cells

upon recognition of viral molecular patterns, in particular nucleic acids such as dsRNAs that are recognized as 'non-self', by cytoplasmic and endosomal receptors such as those from the TLR and RLH family of pattern recognition receptors (Fujita et al., 2007; Kawai et al., 2004). The relationship between a virus and its host is complex; the virus must evolve evasive strategies to avoid detection and immunological defence mechanisms from the host while the host must develop various lines of defence in order to combat viral invasion.

Of particular interest are the pattern recognition receptors from the RLH family of proteins, which are able to recognize RNA viruses through various pathogen associated molecular patterns specific to the latter (Takeuchi and Akira, 2008). In the case of coronaviruses, Li *et al.* has reported the induction of IFN responses in mouse coronavirus MHV infected mouse oligodendrocytes through both RIG-I and MDA5 signalling (Li, Liu, and Zhang, 2010), while Roth-Cross *et al.* has alternatively shown the recognition of MHV by only MDA5 in mouse cells (Roth-Cross, Bender, and Weiss, 2008).

5.2.2.1 The role(s) of RIG-I and/or MDA5 signalling in IBV infection

While Loo *et al*. have also described both the disparate and superfluous roles of RIG-I and/or MDA5 signalling in triggering innate immunity in the same report (Loo et al., 2008), the same cannot really be detailed here in this study. ISG56 expression was induced in IBV-infected MDA5 knockdown and control knockdown cells, but not in IBV-infected RIG-I cells. This strongly suggests the importance of RIG-I in triggering innate immune responses during IBV infection. Nevertheless, as the viral RNA/protein expression in MDA5 knockdown cells was slightly diminished, or delayed, compared to that in control knockdown cells, this could imply that MDA5 may have a supplementary role in boosting innate immune signalling triggered by

RIG-I during IBV infection.

In addition, knockdown of RIG-I was accompanied by a concomitant decrease in MDA expression level during infection. These observations were similarly reported in RIG-I knockout mouse embryo fibroblasts during paramyxovirus and influenza A infection (Loo et al., 2008). However, in comparison to mock-infected cells, while RIG-I expression increased in MDA5 knockdown cells and MDA5 expression was increased in RIG-I knockdown cells at the transcriptional level following virus infection, only infected control knockdown cells achieved the highest expression levels of both. This scenario is also reminiscent of that in dengue or reovirus infection (Loo et al., 2008), and suggests the likely corroborative involvement of perhaps both RIG-I and MDA5 in the recognition of IBV, or the dependence of another novel cytoplasmic PRR that also triggers MAVS activation and downstream signalling. The latter could also explain why transient expression of MDA5 or RIG-I, which has been shown to exist in a state of auto-inhibition in the absence of activating ligands (Gee et al., 2008), did not have a significant effect on the attenuation of virus replication in infected mammalian cells, whereas transient expression of MAVS could almost entirely quell IBV infection as well as the formation of CPE when activated.

5.2.2.2 The role of LGP2 in regulating RIG-I and MDA5 signalling during IBV infection

While the data presented here could not clearly identify the main PRR(s) involved in the recognition of avian IBV, the interplay among RLH signalling components, at least at the transcriptional level, could be briefly outlined. Although similar in structure, the exact function of LGP2 in viral RNA detection is still largely debatable. LGP2 is deficient in the CARDs at the N-terminal, and is currently presumed to be a regulator of RIG-I and MDA5 signalling (Satoh et al., 2010;

Yoneyama et al., 2005). This is also observed in the data presented here, where an increase in LGP2 expression corresponded with an increase in RIG-I levels. Recent reports have highlighted the importance of the LGP2 functional repressor domain (RD) that, when expressed alone, can subdue RIG-I signalling, suggesting the regulation of RLH signalling by LGP2 through RD interactions with RIG-I, and probably with MDA5 as well (Saito et al., 2007). It is therefore likely that distinct RD interactions, and differential RNA ligand binding, could determine the distinct roles of LGP2 as a positive or negative regulator of RLH signalling. Transient expression and site-directed mutagenesis data for LGP2, as well as a more efficient antibody that can distinctly detect LGP2 in immunoblotting experiments, would be useful in the further clarification of the role LGP2 may play in the regulation of RLH signalling during IBV infection.

5.2.2.3 ISG56 negatively regulates virus-induced RIG-I signalling

RIG-I knockdown H1299 cells infected with IBV, exhibited significant attenuation of gene expression, such as that of IFNβ and ISG56, whose gene products are involved in innate immune response. As expected, transient expression of RIG-I in the same cells saw an enhanced expression of ISG56 at the translational level. However, distinct regulation of ISG56 was also observed in $IFN^{-/-}$ cells than that in cells exhibiting normal IFN responses. This is not surprising, given the role of ISG56 in the negative feedback regulation of viral-induced signalling in response to type I interferon induction (Li et al., 2009). This could also explain the reduced levels of ISG56 in cells stably expressing reduced levels of MAVS.

To further validate the results obtained in this study, more work could be done in the generation of stable cell lines that allow for the stable silencing of appropriate genes such as RIG-I and/or MDA5, respectively, without the need for the introduction

of transfection reagents that may unintentionally induce additional cell stress due to the long periods of incubation under serum free conditions. These unfavourable conditions would likely trigger IFN induction in response to stress, and may therefore not genuinely reflect the actual effects of MDA5 and RIG-I signalling during IBV infection in wildtype, untreated cells. The need for stably silenced cells is especially relevant in this study, as reflected in the higher levels of IFN and ISGs induced compared to IBV-infected wildtype cells that have not undergone long hours of incubation during transfection. In the long run, knockout models in mice or other appropriate animal models would also be advantageous in verifying the *in vivo* effects of MDA5 and RIG-I recognition on avian IBV replication and viral progeny production.

5.2.2.4 MAVS is essential in antiviral innate immune response signalling

As with many other RNA viruses (Loo and Gale, 2011), MAVS is also indispensible for the transmittance of innate immune response signals to IBV invasion in mammalian cells. This is evident in the significant attenuation of viral protein production in infected cells transiently expressing MAVS. As such, the requirement for viral replication in MAVS activation of downstream IFN responses at the transcriptional level has also been shown in this study. Given its fundamental role in initiating the activation of downstream immunomodulatory components, MAVS is likely a major focus on which virus-mounted counterattacks of the host defence system is based. Meylan *et al.* have further corroborated this hypothesis by demonstrating the ability of HCV viral NS3/4A protease to cleave and inactivate MAVS signalling (Meylan et al., 2005).

5.2.2.5 MAVS is cleaved during IBV-induced apoptosis

In this study, the cleavage of MAVS was observed in tandem with PARP

cleavage, the latter being a classic hallmark of apoptosis. MAVS cleavage was also observed in chemically-induced apoptosis (staurosporine), synthetic dsRNA-induced apoptosis [poly(I:C)] as well as in IBV-induced apoptosis. MAVS cleavage was also determined to be caspase dependent, and may involve pro-apoptotic members of the Bcl-2 family, as has also been previously shown (Vince and Tschopp, 2010). In contrast, Mcl-1, an anti-apoptotic member from the Bcl-2 family of proteins, was able to reduce IBV-induced MAVS cleavage. The role of MAVS in the regulation of apoptosis, however, is the subject of many debates. Transient expression of MAVS has been shown to induce apoptosis in uninfected cells (Lei et al., 2009). In this study, however, transient MAVS knockdown through RNAi unexpectedly displayed a faster rate of apoptosis when the cells were subjected to IBV infection. This trend has also been previously observed in HEK293 cells, with a decrease in MAVS expression enhancing virus-triggered cell death (Seth et al., 2005).

5.2.2.6 The regulation of IBV-induced apoptosis by MDA5, RIG-I, and MAVS

In a similar vein, MDA5 was also observed to undergo cleavage during poliovirus infection (Barral et al., 2007). While this could not be observed in the data presented here, a decrease in full-length MDA5 was observed with a corresponding increase in the cleavage of both MAVS and PARP during late stages of the infection, suggesting the possibly of enhanced virus-induced cell death. A delayed rate of apoptosis was observed in RIG-I knockdown cells in the late stages of infection, while an increase in the rate of apoptosis was observed at the same time point in infected cells transiently expressing RIG-I, although the rate of apoptosis was still slower than that in infected negative control cells transiently expressing an empty vector. The induction of apoptosis by activated RIG-I has previously been shown in human ovarian cancer cells (Kubler et al., 2010). Thus, as the activation of RIG-I and MDA-5 through

viral RNA recognition triggers MAVS-induced downstream innate immune responses, the concurrent onset of apoptosis may serve as another aspect of host antiviral response (Besch et al., 2009). Yet, as shown in this study, the latter form of host defence appears to be thwarted by viral counterattack mechanisms during the late stages of avian IBV infection.

5.2.2.7 Viral defence mechanisms in the elusion of host antiviral innate immunity

The ability of IBV to evade host antiviral responses was also confirmed through the co-expression studies of RLHs with individual segments of IBV RNA. IFNβ activity was not detected when MDA5 or RIG-I was co-expressed with total IBV RNA, nor through co-expression with the fourth segment of the IBV genome, suggesting the potentiality of certain IBV proteins, possibly from this specific region of the genome, with host antiviral evasive mechanisms.

Viral mechanisms that may thwart MAVS-mediated antiviral responses were then studied. As such, further investigation of MAVS with selected IBV structural and non-structural proteins, mainly from the fourth segment of the IBV genome, called attention to nsp15, which, at high concentrations, was shown to both decrease full-length MAVS expression levels and inhibit MAVS-induced phosphoactivation of IRF3. As IBV nsp15 is a highly conserved endonuclease required for viral replication (Fang et al., 2010), MAVS could be a likely target of nsp15-mediated intervention of downstream innate immunity signalling pathways that ultimately results in an attenuated IFN response. Moreover, as nsp15 lies in the IBV-D segment of the avian coronavirus genome, which did not elicit an increase in IFNβ activity in the presence of MDA5 or RIG-I, this further corroborates with the hypothesized ability of IBV to avoid recognition by PRRs.

Also present in the fourth segment of the IBV genome is nsp16, which has been

associated with 2'-*O*-methyltransferase activity. The 2'-*O*-methylation of human and mouse coronaviral mRNA has recently been found to be vital in the evasion of innate immune responses in the host cell; conferred through the 2'-*O*-methyltransferase activity in nsp16, this is an RNA modification which mimics the ribose 2'-*O*-methylation of higher eukaryotic mRNAs and is known to be a unique molecular motif that differentiates self mRNA from foreign non-self ones (Zust et al., 2011). The ability of coronaviruses from different species to undergo 2'-*O*-methylation of their respective viral mRNA thus collectively prevents the recognition of their 2'-*O*-methylated viral mRNA as non-self mRNA by RLHs, thereby minimizing RLH dependent-dependent IFN response and allowing for the escape of IFN-induced attenuation of coronaviral replication (Zust et al., 2011). Future studies that place emphasis on the significance of coronaviral mRNA modifications by viral proteins such as nsp16 would further shed light on the viral mechanisms behind evasion of avian IBV from MDA5 and/or RIG-I recognition.

A report on the ability of SARS-CoV nsp15 in abrogating MAVS-induced apoptosis (Lei et al., 2009) prompted an examination of IBV nsp15 in the same, here in this study. While FACS analysis did show a slight decrease in the percentage of apoptotic cells in the population of cells co-expressing IBV nsp15 and MAVS, in comparison to cells transiently expressing MAVS alone, the onset of apoptosis was not actually observed at the translational level. As such, this anomaly may need to be addressed by other cell viability assays, such as the XTT (2,3-bis-(2-methoxy-4-nitro-5-sulfophenyl)-2H-tetrazolium-5-carboxanilide) based cell proliferation assay, and/or the Trypan blue exclusion test of cell viability.

5.2.2.8 Conclusion

In conclusion, this study turns the spotlight on the all-important mitochondrion

as a centre stage for the coordination of host antiviral innate immune responses and the mitochondria-mediated apoptotic responses in answer to viral invasion. MAVS is also identified here as a key player in connecting both forms of host defence mechanisms, and appears as an appealing therapeutic target for the future development of antiviral drug tactics.

5.3 FINAL REMARKS

The intricate network between a virus and its host is a complicated affair that involves many players - derived from both virus and host – which are pitted against one other in the battle for ascendancy of one over the other; certain host processes are readily assimilated and manipulated by the virus in its bid to impede host antiviral responses while the host is itself armoured with several lines of defence mechanisms and numerous antiviral factors to combat viral invasion to prevent its spread.

While much progress has been made in the elucidation of the various regulatory pathways that, under the most propitious of conditions, will allow virus and host to co-exist in an uneasy truce, a clearer understanding of the complex interplay between the virus and its host could give new insights into the role of main players, such as those that govern the onset of apoptosis, or type I interferons and their regulators, and lead to the discovery of novel and/or universal targets for the therapeutic mediation against pathogenic infection.

REFERENCES

Aaronson, D. S., and Horvath, C. M. (2002). A road map for those who don't know JAK-STAT. *Science* **296**(5573)**,** 1653-5.

Ablasser, A., Bauernfeind, F., Hartmann, G., Latz, E., Fitzgerald, K. A., and Hornung, V. (2009). RIG-I-dependent sensing of poly(dA:dT) through the induction of an RNA polymerase III-transcribed RNA intermediate. *Nat Immunol* **10**(10)**,** 1065-72.

Adams, J. M., and Cory, S. (2001). Life-or-death decisions by the Bcl-2 protein family. *Trends Biochem Sci* **26**(1)**,** 61-6.

Adams, K. W., and Cooper, G. M. (2007). Rapid turnover of mcl-1 couples translation to cell survival and apoptosis. *J Biol Chem* **282**(9)**,** 6192-200.

Albershardt, T. C., Salerni, B. L., Soderquist, R. S., Bates, D. J., Pletnev, A. A., Kisselev, A. F., and Eastman, A. (2011). Multiple BH3 mimetics antagonize anti-apoptotic MCL1 by inducing the endoplasmic reticulum stress response and up-regulating BH3-only protein NOXA. *J Biol Chem*.

Alcami, A., and Koszinowski, U. H. (2000). Viral mechanisms of immune evasion. *Immunol Today* **21**(9)**,** 447-55.

Ariyama, Y., Tanaka, Y., Shimizu, H., Shimomura, K., Okada, S., Saito, T., Yamada, E., Oyadomari, S., and Mori, M. (2008). The role of CHOP messenger RNA expression in the link between oxidative stress and apoptosis. *Metabolism* **57**(12)**,** 1625-35.

Arndt, A. L., Larson, B. J., and Hogue, B. G. (2010). A conserved domain in the coronavirus membrane protein tail is important for virus assembly. *J Virol* **84**(21)**,** 11418-28.

Ashkenazi, A., and Dixit, V. M. (1998). Death receptors: signaling and modulation. *Science* **281**(5381)**,** 1305-8.

Assuncao Guimaraes, C., and Linden, R. (2004). Programmed cell deaths. Apoptosis and alternative deathstyles. *Eur J Biochem* **271**(9)**,** 1638-50.

Bacon, L. D., Hunter, D. B., Zhang, H. M., Brand, K., and Etches, R. (2004). Retrospective evidence that the MHC (B haplotype) of chickens influences genetic resistance to attenuated infectious bronchitis vaccine strains in chickens. *Avian Pathol* **33**(6)**,** 605-9.

Barber, G. N. (2001). Host defense, viruses and apoptosis. *Cell Death Differ* **8**(2)**,** 113-26.

Barber, M. R., Aldridge, J. R., Jr., Webster, R. G., and Magor, K. E. (2010). Association of RIG-I with innate immunity of ducks to influenza. *Proc Natl Acad Sci U S A* **107**(13)**,** 5913-8.

Baril, M., Racine, M. E., Penin, F., and Lamarre, D. (2009). MAVS dimer is a crucial signaling component of innate immunity and the target of hepatitis C virus NS3/4A protease. *J Virol* **83**(3)**,** 1299-311.

Barral, P. M., Morrison, J. M., Drahos, J., Gupta, P., Sarkar, D., Fisher, P. B., and Racaniello, V. R. (2007). MDA-5 is cleaved in poliovirus-infected cells. *J Virol* **81**(8)**,** 3677-84.

Besch, R., Poeck, H., Hohenauer, T., Senft, D., Hacker, G., Berking, C., Hornung, V., Endres, S., Ruzicka, T., Rothenfusser, S., and Hartmann, G. (2009). Proapoptotic signaling induced by RIG-I and MDA-5 results in type I interferon-independent apoptosis in human melanoma cells. *J Clin Invest* **119**(8)**,** 2399-411.

Bhardwaj, K., Guarino, L., and Kao, C. C. (2004). The severe acute respiratory syndrome coronavirus Nsp15 protein is an endoribonuclease that prefers manganese as a cofactor. *J Virol* **78**(22)**,** 12218-24.

Boulares, A. H., Yakovlev, A. G., Ivanova, V., Stoica, B. A., Wang, G., Iyer, S., and Smulson, M. (1999). Role of poly(ADP-ribose) polymerase (PARP) cleavage in apoptosis. Caspase 3-resistant PARP mutant increases rates of apoptosis in transfected cells. *J Biol Chem* **274**(33)**,** 22932-40.

Bowie, A. G., and Fitzgerald, K. A. (2007). RIG-I: tri-ing to discriminate between self and non-self RNA. *Trends Immunol* **28**(4)**,** 147-50.

Brian, D. A., and Baric, R. S. (2005). Coronavirus genome structure and replication. *Curr Top Microbiol Immunol* **287,** 1-30.

Brockway, S. M., Clay, C. T., Lu, X. T., and Denison, M. R. (2003). Characterization of the expression, intracellular localization, and replication complex association of the putative mouse hepatitis virus RNA-dependent RNA polymerase. *J Virol* **77**(19)**,** 10515-27.

Brockway, S. M., and Denison, M. R. (2005). Mutagenesis of the murine hepatitis virus nsp1-coding region identifies residues important for protein processing, viral RNA synthesis, and viral replication. *Virology* **340**(2)**,** 209-23.

Brojatsch, J., Naughton, J., Rolls, M. M., Zingler, K., and Young, J. A. (1996). CAR1, a TNFR-related protein, is a cellular receptor for cytopathic avian leukosis-sarcoma viruses and mediates

apoptosis. *Cell* **87**(5)**,** 845-55.
Cam, M., Handke, W., Picard-Maureau, M., and Brune, W. (2010). Cytomegaloviruses inhibit Bak- and Bax-mediated apoptosis with two separate viral proteins. *Cell Death Differ* **17**(4)**,** 655-65.
Cao, J., Wu, C. C., and Lin, T. L. (2008). Complete nucleotide sequence of polyprotein gene 1 and genome organization of turkey coronavirus. *Virus Res* **136**(1-2)**,** 43-9.
Cao, X., Yang, M., Wei, R. C., Zeng, Y., Gu, J. F., Huang, W. D., Yang, D. Q., Li, H. L., Ding, M., Wei, N., Zhang, K. J., Xu, B., Liu, X. R., Qian, Q. J., and Liu, X. Y. (2011). Cancer targeting Gene-Viro-Therapy of liver carcinoma by dual-regulated oncolytic adenovirus armed with TRAIL gene. *Gene Ther*.
Casais, R., Dove, B., Cavanagh, D., and Britton, P. (2003). Recombinant avian infectious bronchitis virus expressing a heterologous spike gene demonstrates that the spike protein is a determinant of cell tropism. *J Virol* **77**(16)**,** 9084-9.
Casais, R., Thiel, V., Siddell, S. G., Cavanagh, D., and Britton, P. (2001). Reverse genetics system for the avian coronavirus infectious bronchitis virus. *J Virol* **75**(24)**,** 12359-69.
Castanier, C., Garcin, D., Vazquez, A., and Arnoult, D. (2010). Mitochondrial dynamics regulate the RIG-I-like receptor antiviral pathway. *EMBO Rep* **11**(2)**,** 133-8.
Cavanagh, D. (1997). Nidovirales: a new order comprising Coronaviridae and Arteriviridae. *Arch Virol* **142**(3)**,** 629-33.
Cavanagh, D. (2003). Severe acute respiratory syndrome vaccine development: experiences of vaccination against avian infectious bronchitis coronavirus. *Avian Pathol* **32**(6)**,** 567-82.
Cavanagh, D. (2005). Coronaviruses in poultry and other birds. *Avian Pathol* **34**(6)**,** 439-48.
Cavanagh, D. (2007). Coronavirus avian infectious bronchitis virus. *Vet Res* **38**(2)**,** 281-97.
Cavanagh, D., Brian, D. A., Brinton, M. A., Enjuanes, L., Holmes, K. V., Horzinek, M. C., Lai, M. M., Laude, H., Plagemann, P. G., Siddell, S. G., and et al. (1993). The Coronaviridae now comprises two genera, coronavirus and torovirus: report of the Coronaviridae Study Group. *Adv Exp Med Biol* **342,** 255-7.
Chawla-Sarkar, M., Lindner, D. J., Liu, Y. F., Williams, B. R., Sen, G. C., Silverman, R. H., and Borden, E. C. (2003). Apoptosis and interferons: role of interferon-stimulated genes as mediators of apoptosis. *Apoptosis* **8**(3)**,** 237-49.
Cohen, J. R., Lin, L. D., and Machamer, C. E. (2011). Identification of a Golgi complex-targeting signal in the cytoplasmic tail of the severe acute respiratory syndrome coronavirus envelope protein. *J Virol* **85**(12)**,** 5794-803.
Cottam, E. M., Maier, H. J., Manifava, M., Vaux, L. C., Chandra-Schoenfelder, P., Gerner, W., Britton, P., Ktistakis, N. T., and Wileman, T. (2011). Coronavirus nsp6 proteins generate autophagosomes from the endoplasmic reticulum via an omegasome intermediate. *Autophagy* **7**(11)**,** 1335-47.
Cuconati, A., Degenhardt, K., Sundararajan, R., Anschel, A., and White, E. (2002). Bak and Bax function to limit adenovirus replication through apoptosis induction. *J Virol* **76**(9)**,** 4547-58.
Cuconati, A., Mukherjee, C., Perez, D., and White, E. (2003). DNA damage response and MCL-1 destruction initiate apoptosis in adenovirus-infected cells. *Genes Dev* **17**(23)**,** 2922-32.
Cui, S., Eisenacher, K., Kirchhofer, A., Brzozka, K., Lammens, A., Lammens, K., Fujita, T., Conzelmann, K. K., Krug, A., and Hopfner, K. P. (2008). The C-terminal regulatory domain is the RNA 5'-triphosphate sensor of RIG-I. *Mol Cell* **29**(2)**,** 169-79.
Danial, N. N., and Korsmeyer, S. J. (2004). Cell death: critical control points. *Cell* **116**(2)**,** 205-19.
Danthi, P. (2011). Enter the kill zone: initiation of death signaling during virus entry. *Virology* **411**(2)**,** 316-24.
de Groot, R. J. (2006). Structure, function and evolution of the hemagglutinin-esterase proteins of corona- and toroviruses. *Glycoconj J* **23**(1-2)**,** 59-72.
de Veer, M. J., Holko, M., Frevel, M., Walker, E., Der, S., Paranjape, J. M., Silverman, R. H., and Williams, B. R. (2001). Functional classification of interferon-stimulated genes identified using microarrays. *J Leukoc Biol* **69**(6)**,** 912-20.
Decroly, E., Imbert, I., Coutard, B., Bouvet, M., Selisko, B., Alvarez, K., Gorbalenya, A. E., Snijder, E. J., and Canard, B. (2008). Coronavirus nonstructural protein 16 is a cap-0 binding enzyme possessing (nucleoside-2'O)-methyltransferase activity. *J Virol* **82**(16)**,** 8071-84.
Dong, L., Jiang, C. C., Thorne, R. F., Croft, A., Yang, F., Liu, H., de Bock, C. E., Hersey, P., and Zhang, X. D. (2011). Ets-1 mediates upregulation of Mcl-1 downstream of XBP-1 in human melanoma cells upon ER stress. *Oncogene*.
Du, H., Wolf, J., Schafer, B., Moldoveanu, T., Chipuk, J. E., and Kuwana, T. (2011). BH3 domains other than Bim and Bid can directly activate Bax/Bak. *J Biol Chem* **286**(1)**,** 491-501.
Eckerle, L. D., Brockway, S. M., Sperry, S. M., Lu, X., and Denison, M. R. (2006). Effects of

mutagenesis of murine hepatitis virus nsp1 and nsp14 on replication in culture. *Adv Exp Med Biol* **581,** 55-60.

Egloff, M. P., Ferron, F., Campanacci, V., Longhi, S., Rancurel, C., Dutartre, H., Snijder, E. J., Gorbalenya, A. E., Cambillau, C., and Canard, B. (2004). The severe acute respiratory syndrome-coronavirus replicative protein nsp9 is a single-stranded RNA-binding subunit unique in the RNA virus world. *Proc Natl Acad Sci U S A* **101**(11)**,** 3792-6.

Elmore, S. (2007). Apoptosis: a review of programmed cell death. *Toxicol Pathol* **35**(4)**,** 495-516.

Emmott, E., Rodgers, M. A., Macdonald, A., McCrory, S., Ajuh, P., and Hiscox, J. A. (2010). Quantitative proteomics using stable isotope labeling with amino acids in cell culture reveals changes in the cytoplasmic, nuclear, and nucleolar proteomes in Vero cells infected with the coronavirus infectious bronchitis virus. *Mol Cell Proteomics* **9**(9)**,** 1920-36.

Enjuanes, L., Almazan, F., Sola, I., and Zuniga, S. (2006). Biochemical aspects of coronavirus replication and virus-host interaction. *Annu Rev Microbiol* **60,** 211-30.

Escors, D., Capiscol, C., and Enjuanes, L. (2004). Immunopurification applied to the study of virus protein composition and encapsidation. *J Virol Methods* **119**(2)**,** 57-64.

Fang, S., Shen, H., Wang, J., Tay, F. P., and Liu, D. X. (2010). Functional and genetic studies of the substrate specificity of coronavirus infectious bronchitis virus 3C-like proteinase. *J Virol* **84**(14)**,** 7325-36.

Fang, S. G., Shen, S., Tay, F. P., and Liu, D. X. (2005). Selection of and recombination between minor variants lead to the adaptation of an avian coronavirus to primate cells. *Biochem Biophys Res Commun* **336**(2)**,** 417-23.

Fensterl, V., and Sen, G. C. (2009). Interferons and viral infections. *BioFactors* **35**(1)**,** 14-20.

Fensterl, V., and Sen, G. C. (2011). The ISG56/IFIT1 gene family. *J Interferon Cytokine Res* **31**(1)**,** 71-8.

Ferri, K. F., and Kroemer, G. (2001). Organelle-specific initiation of cell death pathways. *Nat Cell Biol* **3**(11)**,** E255-63.

Frieman, M., Heise, M., and Baric, R. (2008). SARS coronavirus and innate immunity. *Virus Res* **133**(1)**,** 101-12.

Fujita, T., Onoguchi, K., Onomoto, K., Hirai, R., and Yoneyama, M. (2007). Triggering antiviral response by RIG-I-related RNA helicases. *Biochimie* **89**(6-7)**,** 754-60.

Galonek, H. L., and Hardwick, J. M. (2006). Upgrading the BCL-2 network. *Nat Cell Biol* **8**(12)**,** 1317-9.

Garcia, M. A., Meurs, E. F., and Esteban, M. (2007). The dsRNA protein kinase PKR: virus and cell control. *Biochimie* **89**(6-7)**,** 799-811.

Garcia-Sastre, A., and Biron, C. A. (2006). Type 1 interferons and the virus-host relationship: a lesson in detente. *Science* **312**(5775)**,** 879-82.

Gee, P., Chua, P. K., Gevorkyan, J., Klumpp, K., Najera, I., Swinney, D. C., and Deval, J. (2008). Essential role of the N-terminal domain in the regulation of RIG-I ATPase activity. *J Biol Chem* **283**(14)**,** 9488-96.

Goebel, S. J., Hsue, B., Dombrowski, T. F., and Masters, P. S. (2004). Characterization of the RNA components of a putative molecular switch in the 3' untranslated region of the murine coronavirus genome. *J Virol* **78**(2)**,** 669-82.

Goh, P. Y., Tan, Y. J., Lim, S. P., Lim, S. G., Tan, Y. H., and Hong, W. J. (2001). The hepatitis C virus core protein interacts with NS5A and activates its caspase-mediated proteolytic cleavage. *Virology* **290**(2)**,** 224-36.

Gonzalez, J. M., Gomez-Puertas, P., Cavanagh, D., Gorbalenya, A. E., and Enjuanes, L. (2003). A comparative sequence analysis to revise the current taxonomy of the family Coronaviridae. *Arch Virol* **148**(11)**,** 2207-35.

Green, D. R. (2006). At the gates of death. *Cancer Cell* **9**(5)**,** 328-30.

Han, Z., Sun, C., Yan, B., Zhang, X., Wang, Y., Li, C., Zhang, Q., Ma, Y., Shao, Y., Liu, Q., Kong, X., and Liu, S. (2011). A 15-year analysis of molecular epidemiology of avian infectious bronchitis coronavirus in China. *Infect Genet Evol* **11**(1)**,** 190-200.

Harcourt, B. H., Jukneliene, D., Kanjanahaluethai, A., Bechill, J., Severson, K. M., Smith, C. M., Rota, P. A., and Baker, S. C. (2004). Identification of severe acute respiratory syndrome coronavirus replicase products and characterization of papain-like protease activity. *J Virol* **78**(24)**,** 13600-12.

Harding, H. P., Zhang, Y., Zeng, H., Novoa, I., Lu, P. D., Calfon, M., Sadri, N., Yun, C., Popko, B., Paules, R., Stojdl, D. F., Bell, J. C., Hettmann, T., Leiden, J. M., and Ron, D. (2003). An integrated stress response regulates amino acid metabolism and resistance to oxidative stress. *Mol Cell* **11**(3)**,** 619-33.

Hay, S., and Kannourakis, G. (2002). A time to kill: viral manipulation of the cell death program. *J Gen Virol* **83**(Pt 7)**,** 1547-64.

Hitomi, J., Katayama, T., Eguchi, Y., Kudo, T., Taniguchi, M., Koyama, Y., Manabe, T., Yamagishi, S., Bando, Y., Imaizumi, K., Tsujimoto, Y., and Tohyama, M. (2004). Involvement of caspase-4 in endoplasmic reticulum stress-induced apoptosis and Abeta-induced cell death. *J Cell Biol* **165**(3)**,** 347-56.

Holmes, E. C., and Rambaut, A. (2004). Viral evolution and the emergence of SARS coronavirus. *Philos Trans R Soc Lond B Biol Sci* **359**(1447)**,** 1059-65.

Hurst, K. R., Koetzner, C. A., and Masters, P. S. (2009). Identification of in vivo-interacting domains of the murine coronavirus nucleocapsid protein. *J Virol* **83**(14)**,** 7221-34.

Hurst, K. R., Ye, R., Goebel, S. J., Jayaraman, P., and Masters, P. S. (2010). An interaction between the nucleocapsid protein and a component of the replicase-transcriptase complex is crucial for the infectivity of coronavirus genomic RNA. *J Virol* **84**(19)**,** 10276-88.

Hyde, B. B., Twig, G., and Shirihai, O. S. (2010). Organellar vs cellular control of mitochondrial dynamics. *Semin Cell Dev Biol* **21**(6)**,** 575-81.

Ignjatovic, J., and Sapats, S. (2000). Avian infectious bronchitis virus. *Rev Sci Tech* **19**(2)**,** 493-508.

Ivanov, K. A., Hertzig, T., Rozanov, M., Bayer, S., Thiel, V., Gorbalenya, A. E., and Ziebuhr, J. (2004a). Major genetic marker of nidoviruses encodes a replicative endoribonuclease. *Proc Natl Acad Sci U S A* **101**(34)**,** 12694-9.

Ivanov, K. A., Thiel, V., Dobbe, J. C., van der Meer, Y., Snijder, E. J., and Ziebuhr, J. (2004b). Multiple enzymatic activities associated with severe acute respiratory syndrome coronavirus helicase. *J Virol* **78**(11)**,** 5619-32.

Ivanov, K. A., and Ziebuhr, J. (2004). Human coronavirus 229E nonstructural protein 13: characterization of duplex-unwinding, nucleoside triphosphatase, and RNA 5'-triphosphatase activities. *J Virol* **78**(14)**,** 7833-8.

Jiang, C. C., Lucas, K., Avery-Kiejda, K. A., Wade, M., deBock, C. E., Thorne, R. F., Allen, J., Hersey, P., and Zhang, X. D. (2008). Up-regulation of Mcl-1 is critical for survival of human melanoma cells upon endoplasmic reticulum stress. *Cancer Res* **68**(16)**,** 6708-17.

Jurgensmeier, J. M., Krajewski, S., Armstrong, R. C., Wilson, G. M., Oltersdorf, T., Fritz, L. C., Reed, J. C., and Ottilie, S. (1997). Bax- and Bak-induced cell death in the fission yeast Schizosaccharomyces pombe. *Mol Biol Cell* **8**(2)**,** 325-39.

Kato, H., Takeuchi, O., Mikamo-Satoh, E., Hirai, R., Kawai, T., Matsushita, K., Hiiragi, A., Dermody, T. S., Fujita, T., and Akira, S. (2008). Length-dependent recognition of double-stranded ribonucleic acids by retinoic acid-inducible gene-I and melanoma differentiation-associated gene 5. *J Exp Med* **205**(7)**,** 1601-10.

Kawai, T., Sato, S., Ishii, K. J., Coban, C., Hemmi, H., Yamamoto, M., Terai, K., Matsuda, M., Inoue, J., Uematsu, S., Takeuchi, O., and Akira, S. (2004). Interferon-alpha induction through Toll-like receptors involves a direct interaction of IRF7 with MyD88 and TRAF6. *Nat Immunol* **5**(10)**,** 1061-8.

Kawai, T., Takahashi, K., Sato, S., Coban, C., Kumar, H., Kato, H., Ishii, K. J., Takeuchi, O., and Akira, S. (2005). IPS-1, an adaptor triggering RIG-I- and Mda5-mediated type I interferon induction. *Nat Immunol* **6**(10)**,** 981-8.

Kim, H., Rafiuddin-Shah, M., Tu, H. C., Jeffers, J. R., Zambetti, G. P., Hsieh, J. J., and Cheng, E. H. (2006). Hierarchical regulation of mitochondrion-dependent apoptosis by BCL-2 subfamilies. *Nat Cell Biol* **8**(12)**,** 1348-58.

Kim, I., Xu, W., and Reed, J. C. (2008). Cell death and endoplasmic reticulum stress: disease relevance and therapeutic opportunities. *Nat Rev Drug Discov* **7**(12)**,** 1013-30.

King, D. J., and Cavanagh, D. (1991). Infectious Bronchitis. *In* "Disease of Poultry" (B. W. Calnek, H. J. Barnes, C. W. Beard, W. M. Reid, and H. W. J. Yoder, Eds.), pp. 471-84. Iowa State University Press, Ames, Iowa.

Komuro, A., Bamming, D., and Horvath, C. M. (2008). Negative regulation of cytoplasmic RNA-mediated antiviral signaling. *Cytokine* **43**(3)**,** 350-8.

Komuro, A., and Horvath, C. M. (2006). RNA- and virus-independent inhibition of antiviral signaling by RNA helicase LGP2. *J Virol* **80**(24)**,** 12332-42.

Korsmeyer, S. J., Wei, M. C., Saito, M., Weiler, S., Oh, K. J., and Schlesinger, P. H. (2000). Pro-apoptotic cascade activates BID, which oligomerizes BAK or BAX into pores that result in the release of cytochrome c. *Cell Death Differ* **7**(12)**,** 1166-73.

Koshiba, T., Yasukawa, K., Yanagi, Y., and Kawabata, S. (2011). Mitochondrial membrane potential is required for MAVS-mediated antiviral signaling. *Sci Signal* **4**(158)**,** ra7.

Kubler, K., Gehrke, N., Riemann, S., Bohnert, V., Zillinger, T., Hartmann, E., Polcher, M., Rudlowski,

C., Kuhn, W., Hartmann, G., and Barchet, W. (2010). Targeted activation of RNA helicase retinoic acid-inducible gene-I induces proimmunogenic apoptosis of human ovarian cancer cells. *Cancer Res* **70**(13)**,** 5293-304.

Kumar, H., Kawai, T., and Akira, S. (2009). Toll-like receptors and innate immunity. *Biochem Biophys Res Commun* **388**(4)**,** 621-5.

Kumar, H., Kawai, T., Kato, H., Sato, S., Takahashi, K., Coban, C., Yamamoto, M., Uematsu, S., Ishii, K. J., Takeuchi, O., and Akira, S. (2006). Essential role of IPS-1 in innate immune responses against RNA viruses. *J Exp Med* **203**(7)**,** 1795-803.

Kurokawa, M., Koyama, A. H., Yasuoka, S., and Adachi, A. (1999). Influenza virus overcomes apoptosis by rapid multiplication. *Int J Mol Med* **3**(5)**,** 527-30.

Lagos, D., Trotter, M. W., Vart, R. J., Wang, H. W., Matthews, N. C., Hansen, A., Flore, O., Gotch, F., and Boshoff, C. (2007). Kaposi sarcoma herpesvirus-encoded vFLIP and vIRF1 regulate antigen presentation in lymphatic endothelial cells. *Blood* **109**(4)**,** 1550-8.

Lai, M. M. (1990). Coronavirus: organization, replication and expression of genome. *Annu Rev Microbiol* **44,** 303-33.

Lai, M. M., and Cavanagh, D. (1997). The molecular biology of coronaviruses. *Adv Virus Res* **48,** 1-100.

Lai, M. M., and Holmes, K. V. (2001). "Coronaviruses." 4th ed. Fields Virology (D. M. Knipe, and P. M. Howley, Eds.) Lippincott, Williams & Wilkins, Philadelphia, PA.

Landman, W. J., and Feberwee, A. (2004). Aerosol-induced Mycoplasma synoviae arthritis: the synergistic effect of infectious bronchitis virus infection. *Avian Pathol* **33**(6)**,** 591-8.

Laude, H., Rasschaert, D., Delmas, B., Godet, M., Gelfi, J., and Charley, B. (1990). Molecular biology of transmissible gastroenteritis virus. *Vet Microbiol* **23**(1-4)**,** 147-54.

Lei, Y., Moore, C. B., Liesman, R. M., O'Connor, B. P., Bergstralh, D. T., Chen, Z. J., Pickles, R. J., and Ting, J. P. (2009). MAVS-mediated apoptosis and its inhibition by viral proteins. *PLoS One* **4**(5)**,** e5466.

Leu, J. I., Dumont, P., Hafey, M., Murphy, M. E., and George, D. L. (2004). Mitochondrial p53 activates Bak and causes disruption of a Bak-Mcl1 complex. *Nat Cell Biol* **6**(5)**,** 443-50.

Levine, A. J. (1997). p53, the cellular gatekeeper for growth and division. *Cell* **88**(3)**,** 323-31.

Li, F. Q., Tam, J. P., and Liu, D. X. (2007). Cell cycle arrest and apoptosis induced by the coronavirus infectious bronchitis virus in the absence of p53. *Virology* **365**(2)**,** 435-45.

Li, J., Lee, B., and Lee, A. S. (2006). Endoplasmic reticulum stress-induced apoptosis: multiple pathways and activation of p53-up-regulated modulator of apoptosis (PUMA) and NOXA by p53. *J Biol Chem* **281**(11)**,** 7260-70.

Li, J., Liu, Y., and Zhang, X. (2010). Murine coronavirus induces type I interferon in oligodendrocytes through recognition by RIG-I and MDA5. *J Virol* **84**(13)**,** 6472-82.

Li, X. D., Sun, L., Seth, R. B., Pineda, G., and Chen, Z. J. (2005). Hepatitis C virus protease NS3/4A cleaves mitochondrial antiviral signaling protein off the mitochondria to evade innate immunity. *Proc Natl Acad Sci U S A* **102**(49)**,** 17717-22.

Li, Y., Li, C., Xue, P., Zhong, B., Mao, A. P., Ran, Y., Chen, H., Wang, Y. Y., Yang, F., and Shu, H. B. (2009). ISG56 is a negative-feedback regulator of virus-triggered signaling and cellular antiviral response. *Proc Natl Acad Sci U S A* **106**(19)**,** 7945-50.

Liao, Y., Wang, X., Huang, M., Tam, J. P., and Liu, D. X. (2011). Regulation of the p38 mitogen-activated protein kinase and dual-specificity phosphatase 1 feedback loop modulates the induction of interleukin 6 and 8 in cells infected with coronavirus infectious bronchitis virus. *Virology* **420**(2)**,** 106-16.

Lin, R., Heylbroeck, C., Genin, P., Pitha, P. M., and Hiscott, J. (1999). Essential role of interferon regulatory factor 3 in direct activation of RANTES chemokine transcription. *Mol Cell Biol* **19**(2)**,** 959-66.

Liu, C., Xu, H. Y., and Liu, D. X. (2001). Induction of caspase-dependent apoptosis in cultured cells by the avian coronavirus infectious bronchitis virus. *J Virol* **75**(14)**,** 6402-9.

Liu, D. X., and Inglis, S. C. (1991). Association of the infectious bronchitis virus 3c protein with the virion envelope. *Virology* **185**(2)**,** 911-7.

Liu, D. X., and Inglis, S. C. (1992). Identification of two new polypeptides encoded by mRNA5 of the coronavirus infectious bronchitis virus. *Virology* **186**(1)**,** 342-7.

Liu, D. X., Shen, S., Xu, H. Y., and Wang, S. F. (1998). Proteolytic mapping of the coronavirus infectious bronchitis virus 1b polyprotein: evidence for the presence of four cleavage sites of the 3C-like proteinase and identification of two novel cleavage products. *Virology* **246**(2)**,** 288-97.

Liu, T. C., Wang, Y., Hallden, G., Brooks, G., Francis, J., Lemoine, N. R., and Kirn, D. (2005). Functional interactions of antiapoptotic proteins and tumor necrosis factor in the context of a

replication-competent adenovirus. *Gene Ther* **12**(17)**,** 1333-46.
Longo, P. G., Laurenti, L., Gobessi, S., Sica, S., Leone, G., and Efremov, D. G. (2008). The Akt/Mcl-1 pathway plays a prominent role in mediating antiapoptotic signals downstream of the B-cell receptor in chronic lymphocytic leukemia B cells. *Blood* **111**(2)**,** 846-55.
Loo, Y. M., Fornek, J., Crochet, N., Bajwa, G., Perwitasari, O., Martinez-Sobrido, L., Akira, S., Gill, M. A., Garcia-Sastre, A., Katze, M. G., and Gale, M., Jr. (2008). Distinct RIG-I and MDA5 signaling by RNA viruses in innate immunity. *J Virol* **82**(1)**,** 335-45.
Loo, Y. M., and Gale, M., Jr. (2011). Immune Signaling by RIG-I-like Receptors. *Immunity* **34**(5)**,** 680-92.
Lucas, M., Stuart, L. M., Savill, J., and Lacy-Hulbert, A. (2003). Apoptotic cells and innate immune stimuli combine to regulate macrophage cytokine secretion. *J Immunol* **171**(5)**,** 2610-5.
Lv, Y., and Bao, E. (2009). Apoptosis induced in chicken embryo fibroblasts in vitro by a polyinosinic:polycytidylic acid copolymer. *Toxicol In Vitro* **23**(7)**,** 1360-4.
Mamane, Y., Heylbroeck, C., Genin, P., Algarte, M., Servant, M. J., LePage, C., DeLuca, C., Kwon, H., Lin, R., and Hiscott, J. (1999). Interferon regulatory factors: the next generation. *Gene* **237**(1)**,** 1-14.
Marie, I., Durbin, J. E., and Levy, D. E. (1998). Differential viral induction of distinct interferon-alpha genes by positive feedback through interferon regulatory factor-7. *EMBO J* **17**(22)**,** 6660-9.
Masters, P. S. (2006). The molecular biology of coronaviruses. *Adv Virus Res* **66,** 193-292.
Masters, P. S., and Rottier, P. J. (2005). Coronavirus reverse genetics by targeted RNA recombination. *Curr Top Microbiol Immunol* **287,** 133-59.
Matsumiya, T., Imaizumi, T., Yoshida, H., and Satoh, K. (2011). Antiviral signaling through retinoic acid-inducible gene-I-like receptors. *Arch Immunol Ther Exp (Warsz)* **59**(1)**,** 41-8.
Matthijs, M. G., van Eck, J. H., Landman, W. J., and Stegeman, J. A. (2003). Ability of Massachusetts-type infectious bronchitis virus to increase colibacillosis susceptibility in commercial broilers: a comparison between vaccine and virulent field virus. *Avian Pathol* **32**(5)**,** 473-81.
McCullough, K. D., Martindale, J. L., Klotz, L. O., Aw, T. Y., and Holbrook, N. J. (2001). Gadd153 sensitizes cells to endoplasmic reticulum stress by down-regulating Bcl2 and perturbing the cellular redox state. *Mol Cell Biol* **21**(4)**,** 1249-59.
Meylan, E., Curran, J., Hofmann, K., Moradpour, D., Binder, M., Bartenschlager, R., and Tschopp, J. (2005). Cardif is an adaptor protein in the RIG-I antiviral pathway and is targeted by hepatitis C virus. *Nature* **437**(7062)**,** 1167-72.
Mi, J., Li, Z. Y., Ni, S., Steinwaerder, D., and Lieber, A. (2001). Induced apoptosis supports spread of adenovirus vectors in tumors. *Hum Gene Ther* **12**(10)**,** 1343-52.
Mikhailov, V., Mikhailova, M., Degenhardt, K., Venkatachalam, M. A., White, E., and Saikumar, P. (2003). Association of Bax and Bak homo-oligomers in mitochondria. Bax requirement for Bak reorganization and cytochrome c release. *J Biol Chem* **278**(7)**,** 5367-76.
Mir, M. A., and Panganiban, A. T. (2006). Characterization of the RNA chaperone activity of hantavirus nucleocapsid protein. *J Virol* **80**(13)**,** 6276-85.
Moore, C. B., and Ting, J. P. (2008). Regulation of mitochondrial antiviral signaling pathways. *Immunity* **28**(6)**,** 735-9.
Nasirudeen, A. M., Wong, H. H., Thien, P., Xu, S., Lam, K. P., and Liu, D. X. (2011). RIG-I, MDA5 and TLR3 synergistically play an important role in restriction of dengue virus infection. *PLoS Negl Trop Dis* **5**(1)**,** e926.
Nguyen, M., Marcellus, R. C., Roulston, A., Watson, M., Serfass, L., Murthy Madiraju, S. R., Goulet, D., Viallet, J., Belec, L., Billot, X., Acoca, S., Purisima, E., Wiegmans, A., Cluse, L., Johnstone, R. W., Beauparlant, P., and Shore, G. C. (2007). Small molecule obatoclax (GX15-070) antagonizes MCL-1 and overcomes MCL-1-mediated resistance to apoptosis. *Proc Natl Acad Sci U S A* **104**(49)**,** 19512-7.
Nishihara, H., Kizaka-Kondoh, S., Insel, P. A., and Eckmann, L. (2003). Inhibition of apoptosis in normal and transformed intestinal epithelial cells by cAMP through induction of inhibitor of apoptosis protein (IAP)-2. *Proc Natl Acad Sci U S A* **100**(15)**,** 8921-6.
O'Brien, V. (1998). Viruses and apoptosis. *J Gen Virol* **79 (Pt 8),** 1833-45.
Oostra, M., Hagemeijer, M. C., van Gent, M., Bekker, C. P., te Lintelo, E. G., Rottier, P. J., and de Haan, C. A. (2008). Topology and membrane anchoring of the coronavirus replication complex: not all hydrophobic domains of nsp3 and nsp6 are membrane spanning. *J Virol* **82**(24)**,** 12392-405.
Opferman, J. T., and Korsmeyer, S. J. (2003). Apoptosis in the development and maintenance of the immune system. *Nat Immunol* **4**(5)**,** 410-5.
Oyadomari, S., and Mori, M. (2004). Roles of CHOP/GADD153 in endoplasmic reticulum stress. *Cell*

Death Differ **11**(4)**,** 381-9.
Pasternak, A. O., Spaan, W. J., and Snijder, E. J. (2006). Nidovirus transcription: how to make sense...? *J Gen Virol* **87**(Pt 6)**,** 1403-21.
Pearce, A. F., and Lyles, D. S. (2009). Vesicular stomatitis virus induces apoptosis primarily through Bak rather than Bax by inactivating Mcl-1 and Bcl-XL. *J Virol* **83**(18)**,** 9102-12.
Peiris, J. S., Guan, Y., and Yuen, K. Y. (2004). Severe acute respiratory syndrome. *Nat Med* **10**(12 Suppl)**,** S88-97.
Picault, J. P., Drouin, P., Guittet, M., Bennejean, G., Protais, J., L'Hospitalier, R., Gillet, J. P., Lamande, J., and Bachelier, A. L. (1986). Isolation, characterisation and preliminary cross-protection studies with a new pathogenic avian infectious bronchitis virus (strain PL-84084). *Avian Pathol* **15**(3)**,** 367-83.
Pichlmair, A., Lassnig, C., Eberle, C. A., Gorna, M. W., Baumann, C. L., Burkard, T. R., Burckstummer, T., Stefanovic, A., Krieger, S., Bennett, K. L., Rulicke, T., Weber, F., Colinge, J., Muller, M., and Superti-Furga, G. (2011). IFIT1 is an antiviral protein that recognizes 5'-triphosphate RNA. *Nat Immunol*.
Platanias, L. C. (2005). Mechanisms of type-I- and type-II-interferon-mediated signalling. *Nat Rev Immunol* **5**(5)**,** 375-86.
Ploegh, H. L. (1998). Viral strategies of immune evasion. *Science* **280**(5361)**,** 248-53.
Poncet, D., Pauleau, A. L., Szabadkai, G., Vozza, A., Scholz, S. R., Le Bras, M., Briere, J. J., Jalil, A., Le Moigne, R., Brenner, C., Hahn, G., Wittig, I., Schagger, H., Lemaire, C., Bianchi, K., Souquere, S., Pierron, G., Rustin, P., Goldmacher, V. S., Rizzuto, R., Palmieri, F., and Kroemer, G. (2006). Cytopathic effects of the cytomegalovirus-encoded apoptosis inhibitory protein vMIA. *J Cell Biol* **174**(7)**,** 985-96.
Proskuryakov, S. Y., Gabai, V. L., and Konoplyannikov, A. G. (2002). Necrosis is an active and controlled form of programmed cell death. *Biochemistry (Mosc)* **67**(4)**,** 387-408.
Puthalakath, H., O'Reilly, L. A., Gunn, P., Lee, L., Kelly, P. N., Huntington, N. D., Hughes, P. D., Michalak, E. M., McKimm-Breschkin, J., Motoyama, N., Gotoh, T., Akira, S., Bouillet, P., and Strasser, A. (2007). ER stress triggers apoptosis by activating BH3-only protein Bim. *Cell* **129**(7)**,** 1337-49.
Putics, A., Filipowicz, W., Hall, J., Gorbalenya, A. E., and Ziebuhr, J. (2005). ADP-ribose-1"-monophosphatase: a conserved coronavirus enzyme that is dispensable for viral replication in tissue culture. *J Virol* **79**(20)**,** 12721-31.
Rajalingam, K., Sharma, M., Lohmann, C., Oswald, M., Thieck, O., Froelich, C. J., and Rudel, T. (2008). Mcl-1 is a key regulator of apoptosis resistance in Chlamydia trachomatis-infected cells. *PLoS One* **3**(9)**,** e3102.
Rebsamen, M., Meylan, E., Curran, J., and Tschopp, J. (2008). The antiviral adaptor proteins Cardif and Trif are processed and inactivated by caspases. *Cell Death Differ* **15**(11)**,** 1804-11.
Reed, J. C. (2000). Mechanisms of apoptosis. *Am J Pathol* **157**(5)**,** 1415-30.
Ren, J., Shi, M., Liu, R., Yang, Q. H., Johnson, T., Skarnes, W. C., and Du, C. (2005). The Birc6 (Bruce) gene regulates p53 and the mitochondrial pathway of apoptosis and is essential for mouse embryonic development. *Proc Natl Acad Sci U S A* **102**(3)**,** 565-70.
Ross, T. M. (2001). Using death to one's advantage: HIV modulation of apoptosis. *Leukemia* **15**(3)**,** 332-41.
Roth-Cross, J. K., Bender, S. J., and Weiss, S. R. (2008). Murine coronavirus mouse hepatitis virus is recognized by MDA5 and induces type I interferon in brain macrophages/microglia. *J Virol* **82**(20)**,** 9829-38.
Rothenfusser, S., Goutagny, N., DiPerna, G., Gong, M., Monks, B. G., Schoenemeyer, A., Yamamoto, M., Akira, S., and Fitzgerald, K. A. (2005). The RNA helicase Lgp2 inhibits TLR-independent sensing of viral replication by retinoic acid-inducible gene-I. *J Immunol* **175**(8)**,** 5260-8.
Saito, T., Hirai, R., Loo, Y. M., Owen, D., Johnson, C. L., Sinha, S. C., Akira, S., Fujita, T., and Gale, M., Jr. (2007). Regulation of innate antiviral defenses through a shared repressor domain in RIG-I and LGP2. *Proc Natl Acad Sci U S A* **104**(2)**,** 582-7.
Saito, T., Owen, D. M., Jiang, F., Marcotrigiano, J., and Gale, M., Jr. (2008). Innate immunity induced by composition-dependent RIG-I recognition of hepatitis C virus RNA. *Nature* **454**(7203)**,** 523-7.
Satoh, T., Kato, H., Kumagai, Y., Yoneyama, M., Sato, S., Matsushita, K., Tsujimura, T., Fujita, T., Akira, S., and Takeuchi, O. (2010). LGP2 is a positive regulator of RIG-I- and MDA5-mediated antiviral responses. *Proc Natl Acad Sci U S A* **107**(4)**,** 1512-7.
Sawicki, S. G., and Sawicki, D. L. (1995). Coronaviruses use discontinuous extension for synthesis of subgenome-length negative strands. *Adv Exp Med Biol* **380,** 499-506.

Sawicki, S. G., Sawicki, D. L., and Siddell, S. G. (2007). A contemporary view of coronavirus transcription. *J Virol* **81**(1)**,** 20-9.
Schelle, B., Karl, N., Ludewig, B., Siddell, S. G., and Thiel, V. (2005). Selective replication of coronavirus genomes that express nucleocapsid protein. *J Virol* **79**(11)**,** 6620-30.
Schelle, B., Karl, N., Ludewig, B., Siddell, S. G., and Thiel, V. (2006). Nucleocapsid protein expression facilitates coronavirus replication. *Adv Exp Med Biol* **581,** 43-8.
Scott, I. (2009). Degradation of RIG-I following cytomegalovirus infection is independent of apoptosis. *Microbes Infect* **11**(12)**,** 973-9.
Scott, I., and Norris, K. L. (2008). The mitochondrial antiviral signaling protein, MAVS, is cleaved during apoptosis. *Biochem Biophys Res Commun* **375**(1)**,** 101-6.
Seth, R. B., Sun, L., Ea, C. K., and Chen, Z. J. (2005). Identification and characterization of MAVS, a mitochondrial antiviral signaling protein that activates NF-kappaB and IRF 3. *Cell* **122**(5)**,** 669-82.
Shaw, M. H., Reimer, T., Kim, Y. G., and Nunez, G. (2008). NOD-like receptors (NLRs): bona fide intracellular microbial sensors. *Curr Opin Immunol* **20**(4)**,** 377-82.
Shen, H., Fang, S. G., Chen, B., Chen, G., Tay, F. P., and Liu, D. X. (2009). Towards construction of viral vectors based on avian coronavirus infectious bronchitis virus for gene delivery and vaccine development. *J Virol Methods* **160**(1-2)**,** 48-56.
Shen, P., Jiang, T., Lu, H., Han, H., and Luo, R. (2011). Combination of Poly I:C and arsenic trioxide triggers apoptosis synergistically via activation of TLR3 and mitochondrial pathways in hepatocellular carcinoma cells. *Cell Biol Int*.
Shen, S., Law, Y. C., and Liu, D. X. (2004). A single amino acid mutation in the spike protein of coronavirus infectious bronchitis virus hampers its maturation and incorporation into virions at the nonpermissive temperature. *Virology* **326**(2)**,** 288-98.
Shen, S., Wen, Z. L., and Liu, D. X. (2003). Emergence of a coronavirus infectious bronchitis virus mutant with a truncated 3b gene: functional characterization of the 3b protein in pathogenesis and replication. *Virology* **311**(1)**,** 16-27.
Shen, Y., and Shenk, T. E. (1995). Viruses and apoptosis. *Curr Opin Genet Dev* **5**(1)**,** 105-11.
Shi, S. T., and Lai, M. M. (2005). Viral and cellular proteins involved in coronavirus replication. *Curr Top Microbiol Immunol* **287,** 95-131.
Snijder, E. J., Bredenbeek, P. J., Dobbe, J. C., Thiel, V., Ziebuhr, J., Poon, L. L., Guan, Y., Rozanov, M., Spaan, W. J., and Gorbalenya, A. E. (2003). Unique and conserved features of genome and proteome of SARS-coronavirus, an early split-off from the coronavirus group 2 lineage. *J Mol Biol* **331**(5)**,** 991-1004.
Snijder, E. J., van der Meer, Y., Zevenhoven-Dobbe, J., Onderwater, J. J., van der Meulen, J., Koerten, H. K., and Mommaas, A. M. (2006). Ultrastructure and origin of membrane vesicles associated with the severe acute respiratory syndrome coronavirus replication complex. *J Virol* **80**(12)**,** 5927-40.
Stadler, K., Masignani, V., Eickmann, M., Becker, S., Abrignani, S., Klenk, H. D., and Rappuoli, R. (2003). SARS--beginning to understand a new virus. *Nat Rev Microbiol* **1**(3)**,** 209-18.
Stetson, D. B., and Medzhitov, R. (2006). Type I interferons in host defense. *Immunity* **25**(3)**,** 373-81.
Susin, S. A., Lorenzo, H. K., Zamzami, N., Marzo, I., Snow, B. E., Brothers, G. M., Mangion, J., Jacotot, E., Costantini, P., Loeffler, M., Larochette, N., Goodlett, D. R., Aebersold, R., Siderovski, D. P., Penninger, J. M., and Kroemer, G. (1999). Molecular characterization of mitochondrial apoptosis-inducing factor. *Nature* **397**(6718)**,** 441-6.
Suthar, M. S., Ma, D. Y., Thomas, S., Lund, J. M., Zhang, N., Daffis, S., Rudensky, A. Y., Bevan, M. J., Clark, E. A., Kaja, M. K., Diamond, M. S., and Gale, M., Jr. (2010). IPS-1 is essential for the control of West Nile virus infection and immunity. *PLoS Pathog* **6**(2)**,** e1000757.
Sutton, G., Fry, E., Carter, L., Sainsbury, S., Walter, T., Nettleship, J., Berrow, N., Owens, R., Gilbert, R., Davidson, A., Siddell, S., Poon, L. L., Diprose, J., Alderton, D., Walsh, M., Grimes, J. M., and Stuart, D. I. (2004). The nsp9 replicase protein of SARS-coronavirus, structure and functional insights. *Structure* **12**(2)**,** 341-53.
Takeuchi, O., and Akira, S. (2008). MDA5/RIG-I and virus recognition. *Curr Opin Immunol* **20**(1)**,** 17-22.
Takeuchi, O., and Akira, S. (2009). Innate immunity to virus infection. *Immunol Rev* **227**(1)**,** 75-86.
Takeuchi, O., and Akira, S. (2010). Pattern recognition receptors and inflammation. *Cell* **140**(6)**,** 805-20.
Tan, Y. J., Fielding, B. C., Goh, P. Y., Shen, S., Tan, T. H., Lim, S. G., and Hong, W. (2004). Overexpression of 7a, a protein specifically encoded by the severe acute respiratory syndrome coronavirus, induces apoptosis via a caspase-dependent pathway. *J Virol* **78**(24)**,** 14043-7.
Teodoro, J. G., and Branton, P. E. (1997). Regulation of apoptosis by viral gene products. *J Virol* **71**(3)**,**

1739-46.
Theofilopoulos, A. N., Baccala, R., Beutler, B., and Kono, D. H. (2005). Type I interferons (alpha/beta) in immunity and autoimmunity. *Annu Rev Immunol* **23,** 307-36.
Thiel, V., and Siddell, S. G. (2005). Reverse genetics of coronaviruses using vaccinia virus vectors. *Curr Top Microbiol Immunol* **287,** 199-227.
van Vliet, A. L., Smits, S. L., Rottier, P. J., and de Groot, R. J. (2002). Discontinuous and non-discontinuous subgenomic RNA transcription in a nidovirus. *EMBO J* **21**(23)**,** 6571-80.
Venkataraman, T., Valdes, M., Elsby, R., Kakuta, S., Caceres, G., Saijo, S., Iwakura, Y., and Barber, G. N. (2007). Loss of DExD/H box RNA helicase LGP2 manifests disparate antiviral responses. *J Immunol* **178**(10)**,** 6444-55.
Versteeg, G. A., van de Nes, P. S., Bredenbeek, P. J., and Spaan, W. J. (2007). The coronavirus spike protein induces endoplasmic reticulum stress and upregulation of intracellular chemokine mRNA concentrations. *J Virol* **81**(20)**,** 10981-90.
Vince, J. E., and Tschopp, J. (2010). IRF-3 partners Bax in a viral-induced dance macabre. *EMBO J* **29**(10)**,** 1627-8.
Wang, L. F., and Eaton, B. T. (2007). Bats, civets and the emergence of SARS. *Curr Top Microbiol Immunol* **315,** 325-44.
Wang, X., Eno, C. O., Altman, B. J., Zhu, Y., Zhao, G., Olberding, K. E., Rathmell, J. C., and Li, C. (2011a). ER stress modulates cellular metabolism. *Biochem J* **435**(1)**,** 285-96.
Wang, X., Liao, Y., Yap, P. L., Png, K. J., Tam, J. P., and Liu, D. X. (2009). Inhibition of protein kinase R activation and upregulation of GADD34 expression play a synergistic role in facilitating coronavirus replication by maintaining de novo protein synthesis in virus-infected cells. *J Virol* **83**(23)**,** 12462-72.
Wang, X., Olberding, K. E., White, C., and Li, C. (2011b). Bcl-2 proteins regulate ER membrane permeability to luminal proteins during ER stress-induced apoptosis. *Cell Death Differ* **18**(1)**,** 38-47.
Wang, Y. C., Kulp, S. K., Wang, D., Yang, C. C., Sargeant, A. M., Hung, J. H., Kashida, Y., Yamaguchi, M., Chang, G. D., and Chen, C. S. (2008). Targeting endoplasmic reticulum stress and Akt with OSU-03012 and gefitinib or erlotinib to overcome resistance to epidermal growth factor receptor inhibitors. *Cancer Res* **68**(8)**,** 2820-30.
Wei, M. C., Lindsten, T., Mootha, V. K., Weiler, S., Gross, A., Ashiya, M., Thompson, C. B., and Korsmeyer, S. J. (2000). tBID, a membrane-targeted death ligand, oligomerizes BAK to release cytochrome c. *Genes Dev* **14**(16)**,** 2060-71.
Werts, C., Rubino, S., Ling, A., Girardin, S. E., and Philpott, D. J. (2011). Nod-like receptors in intestinal homeostasis, inflammation, and cancer. *J Leukoc Biol*.
Wevers, B. A., and van der Hoek, L. (2009). Recently discovered human coronaviruses. *Clin Lab Med* **29**(4)**,** 715-24.
Wilkins, C., and Gale, M., Jr. (2010). Recognition of viruses by cytoplasmic sensors. *Curr Opin Immunol* **22**(1)**,** 41-7.
Willis, S. N., Chen, L., Dewson, G., Wei, A., Naik, E., Fletcher, J. I., Adams, J. M., and Huang, D. C. (2005). Proapoptotic Bak is sequestered by Mcl-1 and Bcl-xL, but not Bcl-2, until displaced by BH3-only proteins. *Genes Dev* **19**(11)**,** 1294-305.
Willis, S. N., Fletcher, J. I., Kaufmann, T., van Delft, M. F., Chen, L., Czabotar, P. E., Ierino, H., Lee, E. F., Fairlie, W. D., Bouillet, P., Strasser, A., Kluck, R. M., Adams, J. M., and Huang, D. C. (2007). Apoptosis initiated when BH3 ligands engage multiple Bcl-2 homologs, not Bax or Bak. *Science* **315**(5813)**,** 856-9.
Xu, L., Khadijah, S., Fang, S., Wang, L., Tay, F. P., and Liu, D. X. (2010). The cellular RNA helicase DDX1 interacts with coronavirus nonstructural protein 14 and enhances viral replication. *J Virol* **84**(17)**,** 8571-83.
Xu, L. G., Wang, Y. Y., Han, K. J., Li, L. Y., Zhai, Z., and Shu, H. B. (2005). VISA is an adapter protein required for virus-triggered IFN-beta signaling. *Mol Cell* **19**(6)**,** 727-40.
Xu, L. H., Huang, M., Fang, S. G., and Liu, D. X. (2011). Coronavirus infection induces DNA replication stress partly through interaction of its nonstructural protein 13 with the p125 subunit of DNA polymerase delta. *J Biol Chem* **286**(45)**,** 39546-59.
Yamada, Y., Liu, X. B., Fang, S. G., Tay, F. P., and Liu, D. X. (2009). Acquisition of cell-cell fusion activity by amino acid substitutions in spike protein determines the infectivity of a coronavirus in cultured cells. *PLoS One* **4**(7)**,** e6130.
Yan, H., Xiao, G., Zhang, J., Hu, Y., Yuan, F., Cole, D. K., Zheng, C., and Gao, G. F. (2004). SARS coronavirus induces apoptosis in Vero E6 cells. *J Med Virol* **73**(3)**,** 323-31.
Yang, Y., Liang, Y., Qu, L., Chen, Z., Yi, M., Li, K., and Lemon, S. M. (2007). Disruption of innate

immunity due to mitochondrial targeting of a picornaviral protease precursor. *Proc Natl Acad Sci U S A* **104**(17)**,** 7253-8.

Yoneyama, M., and Fujita, T. (2009). RNA recognition and signal transduction by RIG-I-like receptors. *Immunol Rev* **227**(1)**,** 54-65.

Yoneyama, M., Kikuchi, M., Matsumoto, K., Imaizumi, T., Miyagishi, M., Taira, K., Foy, E., Loo, Y. M., Gale, M., Jr., Akira, S., Yonehara, S., Kato, A., and Fujita, T. (2005). Shared and unique functions of the DExD/H-box helicases RIG-I, MDA5, and LGP2 in antiviral innate immunity. *J Immunol* **175**(5)**,** 2851-8.

Yount, B., Curtis, K. M., and Baric, R. S. (2000). Strategy for systematic assembly of large RNA and DNA genomes: transmissible gastroenteritis virus model. *J Virol* **74**(22)**,** 10600-11.

Zhai, Y., Sun, F., Li, X., Pang, H., Xu, X., Bartlam, M., and Rao, Z. (2005). Insights into SARS-CoV transcription and replication from the structure of the nsp7-nsp8 hexadecamer. *Nat Struct Mol Biol* **12**(11)**,** 980-6.

Zhang, X. M., Kousoulas, K. G., and Storz, J. (1992). The hemagglutinin/esterase gene of human coronavirus strain OC43: phylogenetic relationships to bovine and murine coronaviruses and influenza C virus. *Virology* **186**(1)**,** 318-23.

Zhou, Z., Hamming, O. J., Ank, N., Paludan, S. R., Nielsen, A. L., and Hartmann, R. (2007). Type III interferon (IFN) induces a type I IFN-like response in a restricted subset of cells through signaling pathways involving both the Jak-STAT pathway and the mitogen-activated protein kinases. *J Virol* **81**(14)**,** 7749-58.

Ziebuhr, J. (2006). The coronavirus replicase: insights into a sophisticated enzyme machinery. *Adv Exp Med Biol* **581,** 3-11.

Ziebuhr, J., Snijder, E. J., and Gorbalenya, A. E. (2000). Virus-encoded proteinases and proteolytic processing in the Nidovirales. *J Gen Virol* **81**(Pt 4)**,** 853-79.

Zong, W. X., and Thompson, C. B. (2006). Necrotic death as a cell fate. *Genes Dev* **20**(1)**,** 1-15.

Zuniga, S., Sola, I., Alonso, S., and Enjuanes, L. (2004). Sequence motifs involved in the regulation of discontinuous coronavirus subgenomic RNA synthesis. *J Virol* **78**(2)**,** 980-94.

Zust, R., Cervantes-Barragan, L., Habjan, M., Maier, R., Neuman, B. W., Ziebuhr, J., Szretter, K. J., Baker, S. C., Barchet, W., Diamond, M. S., Siddell, S. G., Ludewig, B., and Thiel, V. (2011). Ribose 2'-O-methylation provides a molecular signature for the distinction of self and non-self mRNA dependent on the RNA sensor Mda5. *Nat Immunol* **12**(2)**,** 137-43.